Journal Pre-proof

Wrinkling analysis of a stiff shallow film mounted on a cylindrically curved compliant substrate - Part II: Checkerboard and hexagonal modes

Alexis Kordolemis, Antonios E. Giannakopoulos

PII: S0020-7683(25)00169-6
DOI: https://doi.org/10.1016/j.ijsolstr.2025.113383
Reference: SAS 113383

To appear in: *International Journal of Solids and Structures*

Received date : 30 November 2024
Revised date : 27 March 2025
Accepted date : 8 April 2025

Please cite this article as: A. Kordolemis and A.E. Giannakopoulos, Wrinkling analysis of a stiff shallow film mounted on a cylindrically curved compliant substrate - Part II: Checkerboard and hexagonal modes. *International Journal of Solids and Structures* (2025), doi: https://doi.org/10.1016/j.ijsolstr.2025.113383.

Highlights

- Wrinkling analysis of a stiff shallow film mounted on a cylindrically curved compliant substrate with emphasis to square checkerboard and hexagonal modes is conducted.
- The stability of the bilayer has been explored within the framework of the general theory of thin shallow shells for the film and the general linear theory of solids for the substrate.
- The primary goal of the analysis is to highlight the role of the curvature induced anisotropy to the geometrical parameters of the checkerboard and hexagonal modes, i.e. the wavelengths and the amplitudes.
- Employing the energy minimization approach semi-analytical expressions for the wavelength and the amplitude for both wrinkling modes in the principal directions of the bilayer are presented
- The results have been validated against existing findings in the open literature with very good agreement

Wrinkling analysis of a stiff shallow film mounted on a cylindrically curved compliant substrate - Part II: Checkerboard and hexagonal modes.

Alexis Kordolemis[a,*], Antonios E. Giannakopoulos[b]

[a] *University of Greenwich, Faculty of Engineering and Science, Chatham Maritime, ME4 4TB, Kent, UK*
[b] *National Technical University of Athens, Mechanics Division, 5 Heroes of Polytechnion Avenue, Zografou, Athens, GR-15773, , Greece*

Abstract

A thin film mounted on a compliant substrate under biaxial compressive strains wrinkles in different patterns such as cylindrical, checkerboard, herringbone and hexagonal. In this paper, we provide a thorough analysis of the checkerboard and hexagonal wrinkling modes which have been well documented experimentally and numerically. Particular attention is paid to the role of the curvature-induced anisotropy in the geometrical characteristic of these particular surface wrinkling modes, i.e. the wavelengths in the two principal directions as well as the corresponding amplitudes. The film is assumed to be much stiffer than the substrate and the bilayer system is cylindrically curved and is acted upon biaxial compressive strains. The film is modelled as a shallow shell with finite rotations while the substrate is simulated as a linear three-dimensional elastic solid. Utilising the minimization of the total energy of the system semi-analytical expressions for the critical values of the

*Corresponding author: a.kordolemis@gre.ac.uk

wavelengths and the corresponding amplitudes associated with the onset of the checkerboard and hexagonal mode are provided. The obtained results has been found to be in a very good agreement compared to experimental and numerical findings of other studies. It is shown that the presence of the initial curvature in the bilayer delays the critical strain and the wrinkling amplitudes significantly for both modes, compared to the flat system, and moreover explains the inward buckling of the hexagonal mode which has been observed experimentally.

Keywords: thin film, compliant substrate, wrinkling, square checkerboard, hexagonal, curvature, perturbation method

1. Introduction

In recent years, the study of ordered buckling structures has been in the epicentre of fervent research efforts of the engineering mechanics community due to its importance in the design and manufacturing of novel, high-end technological applications. Early studies on the subject started with the analysis of sandwich panels, (Allen, 1969), while ever since the ordered buckling analysis has been employed to investigate a wide range of natural and advanced synthetic systems, like swelling hydrogels (Hong *et al*, 2008), (Zhang *et al*, 2011), and human skin wrinkling, (Dagdeviren *et al*, 2015). In practical engineering terms, soft electronic devices are very thin multilayered components with high stiffness, attached onto the skin which, in general, is thicker and with much lower stiffness. Thus, the instability analysis of the thin film/substrate bilayer and the associated wrinkling patterns it is reasonable to be investigated mechanically by employing the model of a stiff thin

film mounted on a much thicker compliant substrate.

It has been recognised that the general loading of the bilayer, i.e. film bonded in the substrate, is biaxial strain in the two principal directions of the system. Thus, upon the strain reaches a critical value the bilayer will experience surface wrinkling which manifests itself through different patterns, like cylindrical, checkerboard, herringbone, labyrinths, etc. The source of the biaxial strain varies depending on the nature of the system, thus it can originate from differential thermal expansion between the film and the substrate, swelling of the soft substrate and ultraviolet-ozone (UVO) oxidation process on the thin film, to name but few.

Recently, many theoretical and experimental efforts have been made toward the understanding of the mechanisms that lead to the onset of different wrinkling patterns of these particular kind of bilayers. In their pioneering work in the field, (Bowden *et al*, 1998), studied the spontaneous generation of complex patterns for a vapour deposited thin film on a thermally expanded polymer substrate and the critical stress for the one dimensional cylindrical wrinkling mode presented in a closed form expression. Surface wrinkling instabilities of thin films bonded on compliant substrates have been studied numerically (Nikravesh *et al*, 2019; Nikravesh *et al*, 2019; Nikravesh *et al*, 2020), analytically (Yin *et al*, 2018; Cheng *et al*, 2014; Huang *et al*, 2015; Huang *et al*, 2016; Song *et al*, 2008; Cao *et al*, 2012; Huang *et al*, 2004; Huang *et al*, 2005, Huang, 2005, Huang and Suo, 2002) and experimentally (Jiang *et al*, 2008; Choi *et al*, 2007). All the above studies are focusing on the analysis of flat bilayer systems. However, in nature and in many engineering applications the film/substrate bilayer is not flat but curved.

In their seminar work, (Cai *et al*, 2011), investigated a bilayer under equibiaxial compressive stress states experimentally and provided a theoretical framework employing an analytical upper bound while they performed full numerical analysis for various wrinkling patterns, i.e. cylindrical, checkerboard, herringbone, triangular and hexagonal. Discrepancies between the theoretical analysis and the experimental observations have been attributed to the initial spherical curvature of the system. Surface wrinkling of closed cross-section cylindrical shells supported by a soft core subjected to axial compression combining computational and experimental methods has been the epicentre of many research efforts (Zhao *et al*, 2014; Cao *et al*, 2012; Zhao and Zhao, 2017; Chen and Yin, 2010). In an attempt to provide a deeper understanding of the intriguing wrinkling patterns of the thin film bilayer several studies have focused on the modelling of the substrate as a spherical space (Cao *et al*, 2008; Hao *et al*, 2024; Zhao *et al*, 2020; Breid and Crosby, 2013).

The aim of the present study is to investigate in depth the checkerboard and hexagonal wrinkling modes of the film/substrate system and highlight the role of the curvature-induced anisotropy in the geometric characteristics of the surface wrinkling, i.e. the wavelengths in the two principal curvature directions and their amplitudes. In doing so, the initial configuration of the curved bilayer is considered as an open cylindrical cross-section which differentiates notably the analysis compared to the axisymmetric closed cross-section cylinder and the spherical configurations which have been investigated earlier in other studies. Within this context, semi-analytical expressions for the wavelengths and amplitudes for the squared checkerboard and hexagonal

modes are provided in a comprehensive way. Therefore, the role of every single parameter of the multi-parametric model becomes apparent which can help in the design process. To the best of our knowledge, similar analysis has not been performed so far and is presented in the open literature for the first time in this study.

The paper is structured as follows. In section 2, the theoretical buckling analysis framework is presented for both the film and the substrate and the corresponding energy expressions are established. The displacement components, the accompanied wavelengths and amplitude of the bilayer for the square checkerboard wrinkling mode are presented in Section 3, while the analysis of the hexagonal mode is included in Section 4. In both cases, the analysis initiates with the solution of the flat bilayer which consequently is used as the basis in the perturbation method employed in the analysis of the curved bilayer. In Section 5 the results are presented and discussed in detail while in Section 6 there is a closure summarising the findings of the study.

2. Buckling analysis under biaxial strain

The buckling analysis of the bilayer under biaxial in-plane strains which provides the displacement components and the associated energies of both the thin film and the compliant substrate has been performed analytically in Part I of our study which can be found in our companion paper (Kordolemis and Giannakopoulos, 2024). Here, where necessary, we will be referring to elements of this companion paper by adding the letter "I" as superscript.

2.1. Thin curved film

Consider a curved thin film mounted on a compliant substrate of infinite thickness as shown in Fig.1[I]. The non-linear membrane strains, the in-plane stresses, the membrane forces, the equilibrium equations as well as the expressions for the bending and membrane energy are provided explicitly through Eqs.(2.1)[I] - (2.18)[I].

2.2. Compliant curved substrate

The substrate is modelled as a semi-infinite, linear three-dimensional half space. The strains, the stresses, the equilibrium equations and the associated energy are given analytically through Eqs.(2.19)[I] - (2.26)[I].

3. Square checkerboard mode

In this section we study the stability of the curved film-substrate system and the wavenumbers k_1, k_2 in the principal curvature directions along with the wrinkling amplitude, A_0, are calculated through the minimization of the total energy of the system.

3.1. Curved Thin film

For the case of the two dimensional square checkerboard buckling mode, we assume that the out of plane displacement $w(x, y)$ of the thin curved film is periodic in both directions and it is given from

$$w_f(x, y) = A_0 \cos(k_1 x) \cos(k_2 y) \tag{3.1}$$

Back substitution into Eqs.(2.1)[I] - (2.6)[I] and finally in equilibrium Eqs.(2.13)[I], (2.14)[I], results into a system of coupled equations with respect to the in-plane

displacements which can be solved to yield:

$$u_f^{\text{curved}}(x,y) = \frac{A_0^2\, k_1}{16}\left[2\,\cos^2(k_2\,y) - \nu_f\left(\frac{k_2}{k_1}\right)^2\right]\sin(2\,k_1\,x) - \frac{A_0}{(k\,R)}\,\frac{k_1}{k}\left[\nu_f\left(\frac{k_1}{k}\right)^2 - \left(\frac{k_2}{k}\right)^2\right]\sin(k_1\,x)\,\cos(k_2\,y) \tag{3.2}$$

$$v_f^{\text{curved}}(x,y) = \frac{A_0^2\, k_2}{16}\left[2\,\cos^2(k_1\,x) - \nu_f\left(\frac{k_1}{k_2}\right)^2\right]\sin(2\,k_2\,y) - \frac{A_0}{(k\,R)}\,\frac{k_2}{k}\left[\left(\frac{k_2}{k}\right)^2 + (\nu_f+2)\left(\frac{k_1}{k}\right)^2\right]\sin(k_2\,y)\cos(k_1\,x) \tag{3.3}$$

Note that from Eq.(3.3) it can be concluded that the term containing the initial curvature of the film always decreases the magnitude of the displacement component in the x direction. In contrast, Eq.(3.2) suggests that the contribution of the curvature term is not clear a priori because the sign of the second term depends on the value of the wavelenghts, Poisson's ratio and the sign of the curvature itself. In the special case of a flat film, $R \to \infty$, we obtain the expressions for the in-plane displacement components, u_f, v_f as given in (Song *et al*, 2008).

The bending energy density of the thin film is given by Eq.(2.17)[I], which in view of Eq.(3.1), after integration over one period, is written as:

$$U_{b(f)}^{\text{curved}} = \frac{\bar{E}_f}{96}\,A_0^2\,t_f^3\,k^4 \tag{3.4}$$

The membrane energy density of the film is given by integration oover a

period of Eq.(2.18)[I] as:

$$U_{m(f)}^{\text{curved}} = \frac{\bar{E}_f\, t_f}{256}\Bigg\{128\left[\left(\varepsilon_{xx}^0\right)^2 + \left(\varepsilon_{yy}^0\right)^2 + 2\,\nu_f\,\varepsilon_{xx}^0\,\varepsilon_{yy}^0\right] + 32\,A_0^2\,k_2^2\left[\left[1+\nu_f\left(\frac{k_1}{k_2}\right)^2\right]\varepsilon_{yy}^0 + \left[\left(\frac{k_1}{k_2}\right)^2 + \nu_f\right]\varepsilon_{xx}^0\right] + A_0^4\,k_2^4\left[\left(3-\nu_f^2\right)\left[\left(\frac{k_1}{k_2}\right)^4 + 1\right] + 4\,\nu_f\left(\frac{k_1}{k_2}\right)^2\right] + 32\left(1-\nu_f^2\right)\frac{A_0^2}{R^2}\left(\frac{k_1}{k}\right)^4\Bigg\} \tag{3.5}$$

Note that the expression of the membrane energy of the film is a function of $1/R^2$ alone which in turn implies that the membrane energy remains the same for both convex and concave thin films of the same curvature. For the special case of a flat film, i.e. $R \to \infty$, the above lead to the expression presented in (Song *et al*, 2008) .

3.2. Curved substrate

In this section the displacement components of the linear elastic curved substrate are analysed. The wavelength of the wrinkling is much smaller than the radius of the curvature so as the ratio $\delta = 1/R\sqrt{(k_1^2+k_2^2)}$ is considered to be a small enough quantity. Therefore, the displacement components of the substrate can be expanded as a power series of this small quantity as:

$$u_s\left(x,y,z\right) = A_0\left[u_s^{(0)}(x,y,z) + \delta\,u_s^{(1)}(x,y,z) + \delta^2\,u_s^{(2)}(x,y,z) + O\left(\delta^3\,u_s^{(3)}(x,y,z)\right)\right] \tag{3.6}$$

$$v_s\left(x,y,z\right) = A_0\left[v_s^{(0)}(x,y,z) + \delta\,v_s^{(1)}(x,y,z) + \delta^2\,v_s^{(2)}(x,y,z) + O\left(\delta^2\,v_s^{(2)}(x,y,z)\right)\right] \tag{3.7}$$

$$w_s\left(x,y,z\right)=A_0\Big[w_s^{(0)}(x,y,z)+\delta\, w_s^{(1)}(x,y,z)+\delta^2\, w_s^{(2)}(x,y,z)+O\left(\delta^3\, w_s^{(3)}(x,y,z)\right)\Big] \tag{3.8}$$

where $u_s^{(0)}(x,y,z)=u_s^{\text{flat}}(x,y,z)/A_0$, $v_s^{(0)}(x,y,z)=v_s^{\text{flat}}(x,y,z)/A_0$, $w_s^{(0)}(x,y,z)=w_s^{\text{flat}}(x,y,z)/A_0$ and $u_s^{(i)}, v_s^{(i)}, w_s^{(i)}, i=1,2,...$ are non-dimensional coefficients to be determined through the perturbation method, while O is the Landau's notation indicating that cubic and higher order terms are truncated. The boundary conditions denote that the in-plane shear stresses on the interface of the bilayer ($z=0$) vanish, all the displacement components far away from the interface ($z=-\infty$) are zero, while the out of plane displacement at the interface must follow a sinusoidal pattern. Thus, they read:

$$\begin{aligned}&\sigma_{xz}|_{z=0}=\left(\frac{\partial u_s}{\partial z}+\frac{\partial w_s}{\partial x}\right)\Big|_{z=0}=0,\quad \sigma_{yz}|_{z=0}=\left(\frac{\partial v_s}{\partial z}+\frac{\partial w_s}{\partial y}\right)\Big|_{z=0}=0,\\ &w_s|_{z=0}=A_0\,\cos\left(k_1\,x\right)\cos\left(k_2\,y\right),\quad u_s|_{z=-\infty}=v_s|_{z=-\infty}=w_s|_{z=-\infty}=0\end{aligned} \tag{3.9}$$

Feeding Eqs.(3.6)-(3.8) into equilibrium equations, Eqs.$(2.22)^{\text{I}}$ - $(2.24)^{\text{I}}$, after equating like powers of the small parameter δ, yields the analytical expressions of the non-dimensional coefficients, $u_s^{(i)}, v_s^{(i)}, w_s^{(i)}$, as:

$$u_s^{\text{flat}}\left(x,y,z\right)=\frac{\left(1-2\,\nu_s+k\,z\right)}{2\left(1-\nu_s\right)}\,A_0\,\left(\frac{k_1}{k}\right)\,e^{z\,k}\,\sin\left(k_1\,x\right)\cos\left(k_2\,y\right) \tag{3.10}$$

$$v_s^{\text{flat}}\left(x,y,z\right)=\frac{\left(1-2\,\nu_s+k\,z\right)}{2\left(1-\nu_s\right)}\,A_0\,\left(\frac{k_2}{k}\right)\,e^{z\,k}\,\cos\left(k_1\,x\right)\sin\left(k_2\,y\right) \tag{3.11}$$

$$w_s^{\text{flat}}\left(x,y,z\right)=\frac{\left(2-2\nu_s-k\,z\right)}{2\left(1-\nu_s\right)}\,A_0\,e^{z\,k}\,\cos\left(k_1\,x\right)\cos\left(k_2\,y\right) \tag{3.12}$$

$$u_s^{(1)}(x,y,z) = \frac{2\,(\mathcal{A}_1\,k\,z+\mathcal{A}_2)+1}{2\,(\nu_s-1)\,(2\,\nu_s-1)}\left(\frac{k_1}{k}\right)\,e^{z\,k}\,\sin(k_1\,x)\cos(k_2\,y) \tag{3.13}$$

$$v_s^{(1)}(x,y,z) = \frac{\mathcal{A}_3\,k\,z+\mathcal{A}_4}{(\nu_s-1)\,(2\,\nu_s-1)}\left(\frac{k_2}{k}\right)\,e^{z\,k}\,\cos(k_1\,x)\sin(k_2\,y) \tag{3.14}$$

$$w_s^{(1)}(x,y,z) = \frac{\mathcal{A}_5\,k\,z+\mathcal{A}_6}{4\,k\,R\,(\nu_s-1)^2}\,e^{z\,k}\,\cos(k_1\,x)\cos(k_2\,y) \tag{3.15}$$

$$u_s^{(2)}(x,y,z) = \frac{\mathcal{A}_7\,k\,z+\mathcal{A}_8}{4\,(\nu_s-1)^2\,(2\,\nu_s-1)^2\,\,(k\,R)^2}\left(\frac{k_1}{k}\right)\,e^{z\,k}\,\sin(k_1\,x)\cos(k_2\,y) \tag{3.16}$$

$$v_s^{(2)}(x,y,z) = \frac{\mathcal{A}_9\,k\,z+\mathcal{A}_{10}}{4\,(\nu_s-1)^2\,(2\,\nu_s-1)^2\,\,(k\,R)^2}\left(\frac{k_2}{k}\right)\,e^{z\,k}\,\cos(k_1\,x)\sin(k_2\,y) \tag{3.17}$$

$$w_s^{(2)}(x,y,z) = \frac{\mathcal{A}_{11}\,k\,z+\mathcal{A}_{12}}{8\,(\nu_s-1)^3\,(2\,\nu_s-1)\,\,(k\,R)^2}\,e^{z\,k}\,\cos(k_1\,x)\cos(k_2\,y) \tag{3.18}$$

where the nondimensional auxiliary parameters $\mathcal{A}_i$, $i = 1, 2, ...12$ depend on the substrate's Poisson ratio ν_s, the curvature R and the wavenumbers k_1, k_2 in the two principal directions of the bilayer, i.e.

$$\mathcal{A}_i = \mathcal{A}_i\,(k_1, k_2, \nu_s, R) \tag{3.19}$$

Their analytical closed form expressions are provided through Eqs.(A.1)-(A.12) in the Supporting Information (SI). Note that the series expansion of the substrate's displacement components in Eqs.(3.6)-(3.8) include the first three terms of the non-dimensional coefficients, $u_s^{(i)}, v_s^{(i)}, w_s^{(i)}$, which retains

only up to quadratic terms of the curvature. However, it has been verified that for $k\,R > 100$ and so, these terms are very small compared to the retained ones. Thus, the strain energy for the substrate, U_s, over one period is readily calculated. The analytical expression is appended in the Supporting Information, i.e., Eq. (A.13).

Note that the expression of the substrate's energy includes terms up to the 6^{th} order in terms of the curvature despite of the fact that the displacement field used in the derivation includes quadratic terms. Thus, it would be expected up to 8^{th} order terms to appear in the final energy expression. However, it has been verified that these terms are very small compare to the preceding ones which in turn means the series converges rapidly without the need to include them in the calculations.

The minimization of the total energy of the thin film-substrate system provides the three equations for k_1, k_2, A_0, i.e.

$$\frac{\partial U_{\text{total}}}{\partial A_0} = 0 \tag{3.20}$$

$$\frac{\partial U_{\text{total}}}{\partial k_1} = 0 \tag{3.21}$$

$$\frac{\partial U_{\text{total}}}{\partial k_2} = 0 \tag{3.22}$$

where the non-dimensional parameters are given as:

$$\xi_0 = \frac{A_0}{t_f}, \quad \xi_1 = k_1\,t_f, \quad \xi_2 = k_2\,t_f, \quad \xi_R = \frac{t_f}{R} \tag{3.23}$$

It can be easily verified that the special case where $\xi_R = 0$ regenerates the system of equations for the flat case. Eqs.(3.20)-(3.22) form a highly nonlinear system of ξ_0, ξ_1, ξ_2 which does not admit an analytical solution. However,

it can be solved numerically. In doing so, Eq.(3.20) is solved with respect to ξ_0 and then it is substituted into Eqs.(3.21),(3.22). Thus, the resulting equations include only the two remaining unknowns, i.e ξ_1, ξ_2 in the form:

$$f_A\left(\xi_1, \xi_2; \frac{\bar{E}_s}{\bar{E}_f}, \nu_s, \nu_f, \varepsilon^0_{xx}, \varepsilon^0_{yy}, \xi_R\right) = 0 \tag{3.24}$$

$$f_B\left(\xi_1, \xi_2; \frac{\bar{E}_s}{\bar{E}_f}, \nu_s, \nu_f, \varepsilon^0_{xx}, \varepsilon^0_{yy}, \xi_R\right) = 0 \tag{3.25}$$

The above equations are plotted in Figs.3-5 for various values of the curvature of the bilayer. Once the values of ξ_1, ξ_2 are determined from the above set of equations then the wrinkling amplitude ξ_0 can be readily calculated from Eq.(3.20) by back substitution ending up in an expression of the form:

$$\xi_0 = f_c\left(\frac{\bar{E}_s}{\bar{E}_f}, \nu_s, \nu_f, \varepsilon^0_{xx}, \varepsilon^0_{yy}, \xi_R\right) \tag{3.26}$$

The variation of the amplitude in the non-dimensional form ξ_0 for different values of the curvature is depicted on Fig.7.

4. Hexagonal mode

In this section the hexagonal wrinkling mode is examined. Following the methodology of Section 3, the flat bilayer is analysed by calculating the displacement components of the thin film and the semi-infinite substrate. The results are then used as a perturbation basis in the study of the curved bilayer.

4.1. Flat film

The displacement field of the flat film in the $z-$ direction is assumed to be (Zhao *et al*, 2020):

$$w\left(x, y\right) = A_0\, \cos\left(k\, x\right) + B_0\, \cos\left(\frac{k\, x}{2}\right)\, \cos\left(\frac{\eta\, k\, y}{2}\right) \tag{4.1}$$

Feeding the above expression for $w(x,y)$ into equilibrium equations Eqs.$(2.13)^{\mathrm{I}}$, $(2.14)^{\mathrm{I}}$, considering $R \to \infty$, and solving the resulting system of equations, we obtain analytical expressions for the in-plane displacements of the the flat film as:

$$u^{\mathrm{flat}}_{f,\mathrm{hex}}(x,y) = \frac{k}{32}\Bigg\{ B_0^2\Big[\cos(\eta\, k\, y) + 1 - \nu_f\, \eta^2\Big]\, \sin(k\, x) + 4\, A_0^2\, \sin(2\, k\, x)$$
$$+16\, A_0\, B_0\, \cos\left(\frac{\eta\, k\, y}{2}\right)\left[\frac{\eta^4 - 2\,(1+\nu_f)\,\eta^2 - 1}{(\eta^2+1)^2}\, \sin\left(\frac{k\, x}{2}\right)\right.$$
$$\left. + \frac{\eta^4 + 6\,(1-\nu_f)\,\eta^2 + 27}{(\eta^2+9)^2}\, \sin\left(\frac{3\, k\, x}{2}\right)\right]\Bigg\} \tag{4.2}$$

$$v^{\mathrm{flat}}_{f,\mathrm{hex}}(x,y) = B_0^2\, k\, \frac{\Big[1+\cos(k\, x)\Big]\eta^2 - \nu_f}{32\,\eta}\, \sin(\eta\, k\, y)$$
$$+ A_0\, B_0\, \eta\, k\left[\frac{(1-\nu_f\,\eta^2)}{(\eta^2+1)^2}\, \cos\left(\frac{k\, x}{2}\right) + \frac{(9-\nu_f\,\eta^2)}{(\eta^2+9)^2}\, \cos\left(\frac{3\, k\, x}{2}\right)\right]\, \sin\left(\frac{\eta\, k\, y}{2}\right) \tag{4.3}$$

The bending energy of the film for the hexagonal wrinkling mode over one period, in view of Eq.$(2.17)^{\mathrm{I}}$, is calculated as:

$$U^{\mathrm{flat}}_{b(f),\mathrm{hex}} = \bar{E}_f\, t_f^3\, k^4\left[\frac{A_0^2}{48} + \frac{B_0^2\,(1+\eta^2)^2}{1536}\right] \tag{4.4}$$

The membrane energy of the thin film, over one period, is calculated through Eq.$(2.18)^{\mathrm{I}}$ as:

$$U^{\mathrm{flat}}_{m(f),\mathrm{hex}} = \frac{\bar{E}_f\, t_f}{32}\Bigg\{ (A_0\, k)^4 + 8\,(A_0\, k)^2\left(\varepsilon^0_{xx} + \nu_f\, \varepsilon^0_{yy}\right) + 16\left[\left(\varepsilon^0_{xx}\right)^2 + 2\,\nu_f\, \varepsilon^0_{xx}\, \varepsilon^0_{yy} + \left(\varepsilon^0_{yy}\right)^2\right]$$
$$+ (A_0\, k)^2\, (B_0\, k)^2\left[\left(\nu_f^2 - 1\right)\left[\frac{9\,(2\,\eta^2+9)}{(\eta^2+9)^2} + \frac{(2\,\eta^2+1)}{(\eta^2+1)^2}\right] + \frac{1}{4}\left[\nu_f\left(\eta^2 - 8\,\nu_f\right) + 9\right]\right]$$

$$+\frac{(B_0\,k)^4}{128}\Big[\left(3-\nu_f^2\right)\left(\eta^4+1\right)+4\,\eta^2\,\nu_f\Big]+(B_0\,k)^2\left[\varepsilon^0_{xx}+\eta^2\left(\varepsilon^0_{yy}+\nu_f\,\varepsilon^0_{xx}\right)+\nu_f\,\varepsilon^0_{yy}\right]\Bigg\} \tag{4.5}$$

4.2. Flat substrate

The displacement components of the substrate are assumed to have the form:

$$u^{\text{flat}}_{s,\text{hex}}(x,y,z)=q_1(z)\,\sin\left(k\,x\right)+q_2(z)\,\sin\left(\frac{k\,x}{2}\right)\,\cos\left(\frac{k\,y\,\eta}{2}\right) \tag{4.6}$$

$$v^{\text{flat}}_{s,\text{hex}}(x,y,z)=q_3(z)\,\cos\left(\frac{k\,x}{2}\right)\,\sin\left(\frac{k\,y\,\eta}{2}\right) \tag{4.7}$$

$$w^{\text{flat}}_{s,\text{hex}}(x,y,z)=q_4(z)\,\cos\left(k\,x\right)+q_5(z)\,\cos\left(\frac{k\,x}{2}\right)\,\cos\left(\frac{k\,y\,\eta}{2}\right) \tag{4.8}$$

where $q_1(z), q_2(z), q_3(z), q_4(z), q_5(z)$ are functions of the depth coordinate z of the substrate which after substitution of the above expressions in the equilibrium equations, Eqs.$(2.22)^{\text{I}}$ - $(2.24)^{\text{I}}$, can be calculated analytically. Finally, the analytical expressions of the displacement components of the the flat substrate take the form:

$$u^{\text{flat}}_{s,\text{hex}}(x,y,z)=\frac{1}{4\,(1-\nu_s)}\Bigg\{2\,(1-2\,\nu_s+k\,z)\;A_0\,e^{k\,z}\sin(k\,x)$$
$$+\frac{2\,(1-2\,\nu_s)+k\,\sqrt{\eta^2+1}\,z}{\sqrt{\eta^2+1}}\,B_0\,e^{m\,z}\,\sin\left(\frac{k\,x}{2}\right)\,\cos\left(\frac{\eta\,k\,y}{2}\right)\Bigg\} \tag{4.9}$$

$$v^{\text{flat}}_{s,\text{hex}}(x,y,z)=\frac{2\,(1-2\,\nu_s)+k\,\sqrt{\eta^2+1}\,z}{4\,(1-\nu_s)\,\sqrt{\eta^2+1}}\,B_0\,\eta\;e^{m\,z}\,\cos\left(\frac{k\,x}{2}\right)\,\sin\left(\frac{\eta\,k\,y}{2}\right) \tag{4.10}$$

$$w^{\text{flat}}_{s,\text{hex}}(x,y,z) = \left[\frac{k\,z}{2\,(\nu_s-1)}+1\right] A_0\, e^{k\,z}\cos(k\,x) + \left[\frac{k\,\sqrt{\eta^2+1}\,z}{4\,(\nu_s-1)}+1\right] B_0\, e^{m\,z}\,\cos\left(\frac{k\,x}{2}\right)\cos\left(\frac{\eta\,k\,y}{2}\right) \tag{4.11}$$

where $m = \left(k\,\sqrt{1+\eta^2}\right)/2$. The strain energy of the substrate, over one period, is calculated as:

$$U^{\text{flat}}_{s,\text{hex}} = \frac{\bar{E}_s\,k}{8}\left[A_0^2 + B_0^2\,\frac{\sqrt{1+\eta^2}}{4}\right] \tag{4.12}$$

Minimization of the total energy of the bilayer system, $U^{\text{flat}}_{\text{tot,hex}} = U^{\text{flat}}_{b(f),\text{hex}} + U^{\text{flat}}_{m(f),\text{hex}} + U^{\text{flat}}_{s,\text{hex}}$, with respect to the amplitudes A_0, B_0 and the wavenumbers k, η provides:

$$\frac{\partial U^{\text{flat}}_{\text{tot,hex}}}{\partial A_0} = 0 \tag{4.13}$$

$$\frac{\partial U^{\text{flat}}_{\text{tot,hex}}}{\partial B_0} = 0 \tag{4.14}$$

$$\frac{\partial U^{\text{flat}}_{\text{tot,hex}}}{\partial k} = 0 \tag{4.15}$$

$$\frac{\partial U^{\text{flat}}_{\text{tot,hex}}}{\partial \eta} = 0 \tag{4.16}$$

where the non-dimensional parameters are defined as:

$$\xi_k = k\,t_f, \quad \xi_R = \frac{t_f}{R}, \quad \xi_A = \frac{A_0}{t_f}, \quad \xi_B = \frac{B_0}{t_f} \tag{4.17}$$

Multiplying Eq.(4.13) by $\partial\mathcal{F}_2(\eta)/\partial\eta$ and subtract the resulting equation from Eq.(4.16) we obtain:

$$\xi_B^2 = \frac{1}{6\,\xi_k^3\Big[\mathcal{F}_2(\eta)\,\mathcal{F}_2'(\eta) - 2\,\mathcal{F}_1'(\eta)\Big]}\Bigg\{ -4\,\mathcal{F}_2'(\eta)\left[6\,\frac{\bar{E}_s}{\bar{E}_f} + 12\,\xi_k\left(\varepsilon^0_{xx} + \nu_f\,\varepsilon^0_{yy}\right) + \xi_k^3\right] + \eta\left[\frac{12}{\sqrt{\eta^2+1}}\frac{\bar{E}_s}{\bar{E}_f} + 24\,\xi_k\left(\nu_f\,\varepsilon^0_{xx} + \varepsilon^0_{yy}\right) + \left(\eta^2+1\right)\xi_k^3\right]\Bigg\} \tag{4.18}$$

where

$$\mathcal{F}_1(\eta) = \frac{1}{128}\Big[\left(\eta^4+1\right)\left(3-\nu_f^2\right)+4\,\eta^2\,\nu_f\Big]$$
$$\mathcal{F}_2(\eta) = \left[\frac{2\,\eta^2+1}{\left(\eta^2+1\right)^2}+\frac{9\,(2\,\eta^2+9)}{\left(\eta^2+9\right)^2}\right]\left(\nu_f^2-1\right)+\frac{1}{4}\Big[\nu_f\left(\eta^2-8\,\nu_f\right)+9\Big] \quad (4.19)$$
$$\frac{\partial \mathcal{F}_1(\eta)}{\partial \eta} = \mathcal{F}_1'(\eta),\ \ \frac{\partial \mathcal{F}_2(\eta)}{\partial \eta} = \mathcal{F}_2'(\eta)$$

Solving Eq.(4.13) with respect to ξ_A^2 provides:

$$\xi_A^2 = -\frac{2}{\xi_k^3}\left[\frac{\bar{E}_s}{\bar{E}_f}+2\,\xi_k\left(\varepsilon_{xx}^0+\nu_f\,\varepsilon_{yy}^0\right)\right]-\frac{1}{2}\,\xi_B^2\,\mathcal{F}_2(\eta)-\frac{1}{3} \quad (4.20)$$

Note again that the applied load is compressive, i.e. $\varepsilon_{xx}^0, \varepsilon_{yy}^0 < 0$. Plugging the above expressions for ξ_A, ξ_B into Eqs.(4.15),(4.16) we end up with two equations with respect to ξ_k, η, i.e.

$$G_A\left(\xi_k, \eta; \frac{\bar{E}_s}{\bar{E}_f}, \nu_s, \nu_f, \varepsilon_{xx}^0, \varepsilon_{yy}^0, \xi_R\right) = 0 \quad (4.21)$$

$$G_B\left(\xi_k, \eta; \frac{\bar{E}_s}{\bar{E}_f}, \nu_s, \nu_f, \varepsilon_{xx}^0, \varepsilon_{yy}^0, \xi_R\right) = 0 \quad (4.22)$$

The above system of highly non-linear equations in terms of ξ_k, η, does not admit an analytical solution in terms of ξ_k, η, however it can be solved numerically. The results are presented in Figs. $9(d)$,$11(d)$. Once the wavenumbers are specified then the amplitudes ξ_A, ξ_B are calculated through Eqs.(4.18), (4.20) and the associated numerical results for a range of concve and convex bilayers are shown in Figs.10,13.

4.3. Curved substrate

The wavelength of the wrinkling is much smaller than the radius of the curvature and the ratio $\delta = 1/k\,R\sqrt{(1+\eta^2)}$ is considered to be a small

enough quantity. Therefore, the displacement components of the substrate can be expanded as a power series of this small quantity as:

$$u_s\left(x,y,z\right)=A_0\Big[u_s^{(0)}(x,y,z)+\delta\,u_s^{(1)}(x,y,z)+\delta^2\,u_s^{(2)}(x,y,z)+...\Big] \quad (4.23)$$

$$v_s\left(x,y,z\right)=A_0\Big[v_s^{(0)}(x,y,z)+\delta\,v_s^{(1)}(x,y,z)+\delta^2\,v_s^{(2)}(x,y,z)+...\Big] \quad (4.24)$$

$$w_s\left(x,y,z\right)=A_0\Big[w_s^{(0)}(x,y,z)+\delta\,w_s^{(1)}(x,y,z)+\delta^2\,w_s^{(2)}(x,y,z)+...\Big] \quad (4.25)$$

where $u_s^{(0)}(x,y,z)=u_{s,\mathrm{hex}}^{\mathrm{flat}}(x,y,z)/A_0, v_s^{(0)}(x,y,z)=v_{s,\mathrm{hex}}^{\mathrm{flat}}(x,y,z)/A_0, w_s^{(0)}(x,y,z)=w_{s,\mathrm{hex}}^{\mathrm{flat}}(x,y,z)/A_0$ and $u_s^{(i)},v_s^{(i)},w_s^{(i)},i=1,2,...$ are non-dimensional coefficients determined through the perturbation method as:

$$u_s^{(1)}(x,y,z)=\frac{1}{4\left(1-\nu_s\right)\left(1-2\,\nu_s\right)\,k}\Bigg\{\left(\mathcal{B}_3+\mathcal{B}_4\,k\,z\right)k\,e^{k\,z}\,\sin\left(k\,x\right) + \frac{B_0\,k}{A_0}\left(\mathcal{B}_1+\mathcal{B}_2\,k\,z\right)e^{m\,z}\,\sin\left(\frac{k\,x}{2}\right)\,\cos\left(\frac{k\,y\,\eta}{2}\right)\Bigg\} \quad (4.26)$$

$$u_s^{(2)}(x,y,z)=\frac{1}{\left(1-2\,\nu_s\right)^2\left(\nu_s-1\right)^2}\Bigg\{\left(\mathcal{B}_{13}+\mathcal{B}_{14}\,k\,z\right)\,e^{k\,z}\sin\left(k\,x\right) + \left(\mathcal{B}_{11}+\mathcal{B}_{12}\,k\,z\right)\,\frac{B_0}{4\,A_0}\,e^{m\,z}\,\sin\left(\frac{k\,x}{2}\right)\,\cos\left(\frac{k\,y\,\eta}{2}\right)\Bigg\} \quad (4.27)$$

$$v_s^{(1)}(x,y,z)=\frac{\mathcal{B}_5+\mathcal{B}_6\,k\,z}{4\left(1-\nu_s\right)\left(1-2\,\nu_s\right)}\,\eta\,\frac{B_0}{A_0}\,e^{m\,z}\,\cos\left(\frac{k\,x}{2}\right)\,\sin\left(\frac{k\,y\,\eta}{2}\right) \quad (4.28)$$

$$v_s^{(2)}(x,y,z)=\frac{\mathcal{B}_{15}+\mathcal{B}_{16}\,k\,z}{4\left(1-\nu_s\right)^2\left(1-2\,\nu_s\right)^2}\,\eta\,\frac{B_0}{A_0}\,e^{m\,z}\,\cos\left(\frac{k\,x}{2}\right)\,\sin\left(\frac{k\,y\,\eta}{2}\right) \quad (4.29)$$

$$w_s^{(1)}(x,y,z) = \frac{\mathcal{B}_7 + \mathcal{B}_8\, k\, z}{4\left(1-\nu_s\right)^2}\frac{B_0}{A_0}\, e^{m\, z}\, \cos\left(\frac{k\, x}{2}\right)\, \cos\left(\frac{k\, y\, \eta}{2}\right) + \frac{\mathcal{B}_9 + \mathcal{B}_{10}\, k\, z}{4\left(1-\nu_s\right)^2}\, e^{kz}\cos\left(k\, x\right) \tag{4.30}$$

$$w_s^{(2)}(x,y,z) = \frac{\mathcal{B}_{17} + \mathcal{B}_{18}\, k\, z}{4\left(\nu_s-1\right)^3\left(2\,\nu_s-1\right)}\frac{B_0}{A_0}\, e^{m\, z}\, \cos\left(\frac{k\, x}{2}\right)\, \cos\left(\frac{k\, y\, \eta}{2}\right) \tag{4.31}$$

where

$$\mathcal{B}_i = \mathcal{B}_i\left(k,\, \eta,\, R,\, \nu_s\right), \quad i = 1, 2, ...18, \tag{4.32}$$

are non-dimensional parameters and their analytical expressions are provided in Supporting Information (SI) by Eqs. (B.1)-(B.18).

The energy of the curved substrate is calculated as:

$$U_{s,\mathrm{hex}}^{\mathrm{curved}} = \bar{E}_s\, t_f\left(\xi_A^2\, \mathcal{G}_1 + \xi_B^2\, \mathcal{G}_2\right) \tag{4.33}$$

where

$$\mathcal{G}_i = \mathcal{G}_i\left(\xi_k, \eta, \nu_s, \xi_R\right), \quad i = 1, 2, \tag{4.34}$$

with

$$\begin{aligned}\mathcal{G}_1 = \frac{1}{8\left(\eta^2+1\right)^2\xi_k^5}\Bigg[&\left(\eta^2+1\right)\xi_k^5\,\xi_R\left[\beta_1\left(\eta^2+1\right)+2\sqrt{\eta^2+1}\right]\\ &+\xi_k\,\xi_R^5\left[\beta_{11}+\beta_{12}\,\eta^2+\beta_{13}\sqrt{\eta^2+1}\right]\\ &+\xi_k^2\,\xi_R^4\left[\sqrt{\eta^2+1}\left(\beta_{10}\,\eta^2+\beta_9\right)+\beta_7+\beta_8\,\eta^2\right]\\ &+\xi_k^3\,\xi_R^3\left[\beta_4\left(\eta^2+1\right)+\sqrt{\eta^2+1}\left(\beta_5\,\eta^2+\beta_6\right)\right]\end{aligned}$$

$$+\left(\eta^2+1\right)\xi_k^4\,\xi_R^2\left[\beta_2\sqrt{\eta^2+1}+\beta_3\left(\eta^2+1\right)+3\right]$$

$$+\xi_R^6\left(\beta_{14}+\beta_{15}\,\eta^2+\beta_{16}\sqrt{\eta^2+1}\right)+\left(\eta^2+1\right)^2\,\xi_k^6\Bigg] \tag{4.35}$$

and

$$\mathcal{G}_2=\frac{1}{32\left(\eta^2+1\right)^{11/2}\xi_k^5}\Bigg[4\left(\eta^2+1\right)^{9/2}\xi_k^5\,\xi_R\left[\beta_{17}\left(\eta^2+1\right)+\beta_{18}\right]$$

$$+4\left(\eta^2+1\right)^4\xi_k^4\,\xi_R^2\left(\beta_{19}+\beta_{20}\eta^2\right)$$

$$+\left(\eta^2+1\right)^6\xi_k^6+4\left(\eta^2+1\right)^{5/2}\xi_k^3\,\xi_R^3\left(\beta_{21}+\beta_{22}\eta^2+\beta_{23}\eta^4\right)$$

$$+4\left(\eta^2+1\right)^2\xi_k^2\,\xi_R^4\left(\beta_{24}+\beta_{25}\eta^2+\beta_{26}\eta^4\right)$$

$$+4\left(\eta^2+1\right)^{3/2}\xi_k\,\xi_R^5\left(\beta_{27}+\beta_{28}\eta^2+\beta_{29}\eta^4\right)$$

$$+4\,\xi_R^6\left(\beta_{30}+\beta_{31}\eta^2+\beta_{32}\eta^4+\beta_{33}\eta^6\right)\Bigg] \tag{4.36}$$

In the above expressions of $\mathcal{G}_1,\mathcal{G}_2$ the variables $\beta_i=\beta_i\left(\nu_s\right),\ i=1.2,...33$, are functions of substrate's Poisson ratio only and their analytical expressions are provided in Eqs.(B.19)-(B.22) in Supporting Information (SI). Note that for $\xi_R\to 0$ the energy of the flat substrate as given in Eq.(4.12) is recovered.

4.4. Curved film

Feeding the expression of $w(x,y)$ from Eq.(4.1) into equilibrium equations Eqs.$(2.13)^{\mathrm{I}}$, $(2.14)^{\mathrm{I}}$ and solving the resulting system of equations we obtain:

$$u_{f,\mathrm{hex}}^{\mathrm{curved}}(x,y,z)=\left\{-\frac{A_0\,\nu_f}{k\,R}+\frac{B_0^2\,k}{32}\Big[\cos\left(k\,y\,\eta\right)+1-\eta^2\,\nu_f\Big]\right\}\sin(k\,x)$$

$$+\frac{B_0}{2\,k}\left\{\left[\frac{4\left(\eta^2-\nu_f\right)}{\left(\eta^2+1\right)^2\,R}+\frac{A_0\,k^2\left[\eta^4-1-2\,\eta^2\left(\nu_f+1\right)\right]}{\left(\eta^2+1\right)^2}\right]\sin\left(\frac{k\,x}{2}\right)\right.$$
$$\left.+A_0\,k^2\,\frac{\left[\eta^4-6\,\eta^2\left(\nu_f-1\right)+27\right]}{\left(\eta^2+9\right)^2}\,\sin\left(\frac{3\,k\,x}{2}\right)\right\}\cos\left(\frac{k\,y\,\eta}{2}\right)+\frac{1}{8}\,A_0^2\,k\,\sin(2\,k\,x) \tag{4.37}$$

$$v_{f,\mathrm{hex}}^{\mathrm{curved}}(x,y,z)=B_0^2\,k\,\frac{\eta^2\left[1+\cos(k\,x)\right]-\nu_f}{32\,\eta}\,\sin\left(k\,y\,\eta\right)$$
$$+\,B_0\,\eta\left[\frac{A_0\,k\left(9-\eta^2\,\nu_f\right)}{\left(\eta^2+9\right)^2}\cos\left(\frac{3\,k\,x}{2}\right)\right.$$
$$\left.+\,\frac{\left[A_0\,k\left(1-\eta^2\,\nu_f\right)-\frac{2\left(\eta^2+\nu_f+2\right)}{k\,R}\right]}{\left(\eta^2+1\right)^2}\cos\left(\frac{k\,x}{2}\right)\right]\sin\left(\frac{k\,y\,\eta}{2}\right) \tag{4.38}$$

The bending energy of the curved film for the hexagonal wrinkling mode over one period, in view of Eq.(2.17)[I], is calculated as:

$$U_{b(f),\mathrm{hex}}^{\mathrm{curved}}=\bar{E}_f\,t_f\left[\xi_A^2\,\mathcal{G}_3+\xi_B^2\,\mathcal{G}_4\right] \tag{4.39}$$

where

$$\mathcal{G}_3=\frac{\xi_k^4}{48},\quad \mathcal{G}_4=\frac{\left(\eta^2+1\right)^2\xi_k^4}{1536} \tag{4.40}$$

Eq.(4.39) reveals that the bending energy in the curved film is the same with the bending energy provided in Eq.(4.4), as expected, because there is no direct involvement of the curvature in the displacement component $w(x,y,z)$. For the special case where $B_0=0$ the energy of the 1D bilayer is retrieved, (Kordolemis and Giannakopoulos, 2024). The membrane energy is

calculated over a period through Eq.(2.18)$^{\mathrm{I}}$ as:

$$U^{\text{curved}}_{m(f),\text{hex}} = \bar{E}_f\, t_f \Bigg[\xi_B^2 \left[\mathcal{G}_{12} + \xi_B^2\, \mathcal{G}_6 + \xi_A \left(\xi_A\, \mathcal{G}_7 + \mathcal{G}_8 \right) \right] + \mathcal{G}_9 \left[\left(\varepsilon^0_{xx} \right)^2 + \left(\varepsilon^0_{yy} \right)^2 + 2\, \nu_f\ \varepsilon^0_{xx}\, \varepsilon^0_{yy} \right] + \xi_A^2\, \mathcal{G}_{11} + \xi_A^4\, \mathcal{G}_5 \Bigg] \tag{4.41}$$

where

$$\begin{aligned}
\mathcal{G}_5 &= \frac{\xi_k^4}{32} \\
\mathcal{G}_6 &= -\frac{\eta^4 \left(\nu_f^2 - 3 \right) - 4\, \eta^2\, \nu_f + \nu_f^2 - 3}{4096}\, \xi_k^4 \\
\mathcal{G}_7 &= \frac{\xi_k^4}{32} \left\{ \left[\frac{2\, \eta^2 + 1}{\left(\eta^2 + 1 \right)^2} + \frac{9 \left(2\, \eta^2 + 9 \right)}{\left(\eta^2 + 9 \right)^2} \right] \left(\nu_f^2 - 1 \right) + \frac{1}{4} \left[\nu_f \left(\eta^2 - 8\, \nu_f \right) + 9 \right] \right\} \\
\mathcal{G}_8 &= \frac{\eta^2}{32} \left[\frac{4}{\left(\eta^2 + 1 \right)^2} + \frac{1}{2} \right] \left(1 - \nu_f^2 \right)\, \xi_k^2\, \xi_R \\
\mathcal{G}_9 &= \frac{1}{2} \\
\mathcal{G}_{10} &= \mathcal{G}_{11}\, \xi_A^2 + \mathcal{G}_{12}\, \xi_B^2 \\
\mathcal{G}_{11} &= \frac{1}{4} \left[\xi_k^2 \left(\varepsilon^0_{xx} + \nu_f\, \varepsilon^0_{yy} \right) - \left(\nu_f^2 - 1 \right) \xi_R^2 \right] \\
\mathcal{G}_{12} &= \frac{1}{32} \left[\xi_k^2 \left[\varepsilon^0_{xx} \left(\eta^2\, \nu_f + 1 \right) + \varepsilon^0_{yy} \left(\eta^2 + \nu_f \right) \right] - \frac{4 \left(\nu_f^2 - 1 \right)}{\left(\eta^2 + 1 \right)^2}\, \xi_R^2 \right]
\end{aligned} \tag{4.42}$$

Minimization of the total energy, $U^{\text{curved}}_{\text{tot,hex}} = U^{\text{curved}}_{b(f),\text{hex}} + U^{\text{curved}}_{m(f),\text{hex}} + U^{\text{curved}}_{s,\text{hex}}$, of the bilayer with respect to the wavenumbers k, η and the two amplitudes A_0, B_0, which is equivalent to minimizing with respect to the non-dimensional counterparts $\xi_A, \xi_B, \xi_k, \eta$, provides:

$$\frac{\partial U^{\text{curved}}_{\text{tot,hex}}}{\partial \xi_A} = 2\, \xi_A \left(\frac{\bar{E}_s}{\bar{E}_f}\, \mathcal{G}_1 + \xi_B^2\, \mathcal{G}_7 + \mathcal{G}_{11} + \mathcal{G}_3 + 2\, \xi_A^2\, \mathcal{G}_5 \right) + \xi_B^2\, \mathcal{G}_8 = 0 \tag{4.43}$$

$$\frac{\partial U^{\text{curved}}_{\text{tot,hex}}}{\partial \xi_B} = \frac{\bar{E}_s}{\bar{E}_f}\,\mathcal{G}_2 + \mathcal{G}_{12} + \mathcal{G}_4 + 2\,\xi_B^2\,\mathcal{G}_6 + \xi_A\,(\xi_A\,\mathcal{G}_7 + \mathcal{G}_8) = 0 \tag{4.44}$$

$$\begin{aligned}\frac{\partial U^{\text{curved}}_{\text{tot,hex}}}{\partial \xi_k} = {} & \frac{\bar{E}_s}{\bar{E}_f}\left(\xi_A^2\,\mathcal{G}_{1,\xi_k} + \xi_B^2\,\mathcal{G}_{2,\xi_k}\right) + \xi_A^2\left(\mathcal{G}_{11,\xi_k} + \mathcal{G}_{3,\xi_k} + \xi_A^2\,\mathcal{G}_{5,\xi_k}\right) \\ & + \xi_B^2\left[\mathcal{G}_{4,\xi_k} + \mathcal{G}_{12,\xi_k} + \xi_B^2\,\mathcal{G}_{6,\xi_k} + \xi_A\,(\xi_A\,\mathcal{G}_{7,\xi_k} + \mathcal{G}_{8,\xi_k})\right] = 0\end{aligned} \tag{4.45}$$

$$\begin{aligned}\frac{\partial U^{\text{curved}}_{\text{tot,hex}}}{\partial \eta} = {} & \xi_B^2\left[\frac{\bar{E}_s}{\bar{E}_f}\,\mathcal{G}_{2,\eta} + \mathcal{G}_{12,\eta} + \mathcal{G}_{4,\eta} + \xi_B^2\,\mathcal{G}_{6,\eta} + \xi_A\,(\xi_A\,\mathcal{G}_{7,\eta} + \mathcal{G}_{8,\eta})\right] \\ & + \frac{\bar{E}_s}{\bar{E}_f}\,\xi_A^2\,\mathcal{G}_{1,\eta} = 0\end{aligned} \tag{4.46}$$

where the following notation has been adopted for differentiation:

$$(\ldots)_{,\xi_k} = \frac{\partial\,(\ldots)}{\partial \xi_k}, \quad (\ldots)_{,\eta} = \frac{\partial\,(\ldots)}{\partial \eta} \tag{4.47}$$

The above system of Eqs.(4.43)-(4.46) is highly non-linear in terms of $\xi_A, \xi_B, \xi_k, \eta$ and cannot be solved analytically. However, it can be solved numerically. In doing so, we solve Eq.(4.43) with respect to ξ_B^2 and we substitute the resulting expression to Eq.(4.44) to obtain:

$$\xi_B^2 = -\frac{1}{2\,\mathcal{G}_6}\left[\frac{\bar{E}_s}{\bar{E}_f}\,\mathcal{G}_2 + \mathcal{G}_{12} + \mathcal{G}_4 + \xi_A\,(\xi_A\,\mathcal{G}_7 + \mathcal{G}_8)\right] \tag{4.48}$$

$$\xi_A = \frac{3\,\mathcal{S}_1\,\mathcal{G}_7\,\mathcal{G}_8 + 3^{1/3}\,\mathcal{S}_1^2 - 3^{2/3}\,\mathcal{S}_2}{6\,\mathcal{S}_1\mathcal{P}_3} \tag{4.49}$$

where

$$\begin{aligned}\mathcal{S}_1 = {} & \left[36\,\mathcal{G}_6\,\mathcal{G}_8\left[\mathcal{P}_3\,(2\,\mathcal{P}_1\,\mathcal{G}_5 - \mathcal{P}_2\,\mathcal{G}_7) + \mathcal{P}_4\right]\right. \\ & \left. + \frac{1}{6}\sqrt{46656\,\mathcal{G}_6^2\,\mathcal{G}_8^2\left[\mathcal{P}_3\,(2\,\mathcal{P}_1\,\mathcal{G}_5 - \mathcal{P}_2\,\mathcal{G}_7) + \mathcal{P}_4\right]^2 + 4\left[6\,\mathcal{P}_3\,(4\,\mathcal{P}_2\,\mathcal{G}_6 - 2\,\mathcal{P}_1\,\mathcal{G}_7 - \mathcal{G}_8^2) - 9\,\mathcal{G}_7^2\,\mathcal{G}_8^2\right]^3}\right]^{1/3}\end{aligned} \tag{4.50}$$

$$\mathcal{S}_2 = 4\left(4\,\mathcal{G}_5\,\mathcal{G}_6 - \mathcal{G}_7^2\right)\left[2\,\mathcal{G}_6\left(\frac{\bar{E}_s}{\bar{E}_f}\,\mathcal{G}_1 + \mathcal{G}_{11} + \mathcal{G}_3\right) - \mathcal{G}_7\left(\frac{\bar{E}_s}{\bar{E}_f}\,\mathcal{G}_2 + \mathcal{G}_{12} + \mathcal{G}_4\right)\right] - \mathcal{G}_8^2\left(8\,\mathcal{G}_5\,\mathcal{G}_6 + \mathcal{G}_7^2\right) \tag{4.51}$$

with

$$\mathcal{P}_1 = \frac{\bar{E}_s}{\bar{E}_f}\,\mathcal{G}_2 + \mathcal{G}_{12} + \mathcal{G}_4, \quad \mathcal{P}_2 = \frac{\bar{E}_s}{\bar{E}_f}\,\mathcal{G}_1 + \mathcal{G}_{11} + \mathcal{G}_3,$$
$$\mathcal{P}_3 = 4\,\mathcal{G}_5\,\mathcal{G}_6 - \mathcal{G}_7^2, \quad \mathcal{P}_4 = \mathcal{G}_5\,\mathcal{G}_7\,\mathcal{G}_8^2 \tag{4.52}$$

Note that the amplitudes ξ_A, ξ_B given in Eqs.(4.48),(4.49) respectively, are functions of the wavenumbers ξ_k, η only. Thus, plugging these expressions back to Eqs.(4.45),(4.46) we end up with two equations with the only unknowns the wavenumbers ξ_k, η, i.e.:

$$G_C\left(\xi_k, \eta; \frac{\bar{E}_s}{\bar{E}_f}, \nu_s, \nu_f, \varepsilon^0_{xx}, \varepsilon^0_{yy}, \xi_R\right) = 0 \tag{4.53}$$

$$G_D\left(\xi_k, \eta; \frac{\bar{E}_s}{\bar{E}_f}, \nu_s, \nu_f, \varepsilon^0_{xx}, \varepsilon^0_{yy}, \xi_R\right) = 0 \tag{4.54}$$

The above system of equations is highly non-linear in ξ_k, η and can be solved numerically. The solutions for various values of the curvature are shown in Figs.12,14. After the specification of the wavenumbers ξ_k, η the calculation of the amplitudes ξ_A, ξ_B is straightforward, as shown in Figs.13,15.

5. Results and discussion

In this section numerical results regarding the three geometrical variables of the checkerboard wrinkling mode, i.e. $\xi_1, \xi_2\,\xi_0$, and the four geometrical parameters of the hexagonal wrinkling mode, i.e.$\xi_k, \eta\,\xi_A, \xi_B$, for the

film/substrate system are presented. Specific attention is paid on the dependence of those variables to the magnitude of the curvature, (ξ_R), while conclusions are drawn regarding the convexity, $\xi_R > 0$, and concavity, $\xi_R < 0$, of the bilayer. Therefore, the dependency of the wrinkling modes' characteristics on Poisson's ratios is not presented explicitly in the following discussion but the interested reader can readily extract it from the analytical set up of the equations. For the numerical analysis the thin film is assumed to be made from silicon, (Si), while the substrate is made by polydimethylsiloxane (PDMS). The mechanical properties of these two materials are well documented in experimental studies, (Bietsch and Michel, 2000) and the numerical values used in our analysis, along with the film thickness t_f, are presented in Table.3. Note that the reduced moduli for the film and the substrate are calculated as: $\bar{E}_f = E_f/\left(1-\nu_f^2\right)$ and $\bar{E}_s = E_f/\left(1-\nu_s^2\right)$, respectively.

In Figs.3-5 the graphical specification of the wavelengths ξ_1, ξ_2 for the checkerboard wrinkling mode for various magnitudes of concave bilayers $(\xi_R > 0)$ is presented. Similar plots can be extracted for convex bilayers as well and the differences in the critical compressive strain are shown in Table. 4. The red lines denote the solution, i.e. the pairs of ξ_1, ξ_2, that satisfy Eq.(3.24), while the black lines denote the solution of Eq.(3.25). Solid, dashed and dashed-dot lines are referring to different levels of biaxially strain loading. The intersection points of the two curve sets, are unique for a predefined value of the biaxial strain and they are highlighted through a data tip label on each plot. As expected, the pair of the wavenumbers ξ_1, ξ_2 that satisfies simultaneously Eqs.(3.24),(3.25) is independent of the applied strain load $\varepsilon_{xx}^0, \varepsilon_{yy}^0$ in the two principal directions of the system x, y, respectively.

However, for the case of finite deformations it has been shown that there is a dependency between the wavenumbers and the applied strain, (Jiang *et al*, 2007).

The insets in Figs.3-5 denote the change of the wavelengths λ_1, λ_2 of the checkerboard mode with respect to the magnitude of the curvature. Upon the calculation of the wavenumbers, $\xi_1 \,(= k_1\, t_f)\,, \xi_2 \,(= k_2\, t_f)$, the corresponding wavelengths λ_1, λ_2 are calculated through $\lambda_i = 2\,\pi/k_i,\ i = 1, 2$. The insets are referring to the projected area of the bilayer in the xy plane and the dimensions are $\lambda_1 \times \lambda_2$ depicting one period of the checkerboard in both directions. Figs.3$(a) - (c)$ show the change of the wavelengths within the same projected area along one period due to the variation of the curvature. The flat bilayer acts as the baseline to demonstrate the role of the curvature in the change of the wavelengths. It can be seen that there is a significant decrease of both wavelengths due to the presence of the curvature. This observation is true not only for equibiaxial compressive strain of the bilayer, as shown in Figs.4 and 5, but in occasions where the biaxial strain loading is not symmetric in the two principal directions. In particular, comparing Fig.4(a) referring to concave bilayer with $\xi_R = 1/25$ there is a tenfold decrease of the wavenumbers of the checkerboard mode compared to the flat bilayer which indicates the curvature increases significantly the wrinkling waviness of the bilayer. Interestingly, despite the fact the strain is equibiaxial the decrease of the wavelength λ_2, along the $y-$ direction is higher compared to the decrease of wavelength λ_1, in the transverse $x-$ direction.

In Fig.6 the variation of the wavenumbers ξ_1, ξ_2 for various values of the moduli mismatch $\bar{E}_s/\bar{E}_f$ for the checkerboard mode is shown. For the

calculations the value of the compressive equibiaxial strain load was taken equal to 5% for illustrative reasons because as it was shown in Figs.3-5 the values of the wavenumbers are independent of the loading. As it can be seen, for both the flat and the curved bilayer (either concave or convex) the higher the value of the moduli mismatch the higher the corresponding wavenumbers ξ_1, ξ_2 and in turn the lower the associated wavelengths, λ_1, λ_2. Also, for relative high values of the moduli mismatch, i.e. $\bar{E}_s/\bar{E}_f = 1.5 \times 10^{-2}$ and above the wavenumbers ξ_1, ξ_2 seems to be almost equal to each other either the bilayer is curved or not.

The analysis shows that the wavelengths λ_1, λ_2 are equal to each other only in the case of the flat bilayer under equibiaxial compressive strain, as demonstrated in other studies (Song *et al*, 2008) . However, when the curvature comes in the analysis the wavelengths are no longer equal to each other even under equibiaxial strain loading conditions. Upon the calculation of the wavenumbers ξ_1, ξ_2 from Figs.3-5, their values are substituted back to Eq.(3.20) and a closed form expression for the wrinkling amplitude ξ_0 is obtained in the form of Eq.(3.26), as a function of the material properties of the bilayer and the curvature.

Fig.7 shows the variation of the wrinkling amplitude, ξ_0, against various values of the curvature of the bilayer for equibiaxial strain loading, Fig.7(a), and for strain loading ratios of 2 and 1/2 in the two principal directions, Figs. 7(b),(c) respectively. Fig.7(d) is referring to uniaxial compression along the $x-$ direction and the critical strain values on this plot are included in Table 5 where the results are compared with the findings of other studies. It can be seen that the magnitude of the curvature reduces significantly the wrinkling

amplitude with respect to the flat bilayer by a factor of 15 for $\xi_R = \pm 1/25$ compared to the flat bilayer for a strain loading up to 3%. The analysis shows that the convex bilayer ($\xi_R < 0$) is experiencing higher values in the amplitude ξ_0 compared to the concave bilayer within the range of $10\% - 14\%$ for $|\xi_R| = 1/25$ and $|\xi_R| = 1/100$, respectively. The intersection points of the curves with the horizontal axis of strain loading denote the critical values of strain load for different values of ξ_R. These values are presented explicitly in Table.4 for convex and concave bilayer. It can be easily verified that the non-dimensional wavelength ξ_0 for the flat bilayer under equibiaxial compressive strain can be calculated as a function of the critical load of the checkerboard mode through the simple closed form expression

$$\xi_0^{\text{flat}} = \sqrt{\frac{8}{(3-\nu_f)(1+\nu_f)}}\sqrt{\frac{\varepsilon_{yy}^0}{\varepsilon_{\text{critical}}} - 1} = 1.52\sqrt{\frac{\varepsilon_{yy}^0}{\varepsilon_{\text{critical}}} - 1}, \text{ for } \quad \nu_f = 0.27, \tag{5.1}$$

For the case of the curved bilayer under equibiaxial compressive strain the non-dimensional wrinkling amplitude can be calculated numerically through a similar expression:

$$\xi_0^{\text{R}} = 1.05\sqrt{\frac{\varepsilon_{yy}^0}{\varepsilon_{\text{critical}}} - 1}, \quad \text{for} \quad \left|\frac{1}{100}\right| \leq \xi_R \leq \left|\frac{1}{25}\right| \quad \text{and} \quad \nu_f = 0.27. \tag{5.2}$$

A direct comparison of Eqs.(5.1),(5.2) demonstrates that for the particular value of $\nu_f = 0.27$ there is a considerable decrease of 30% in the wrinkling amplitude for the specified range of the bilayer's curvature.

The variation of the ratio of the total energy in the buckled state, $U_{\text{tot}}^{\text{buck}}$ over the total energy in the unbuckled state, $U_{\text{tot}}^{\text{unbuck}} = \bar{E}_f\, t_f \left[(\varepsilon_{xx}^0)^2 + \nu_f\, (\varepsilon_{yy}^0)^2\right]$, is presented in Fig.8($a$). It is shown that the energy in the buckled state for

a curved substrate is considerably higher compared to the energy of the flat bilayer. Similar to the case of the wrinkling amplitude, the convexity of the system suggests a slight decrease of the energy in the buckled state compared to the energy of the concave layer. Fig.8(b) presents the variation of the three different components of the system, i.e. bending $U_{b(f)}$ and membrane $U_{m(f)}$ energy of the film and the energy of the substrate, U_s, for equibiaxial loading. For both cases of flat and curved bilayer it appears that the membrane energy of the thin film provides the higher contribution in the buckled state. For the flat bilayer the contribution of the substrate is higher compared to the bending energy of the film however this contribution reverses when the curvature is introduced. Furthermore, the convexity of the bilayer reduces slightly the membrane energy of the film and the energy of the substrate.

In Figs.9,11 the calculation of the wavenumbers ξ_k, η for the hexagonal wrinkling mode lines are presented for various values of the curvature for the case on convex ($\xi_R < 0$) and concave ($\xi_R > 0$) bilayers. The red and black lines in the figures correspond to the solutions of Eqs.(4.53), (4.54), respectively. The intersection points of the curves for different curvatures constitute the solution of the system of the two equations and are marked with a data tip label. Note that the marked values are independent of the equibiaxial strain which is kept within the theoretical small strain and moderate rotation elastic regime, i.e. $1-5\%$. Note that for the case of the flat bilayer more than one solution of the system has been found as denoted in Figs. 9(d),11(d), by the points a, b, c, d. From all these pairs the solution that minimises the total energy of the system is that at point a which essentially corresponds to, $\eta = \sqrt{3}$ and $\xi_k = \left(3\,\bar{E}_s/\bar{E}_f\right)^{1/3} = 0.0355$, in agreement with

what has been conjectured in other studies,(Cai *et al*, 2011).

Furthermore, Fig.10 reveals that for the flat bilayer the amplitude ξ_B is twice as much as the amplitude ξ_B, for convex bilayers. However, this analogy between the amplitudes breaks off for concave bilayers, as can be seen in Fig.13(b). It is noteworthy that the hexagonal mode is highly sensitive to the applied load, especially for the case of concave bilayers. Fig.13(a) demonstrates that the amplitude ξ_A becomes negative showing a preference of the film to buckle inward to the substrate. This conclusion verifies the experimental findings presented in other studies,(Cai *et al*, 2011).

The variation of the wavenumbers ξ_k, η for the hexagonal mode for various vlaues of the moduli mismatch $\bar{E}_s/\bar{E}_f$ is depicted in Fig.12. In particular, Figs.12(a), (b), show that for concave bilayers the value of the wavenumber η seems to be locked to 1.793 while the wavenumber in the transverse direction ξ_k is increasing along the value of the moduli mismatch. Fig.12(c) reveals a reversed pattern for concave bilayers because while η remains roughly unchanged for all curvatures, ξ_k is decreasing with increasing values of the moduli mismatch.

In Fig.14(a) the variation of the ratio of the total energy in the buckled state over the total energy in the unbuckled state is presented for the hexagonal mode. Note that for the case of the concave bilayer the onset of the wrinkling initiation is delayed significantly compared to that of a convex bilayer. Fig.14(b) shows the contribution of the film and substrate energies to the overall energy of the system. Fig.15 shows the variation of the ratio of the total energy in the buckled state over the energy on the unbuckled state for the cylindrical, squared checkerboard and the hexagonal wrinkling mode

for various convexities and concavities of the bilayer. It can be seen that the checkerboard mode is the most favourable due to the lowest energy followed by the hexagonal and the cylindrical modes respectively. The presence of the initial curvature in the bilayer does not alter the sequence of the buckling modes but translates the values of all the corresponding energies into higher levels, compared to the flat case denoted with solid lines, indicating a delay in the onset of wrinkling.

(Zhao *et al*, 2020) investigated the effects of surface curvature on the wrinkling pattern evolution in soft materials and they have shown that for the case of the square checkerboard mode the critical wavenumber and the accompanied critical strain may be calculated through the analytical expressions:

$$\xi_{2c} = 0, \quad \xi_{1c} = \phi\,\xi_1^0, \quad \text{with} \quad \xi_1^0 = \left(\frac{3\,\bar{E}_s}{\bar{E}_f}\right)^{1/3} \tag{5.3}$$

while the critical strain is provided as:

$$\varepsilon_{\text{critical}}^{\text{checkerboard}} = \frac{2\,\phi^2 + \phi^{-1}}{3}\,\varepsilon_c^0, \quad \text{with} \quad \varepsilon_c^0 = \frac{1}{4}\left(\frac{3\,\bar{E}_s}{\bar{E}_f}\right)^{2/3} \tag{5.4}$$

The parameter ϕ is determined by the equation

$$\phi^4 - \phi - 3\,\Omega_2^2 = 0 \tag{5.5}$$

where Ω_2 is dimensional curvature that determines the critical buckling of a sphere system and is provided by (Cai *et al*, 2011) as:

$$\Omega_2 = 2\sqrt{1-\nu_f^2}\,\xi_R\left(\frac{\bar{E}_f}{3\bar{E}_s}\right)^{2/3} \tag{5.6}$$

Table.5 shows that the critical strain of the checkerboard mode evaluated in the present study for various positive values of the curvature, see Fig.11(d),

is in a very good agreement with the critical strain values provided through Eq.(5.4).

In the post-bifurcation analysis, (Zhao *et al*, 2020), have shown that the sinusoidal mode evolves to the hexagonal mode if the modulus ratio reaches a critical value which is calculated numerically and verified experimentally for various curvatures. (Xu and Potier-Ferry, 2016) investigated the post-buckling behaviour of core-shell cylinders beyond the first bifurcation employing a 3D finite element model and provided a closed form expression for the transition from the sinusoidal to the hexagonal wrinkling mode as:

$$C_s = \frac{E_s}{E_f}\left(\frac{1}{\xi_R}\right)^{3/2} < 0.70 \tag{5.7}$$

for $C_s > 0.90$ the axisymmetric mode prevails while for values in between, i.e. $0.70 < C_s < 0.90$, the preferred pattern remains unclear due to the high sensitivity in the numerical results. (Zhao *et al*, 2021) studied the effect of the sign of Gauss curvature and curvature anisotropy on the wrinkling patterns of the bilayer and calculated numerically that the critical curvature for the transition from the sinusoidal to the hexagonal mode is $\Omega_2 = 0.94$.

6. Closure

In this paper, we provide a thorough wrinkling analysis of cylindrically curved thin film attached on a curved substrate under biaxial strain, focusing on the onset of the checkerboard and hexagonal buckling modes. The geometrical parameters of the buckling modes are specified semi-analytically and special attention has been paid on the role of the curvature-induced anisotropy in the elastic analysis. The film has been analysed by employing

the shallow shell theory and the substrate as a three-dimensional semi-infinite solid where the displacement components have been specified through the perturbation method. We show that the critical strain is increasing due to the curvature and the wrinkling amplitude is decreasing substantially. The analysis suggests that, energetically, the checkerboard wrinkling mode is more favourable compared to the one-dimensional and the hexagonal mode, see Fig 15. Finally, the convexity and concavity of the bilayer is discussed in detail for both wrinkling modes and it is shown that convex bilayers are favoured in the checkerboard mode while for hexagonal modes concavity favours buckling inward the substrate as has been observed in experiments.

References

[1] Allen H.G., 1969, Analysis and design of structural sandwich panels, Pergamon Press, New York.

[2] Bietsch A., Michel B., 2000, Conformal contact and pattern stability of stamps used for soft lithography, Journal of Applied Physics, vol. 88, pp. 4310-4318.

[3] Bowden N., Brittain S.,Evans A.G., Hutchinson J.W., Whitesides G., 1998, Spontaneous formation of ordered structures in thin films of metals supported on an elastomeric polymer, Nature , vol. 393, pp. 146-149.

[4] Breid D. and Crosby A.J., 2013, Curvature-controlled wrinkle morphologies, Soft Matter, vol. 9, pp. 3624-3630.

[5] Cai S., Breid D., Crosby A.J., Suo Z., Hutchinson J.W., 2011, Periodic

patterns and energy states of buckled films on compliant substrates, Journal of the Mechanics and Physics of Solids, vol. 59, pp. 1094-1114.

[6] Cao G., Chen X., Li C., Ji A., Cao Z., 2008, Self-assembled triangular and labyrinth buckling patterns of thin films on spherical substrates, Physical Review Letters, vol. 100, pp. 1-4.

[7] Cao Y., Li B., Feng X., 2012, Surface wrinkling and folding of core-shell soft cylinders, Soft Matter, vol. 8, pp. 556- 562.

[8] Cao Y., Jia F., Zhao Y., Feng X., Yu S., 2012, Buckling and post-buckling of a stiff film resting on an elastic graded substrate, International Journal of Solids and Structures, vol. 49, pp. 1656-1664.

[9] Cheng H., Zhang Y., Hwang K., Rogers J.A., Huang Y., 2014, Buckling of a stiff thin film on a pre-strained bi-layer substrate, International Journal of Solids and Structures, vol.51, pp. 3113-3118.

[10] Chen X. and Yin J., 2010, Buckling patterns of thin films on curved compliant substrates with applications to morphogenesis and three-dimensional micro-fabrication, Soft Matter, vol. 6, pp. 5667-5680.

[11] Choi W. M., Song J.,Khang D., Jiang H., Huang Y.Y., Rogers J.A., 2007, Biaxially stretchable "wavy" silicon nanomembranes, Nano Letters, vol. 7, pp. 1655-1663.

[12] Dagdeviren C., Shi Y., Joe P., Ghaffari R., Balooch G., Usgaonkar K., Gur O., Tran P.L., Crosby J.R., Meyer Su Y.M., Chad Webb R., Tedesco

A.S., Slepian M.J., Huang Y., and Rogers J.A., 2015, Conformal piezoelectric systems for clinical and experimental characterization of soft tissue biomechanics, Nature Materials, vol. 14, pp. 728-738.

[13] Hao Y., Li B., Feng X., Gao H., 2024, Wrinkling-dewrinkling transitions in stretched soft spherical shells, International Journal of Solids and Structures, vol.294, pp.1-12.

[14] Hong W., Zhao X., Zhou J., Suo Z., 2008, A theory of coupled diffusion and large deformation in polymeric gels,Journal of the Mechanics and Physics of Solids, vol. 56, pp. 1779-1793.

[15] Huang R, 2005, Kinetic wrinkling of an elastic film on a viscoelastic substrate, Journal of the Mechanics and Physics of Solids, vol. 53, pp. 63 - 89.

[16] Huang R., Suo Z., 2002, Wrinkling of a compressed elastic film on a viscous layer, Journal of Applied Physics, vol. 91, pp. 1135 - 1142.

[17] Huang X., Li B., Hong W., Cao Y., Feng X., 2016, Effects of tension-compression asymmetry on the surface wrinkling of film-substrate systems, Journal of the Mechanics and Physics of Solids, vol. 94, pp. 88-104.

[18] Huang X., Zhao H., Xie W., Hong W., Feng X., 2015, Radial wrinkles on film-substrate system induced by local pre-stretch: A theoretical analysis, International Journal of Solids and Structures, vol.58, pp. 12-19.

[19] Huang Z., Hong W., Suo Z., 2004, Evolution of wrinkles in hard films on soft substrates, Physical Review E, vol. 70, pp. 030601-4.

[20] Huang Z.Y., Hong W., Suo Z., 2005, Nonlinear analyses of wrinkles in a film bonded to a compliant substrate, Journal of the Mechanics and Physics of Solids, vol. 53, pp. 2101-2118.

[21] Jiang H., Khang D., Fei H, Kim H., Huang Y., Xiao J., Rogers J.A., 2008, Finite width effect of thin films buckling on compliant substrate:Experimental and theoretical studies, Journal of the Mechanics and Physics of Solids, vol. 56, pp. 2585-2598.

[22] Jiang H., Khang D., Song J., Sun Y., Huang Y., Rogers J.A., 2007, Finite deformation mechanics in buckled thin films on compliant supports, Proceedings of the National Academy of Sciences, vol. 104, pp. 15607-15612.

[23] Karam G. N. and Gibson L. J., 1995, Elastic buckling of cylindrical shells with elastic cores - I. Analysis. International Journal of Solids and Structures, vol. 32, pp. 1259-1283.

[24] Kordolemis A., Giannakopoulos A.E., 2024, Wrinkling analysis of a stiff shallow film mounted on a cylindrically curved compliant substrate - Part I: Cylindrical mode., IJSS submitted.

[25] Nikravesh, S., Ryu, D. and Shen, Y.-L., 2019, Surface instability of composite thin films on compliant substrates: Direct Simulation Approach, Frontiers in Materials vol.6, pp. 214-224.

[26] Nikravesh, S., Ryu, D. and Shen, Y.-L., 2019, Direct numerical simulation of buckling instability of thin films on a compliant substrate, Advances in Mechanical Engineering, vol. 11, 1687814019840470

[27] Nikravesh, S., Ryu, D. and Shen, Y.-L., 2020, Instabilities of thin films on a compliant substrate: Direct numerical simulations from surface wrinkling to global buckling, Nature, vol.10, pp.1-19.

[28] Song J., Jiang H., Choi W.M, Khang D.Y., Huang Y.Y., Rogers J.A., 2008, An analytical study of two-dimensional buckling of thin films on compliant substrates, Journal of Applied Physics, vol. 103, pp. 014303-10.

[29] Xu F. and Potier-Ferry M., 2016, On axisymmetric/diamond like mode transitions in axially compressed core-shell cylinders, Journal of the Mechanics and Physics of Solids, vol.94, pp. 68-87.

[30] Yin S., Li B., Cao Y.P., Feng X., 2018, Surface wrinkling of anisotropic films bonded on a compliant substrate, International Journal of Solids and Structures, vol. 141-142, pp. 219-231.

[31] Zhang X., Guo T., Zhang Y., 2011, Instability analysis of a programmed hydrogel plate under swelling, Journal of Applied Physics, vol. 109, 063527.

[32] Zhao R. and Zhao X., 2017, Multimodal surface instabilities in curved film-substrate structures, Journal of Applied Mechanics, vol. 84, pp.1-13.

[33] Zhao Y., Cao Y., Feng X., Ma K., 2014, Axial compression induced wrinkles on a core shell soft cylinder: Theoretical analysis, simulations and experiments, Journal of the Mechanics and Physics of Solids, vol.73, pp. 212-227.

[34] Zhao Y., Guo W., Zhu H., He Y., Jiang C., Cao Y., 2021, Pattern selection on axial compressed bilayer systems with a non-zero Gauss curvature, Journal of the Mechanics and Physics of Solids, vol.154, pp. 1-12.

[35] Zhao Y., Zhu H., Jiang C., Cao Y., Feng X., 2020, Wrinkling pattern evolution on curved surfaces, Journal of the Mechanics and Physics of Solids, vol.135, pp. 1-15.

List of Table captions

Table 1. Variation of the parameters $\alpha_i\,(\nu_s)$ for different values of substrate's Poisson's ratio.

Table 2. Variation of the parameters $\beta_i\,(\nu_s)$ for different values of substrate's Poisson's ratio.

Table 3. Numerical values used in the numerical analysis for the thin film, quantities with subscript f, and the substrate, quantities with subscript s.

Table 4. Compressive critical load, as (%), of the checkerboard mode for various ratios of the loading in the two principal directions x, y of the bilayer. The values within the parenthesis are referring to the critical load of a convex bilayer, i.e. $\xi_R < 0$.

Table 5. Numerical values of the critical strain (%) for the squared checkerboard mode for various values of the curvature ($\xi_R > 0$). The values from Table.1. have been used for the calculations.

List of Figure captions

Figure 1. (a) Stereoscopic view and (b) top view of the square checkerboard mode wrinkling and the accompanied geometrical quantities, i.e. the wavelengths λ_1, λ_2 in x, y direction respectively and the wrinkling amplitude A_0.

Figure 2. (a) Stereoscopic view and (b) top view of the hexagonal wrinkling mode and the accompanied geometrical quantities, i.e. the wavelengths $\lambda_1 = 4\,\pi/k\,\eta, \lambda_2 = 4\,\pi/k$ in x, y direction, respectively, and the wrinkling amplitudes A_0, B_0.

Figure 3. Graphical calculation of the wavenumbers ξ_1, ξ_2 for the squared checkerboard mode. Calculations are referring to equibiaxial compression $\left(\varepsilon^0_{xx} = \varepsilon^0_{yy} = \varepsilon^{\text{eq}}\right)$ of a concave ($\xi_R > 0$) thin film-substrate system. The numerical values used for the curvature are: (a) $\xi_R = +1/25$, (b) $\xi_R = +1/50$, (c) $\xi_R = +1/100$, (d) $\xi_R = 0\,(\text{flat})$. The insets represent the evolution of the the wrinkling as the curvature is changing.

Figure 4. Graphical calculation of the wavenumbers ξ_1, ξ_2 for the checkerboard mode. Calculations are referring to higher compression of the concave ($\xi_R > 0$)bilayer in the $x-$ direction, i.e. $\varepsilon^0_{xx} = 2\,\varepsilon^0_{yy}$. The numerical values used for the curvature are: (a) $\xi_R = +1/25$, (b) $\xi_R = +1/50$, (c) $\xi_R = +1/100$, (d) $\xi_R = 0\,(\text{flat})$.

Figure 5. Graphical calculation of the wavenumbers ξ_1, ξ_2 for the checkerboard mode. Calculations are referring to higher compression of the concave ($\xi_R > 0$) bilayer in the $y-$ direction, i.e. $\varepsilon^0_{yy} = 2\,\varepsilon^0_{xx}$. The numerical values used for the curvature are: (a) $\xi_R = +1/25$, (b) $\xi_R = +1/50$, (c) $\xi_R = +1/100$, (d) $\xi_R = 0\,(\text{flat})$.

Figure 6. Variation of the wavenumbers ξ_k, η for the checkerboard wrinkling mode for different values of the moduli mismatch $\bar{E}_s/\bar{E}_f$. Calculations are referring to 5% equibiaxial compression but the values marked on the figures are independent of the applied strain. The numerical values used for the curvature are: (a) $\xi_R = +1/25$, (b) $\xi_R = +1/100$, (c)

$\xi_R = -1/25$, (d) $\xi_R = 0$ (flat).

Figure 7. Numerical calculation of the amplitude ξ_0 for various values of curvature for the checkerboard mode. The intersection points of the curves with the horizontal axis of equibiaxial strains denote the critical load for different values of ξ_R. (a) equibiaxial loading, i.e. $\varepsilon^0_{xx} = \varepsilon^0_{yy} = \varepsilon_{\text{eq}}$ and (b) $\varepsilon^0_{xx} = 2\,\varepsilon^0_{yy}$, (c) $\varepsilon^0_{xx} = 1/2\,\varepsilon^0_{yy}$,$(d)$ uniaxial loading along the $x-$ direction, i.e., $\varepsilon^0_{yy} = 0$.

Figure 8. (a) Variation of the ratio of the total energy in the buckled state, $U^{\text{buck}}_{\text{tot}}$, over the total energy in the unbuckled state, $U^{\text{unbuck}}_{\text{tot}}$ for the checkerboard mode. (b) Variation of the ratios of the substrate U_s, the film bending $U_{b(f)}$, and the film membrane $U_{m(f)}$ energies to the total energy in the unbuckled state. Calculations are referring to equibiaxial compression (negative strain) of the bilayer.

Figure 9. Graphical calculation of the wavenumbers ξ_k, η for the hexagonal wrinkling mode. Calculations are referring to equibiaxial compression $\left(\varepsilon^0_{xx} = \varepsilon^0_{yy} = \varepsilon^{\text{eq}}\right)$ of a convex $(\xi_R < 0)$ thin film-substrate system. The numerical values used for the curvature are: (a) $\xi_R = +1/25$, (b) $\xi_R = +1/50$, (c) $\xi_R = +1/100$, (d) $\xi_R = 0$ (flat).

Figure 10. Numerical calculation of the amplitudes ξ_A, ξ_B for the hexagonal mode for various values of the negative curvature of the bilayer. Calculations are referring to equibiaxial compression $\left(\varepsilon^0_{xx} = \varepsilon^0_{yy} = \varepsilon^{\text{eq}} < 0\right)$.

Figure 11. Graphical calculation of the wavenumbers ξ_k, η for the hexagonal wrinkling mode. Calculations are referring to equibiaxial compression $\left(\varepsilon^0_{xx} = \varepsilon^0_{yy} = \varepsilon^{\text{eq}}\right)$ of a convex $(\xi_R < 0)$ thin film-substrate system. The numerical values used for the curvature are: (a) $\xi_R = +1/25$, (b) $\xi_R = +1/50$, (c) $\xi_R = +1/100$, (d) $\xi_R = 0$ (flat). Note the change of scale in the abscissa in the flat bilayer.

Figure 12. Variation of the wavenumbers ξ_k, η for the hexagonal wrinkling mode for different values of the moduli mismatch $\bar{E}_s/\bar{E}_f$. Calculations are referring to 5% equibiaxial compression but the values marked on the figures are independent of the applied strain. The numerical values used for the curvature are: (a) $\xi_R = -1/25$, (b) $\xi_R = -1/100$, (c) $\xi_R = +1/25$, (d) $\xi_R = 0$ (flat).

Figure 13. Numerical calculation of the amplitudes ξ_A, ξ_B for the hexagonal mode for various values of the positive curvature of the bilayer. Calculations are referring to equibiaxial compression $\left(\varepsilon^0_{xx} = \varepsilon^0_{yy} = \varepsilon^{\text{eq}} < 0\right)$.

Figure 14. (a) Variation of the ratio of the total energy in the buckled state, $U^{\text{buck}}_{\text{tot}}$, over the total energy in the unbuckled state, $U^{\text{unbuck}}_{\text{tot}}$ for the hexagonal mode. (b) Variation of the ratios of the substrate U_s, the film bending $U_{b(f)}$, and the film membrane $U_{m(f)}$ energies to the total energy in the unbuckled state. Calculations are referring to equibiaxial compression (negative strain) of the bilayer.

Figure 15. Variation of the ratio of the total energy in the buckled state, $U^{\text{buck}}_{\text{tot}}$, over the total energy in the unbuckled state, $U^{\text{unbuck}}_{\text{tot}}$, for the 1D, checkerboard and hexagonal wrinkling modes, for (a) concave $(\xi_R > 0)$ and (b) convex $(\xi_R < 0)$ bilayer.

Figure(s)

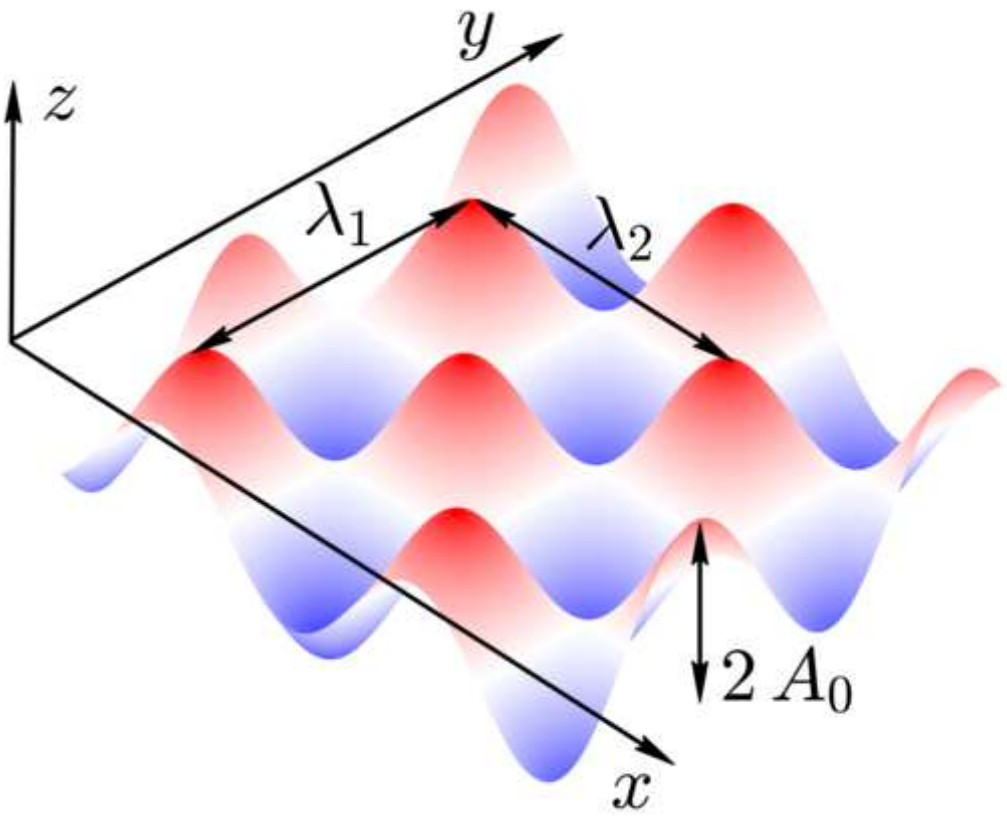

Figure(s)

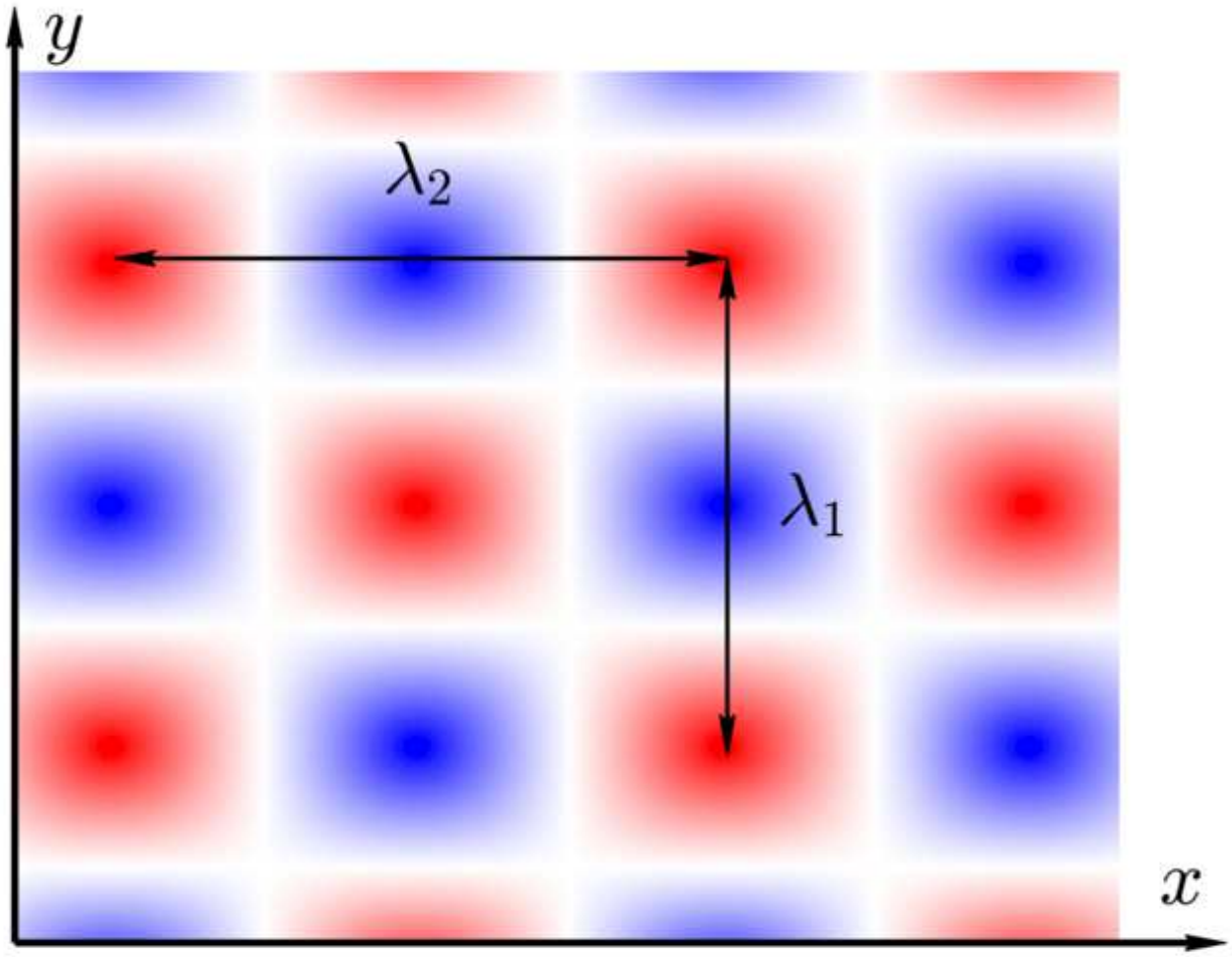

Figure(s)

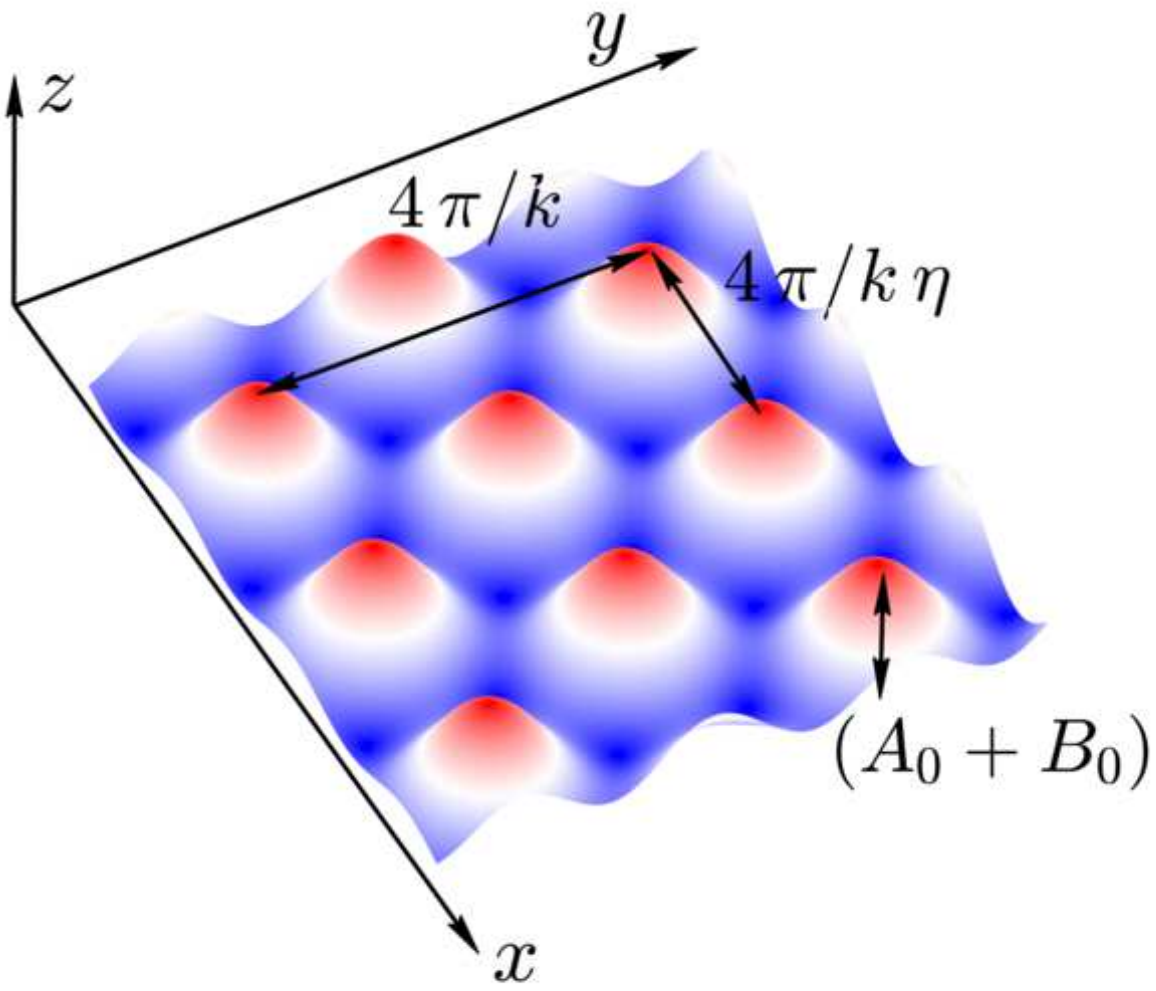

Figure(s)

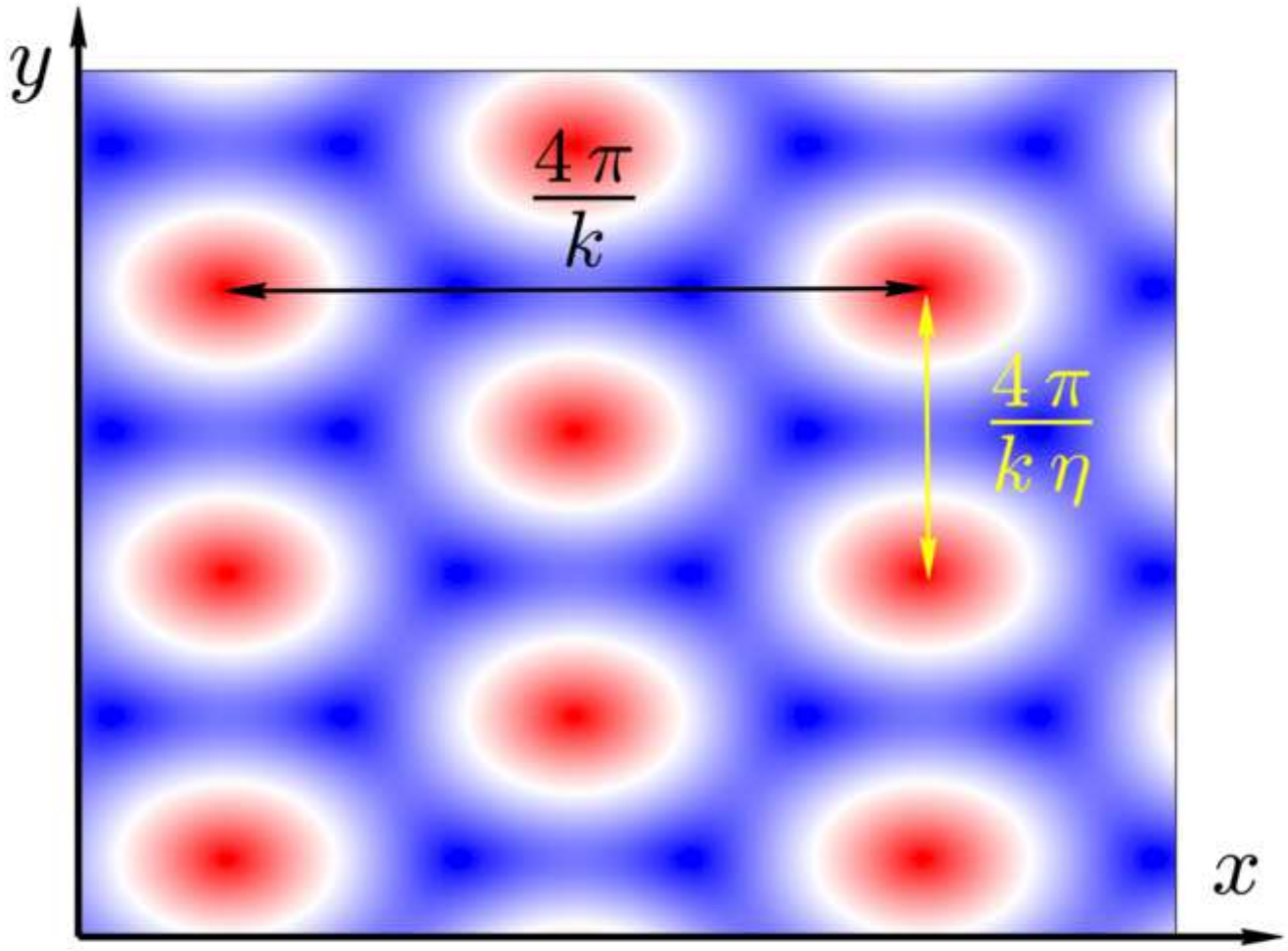

Figure(s)

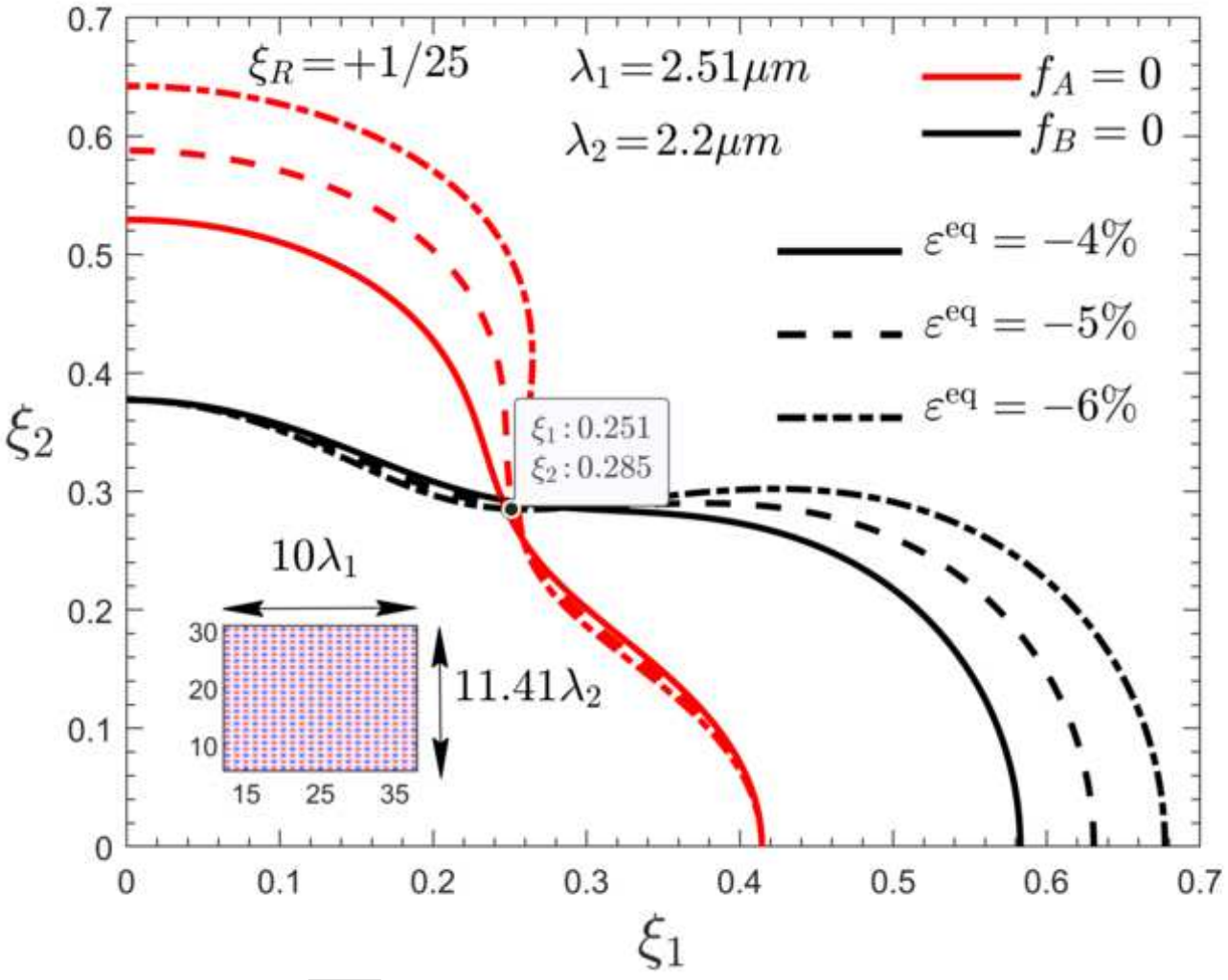

Figure(s)

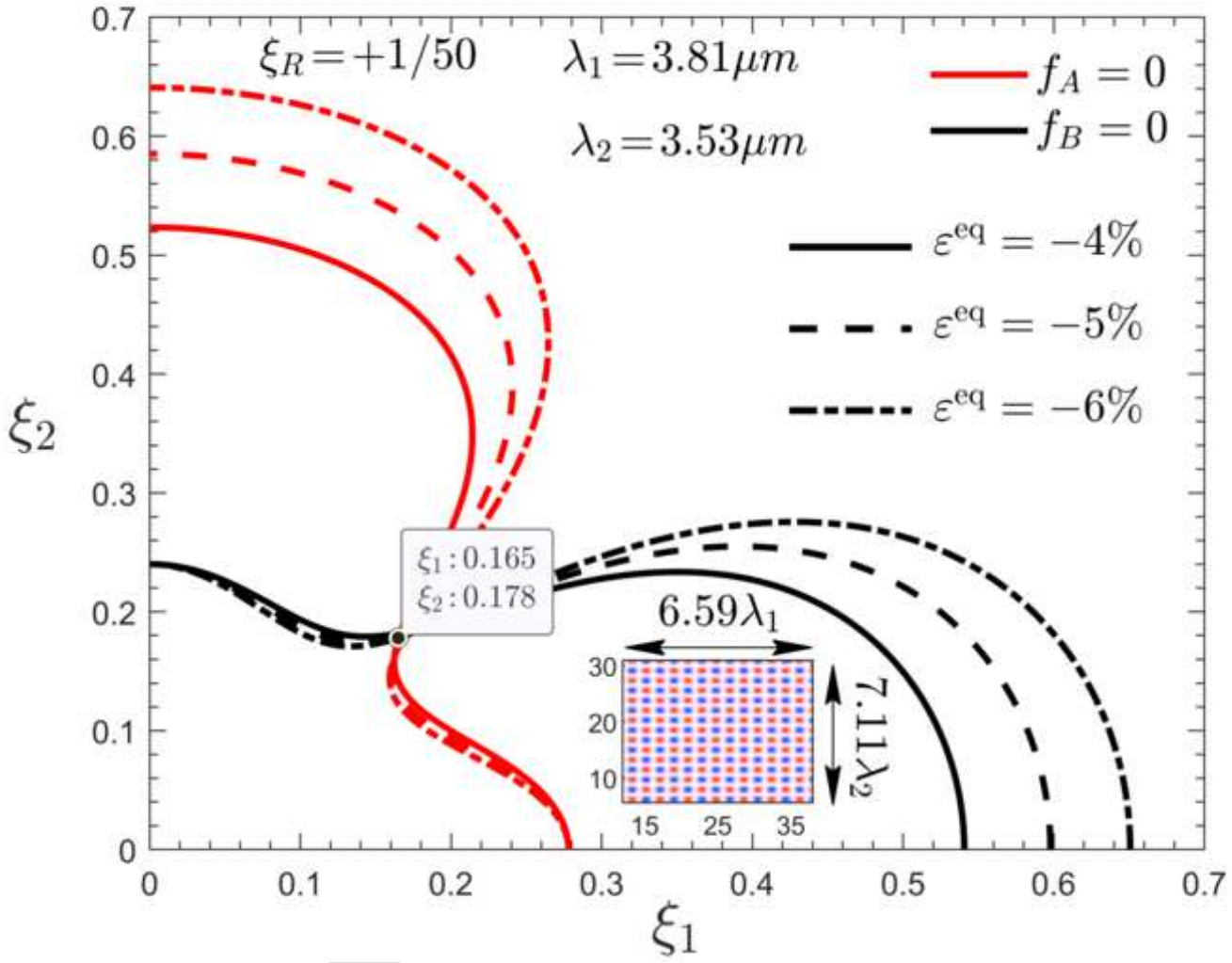
$\xi_R = +1/50$
$\lambda_1 = 3.81\mu m$
$\lambda_2 = 3.53\mu m$
$f_A = 0$
$f_B = 0$
$\varepsilon^{eq} = -4\%$
$\varepsilon^{eq} = -5\%$
$\varepsilon^{eq} = -6\%$
$\xi_1 : 0.165$
$\xi_2 : 0.178$
$6.59\lambda_1$
$7.11\lambda_2$
ξ_1
ξ_2

Figure(s)

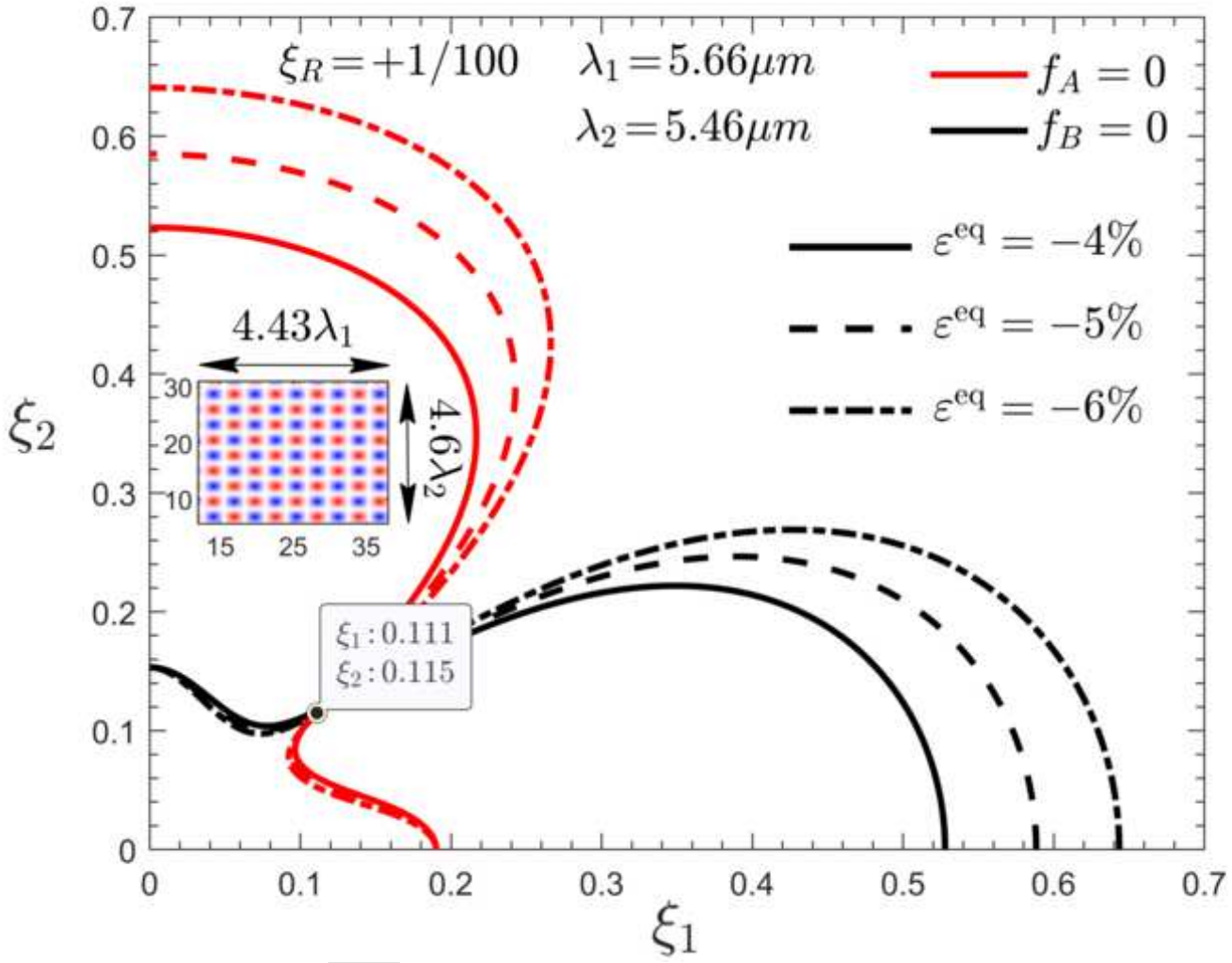
$\xi_R = +1/100$
$\lambda_1 = 5.66\mu m$
$\lambda_2 = 5.46\mu m$
$f_A = 0$
$f_B = 0$
$\varepsilon^{eq} = -4\%$
$\varepsilon^{eq} = -5\%$
$\varepsilon^{eq} = -6\%$
$4.43\lambda_1$
$4.6\lambda_2$
$\xi_1 : 0.111$
$\xi_2 : 0.115$
ξ_1
ξ_2

Figure(s)

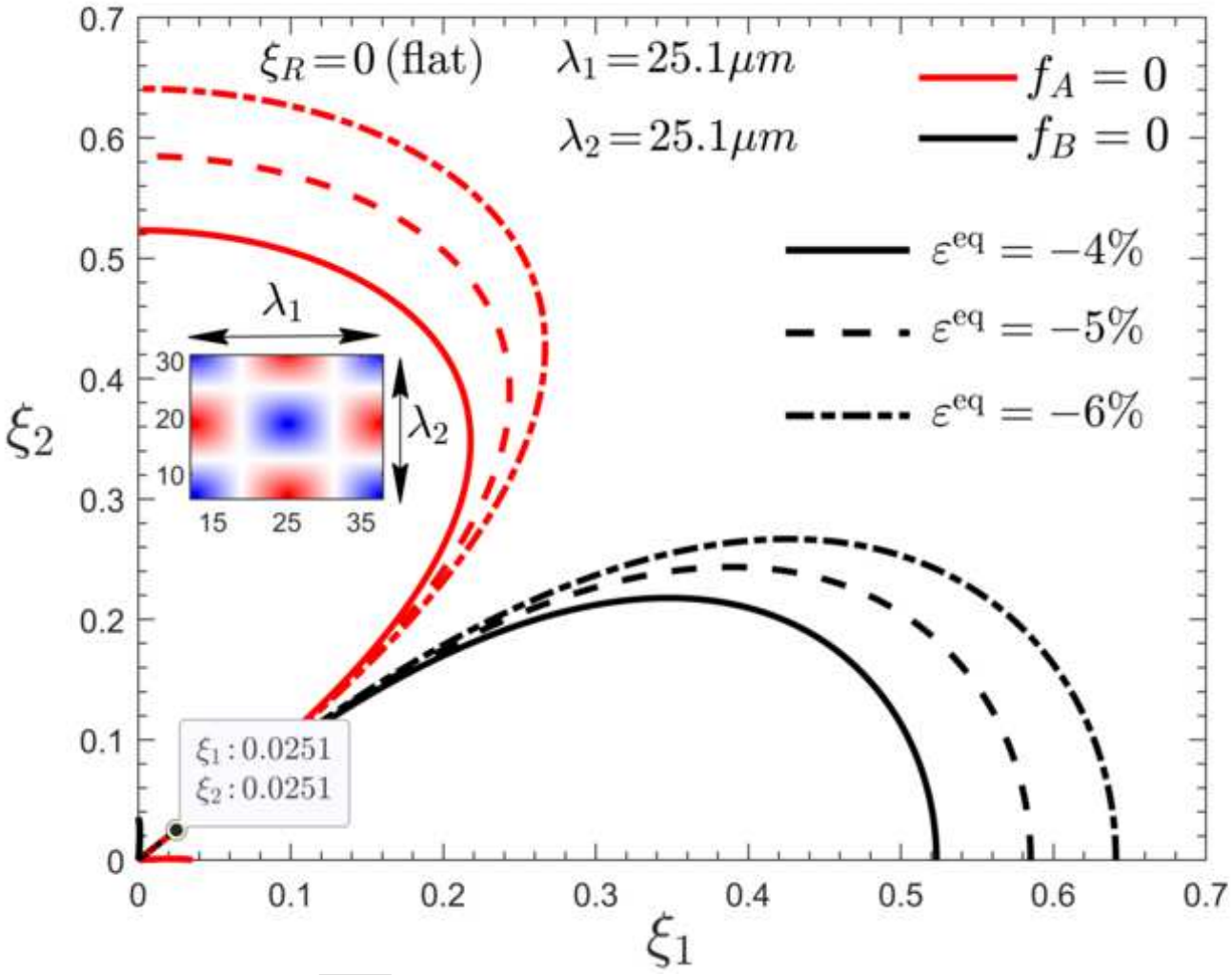
$\xi_R = 0$ (flat)
$\lambda_1 = 25.1\mu m$
$\lambda_2 = 25.1\mu m$
$f_A = 0$
$f_B = 0$
$\varepsilon^{eq} = -4\%$
$\varepsilon^{eq} = -5\%$
$\varepsilon^{eq} = -6\%$
λ_1
λ_2
$\xi_1 : 0.0251$
$\xi_2 : 0.0251$
ξ_1
ξ_2

Figure(s)

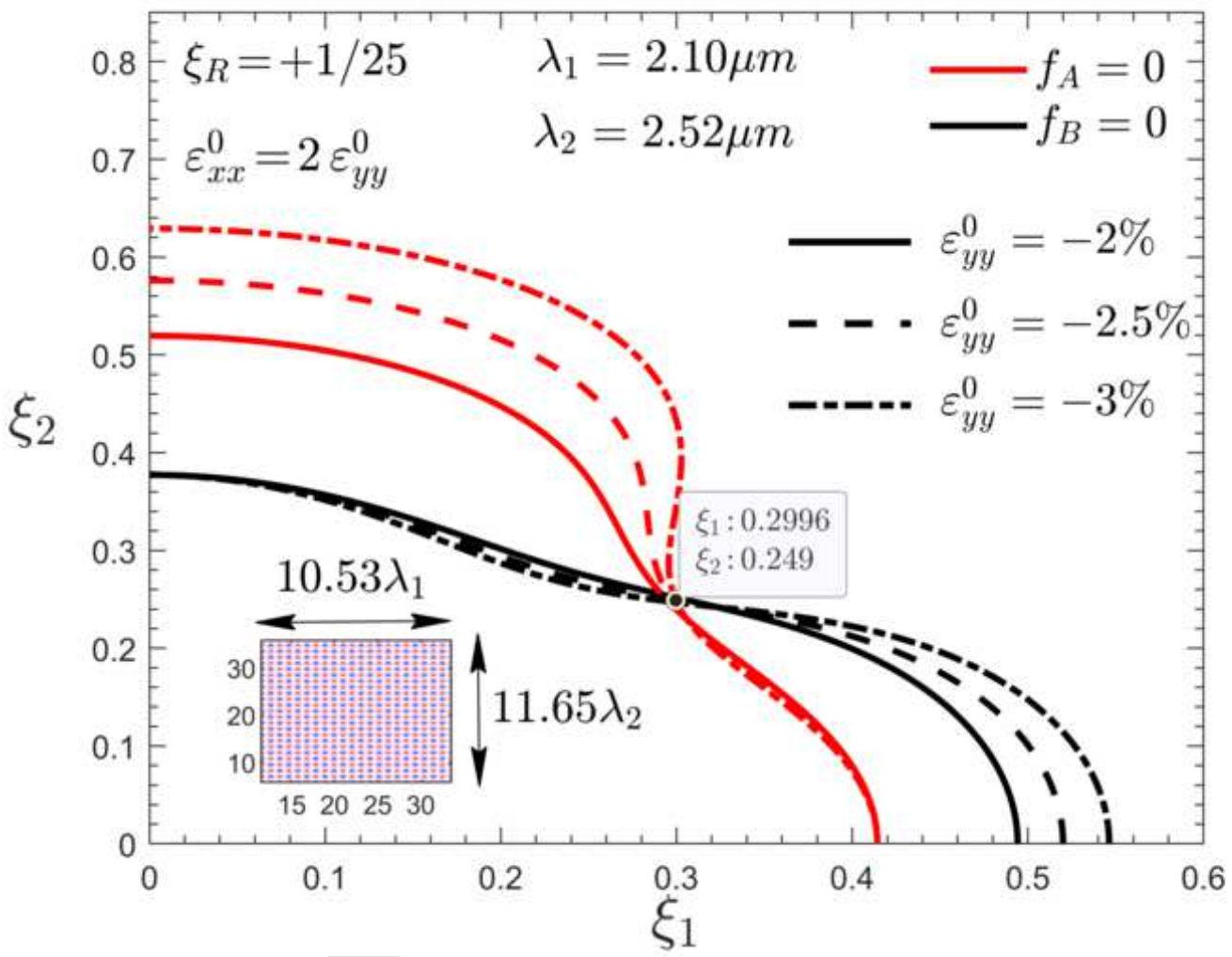
$\xi_R = +1/25$
$\varepsilon^0_{xx} = 2\,\varepsilon^0_{yy}$
$\lambda_1 = 2.10\mu m$
$\lambda_2 = 2.52\mu m$
$f_A = 0$
$f_B = 0$
$\varepsilon^0_{yy} = -2\%$
$\varepsilon^0_{yy} = -2.5\%$
$\varepsilon^0_{yy} = -3\%$
$\xi_1 : 0.2996$
$\xi_2 : 0.249$
$10.53\lambda_1$
$11.65\lambda_2$
ξ_1
ξ_2

Figure(s)

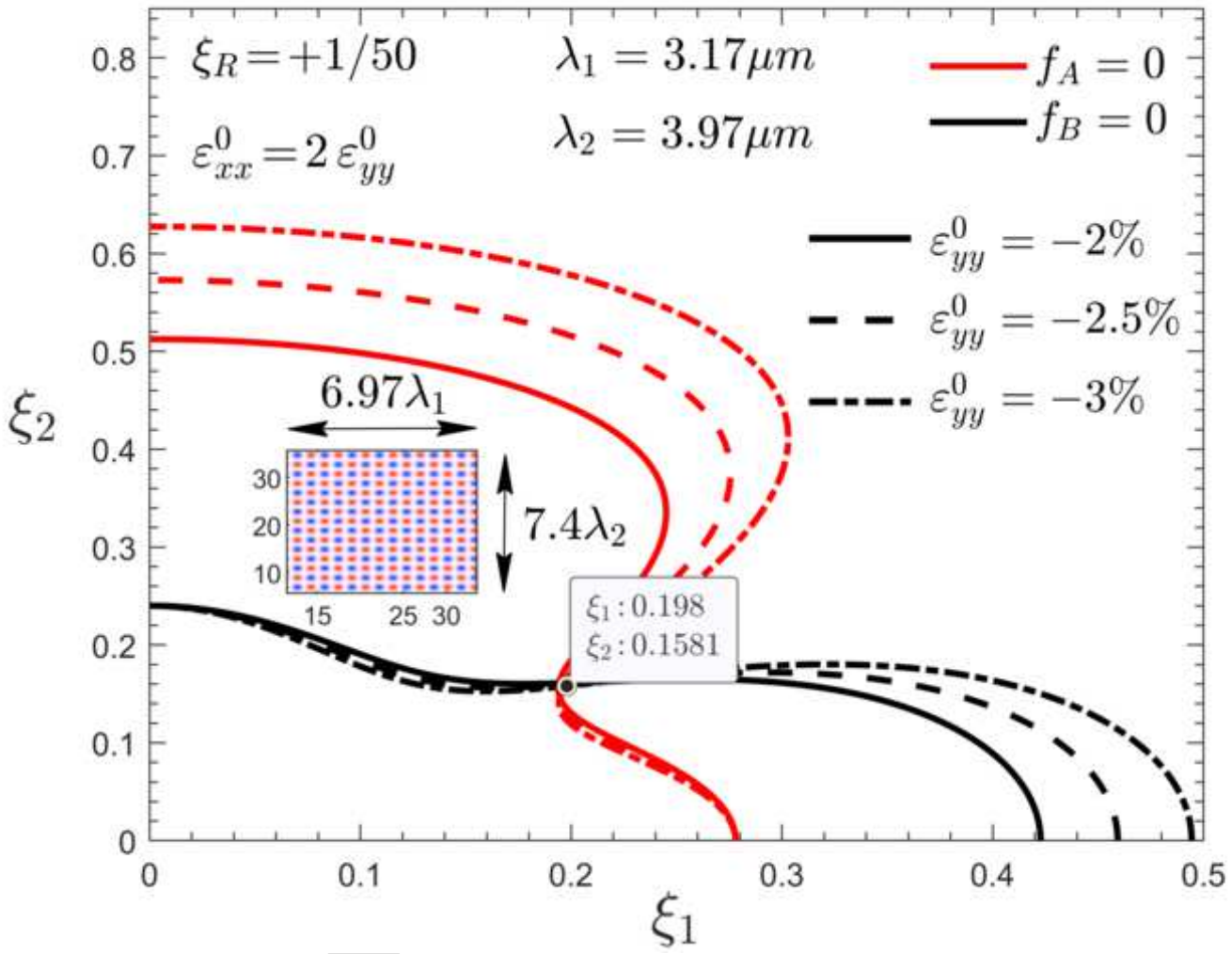
$\xi_R = +1/50$
$\varepsilon^0_{xx} = 2\,\varepsilon^0_{yy}$
$\lambda_1 = 3.17\mu m$
$\lambda_2 = 3.97\mu m$
$f_A = 0$
$f_B = 0$
$\varepsilon^0_{yy} = -2\%$
$\varepsilon^0_{yy} = -2.5\%$
$\varepsilon^0_{yy} = -3\%$
$6.97\lambda_1$
$7.4\lambda_2$
$\xi_1 : 0.198$
$\xi_2 : 0.1581$
ξ_1
ξ_2

Figure(s)

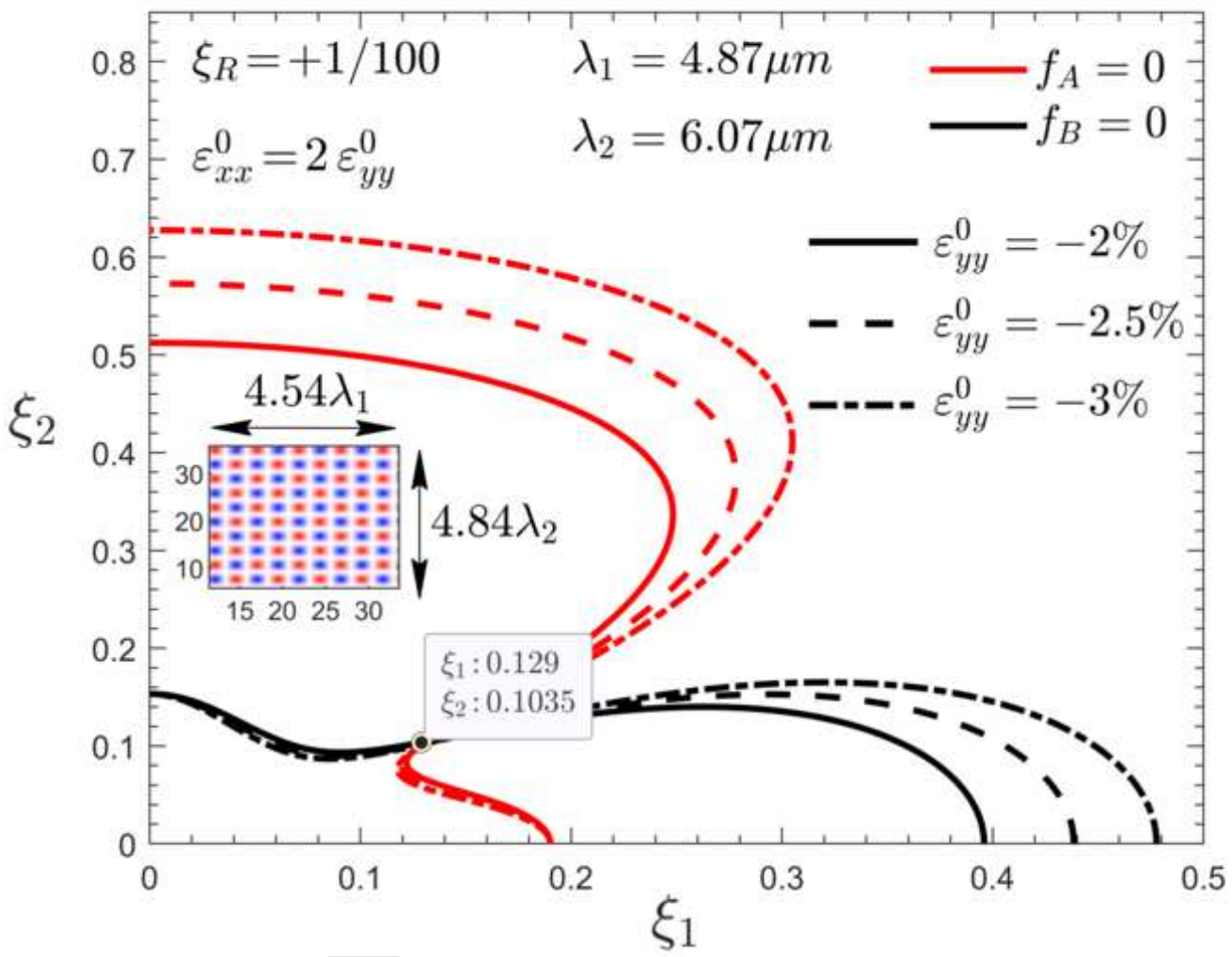
$\xi_R = +1/100$
$\varepsilon^0_{xx} = 2\,\varepsilon^0_{yy}$
$\lambda_1 = 4.87\mu m$
$\lambda_2 = 6.07\mu m$
$f_A = 0$
$f_B = 0$
$\varepsilon^0_{yy} = -2\%$
$\varepsilon^0_{yy} = -2.5\%$
$\varepsilon^0_{yy} = -3\%$
$4.54\lambda_1$
$4.84\lambda_2$
$\xi_1 : 0.129$
$\xi_2 : 0.1035$
ξ_1
ξ_2

Figure(s)

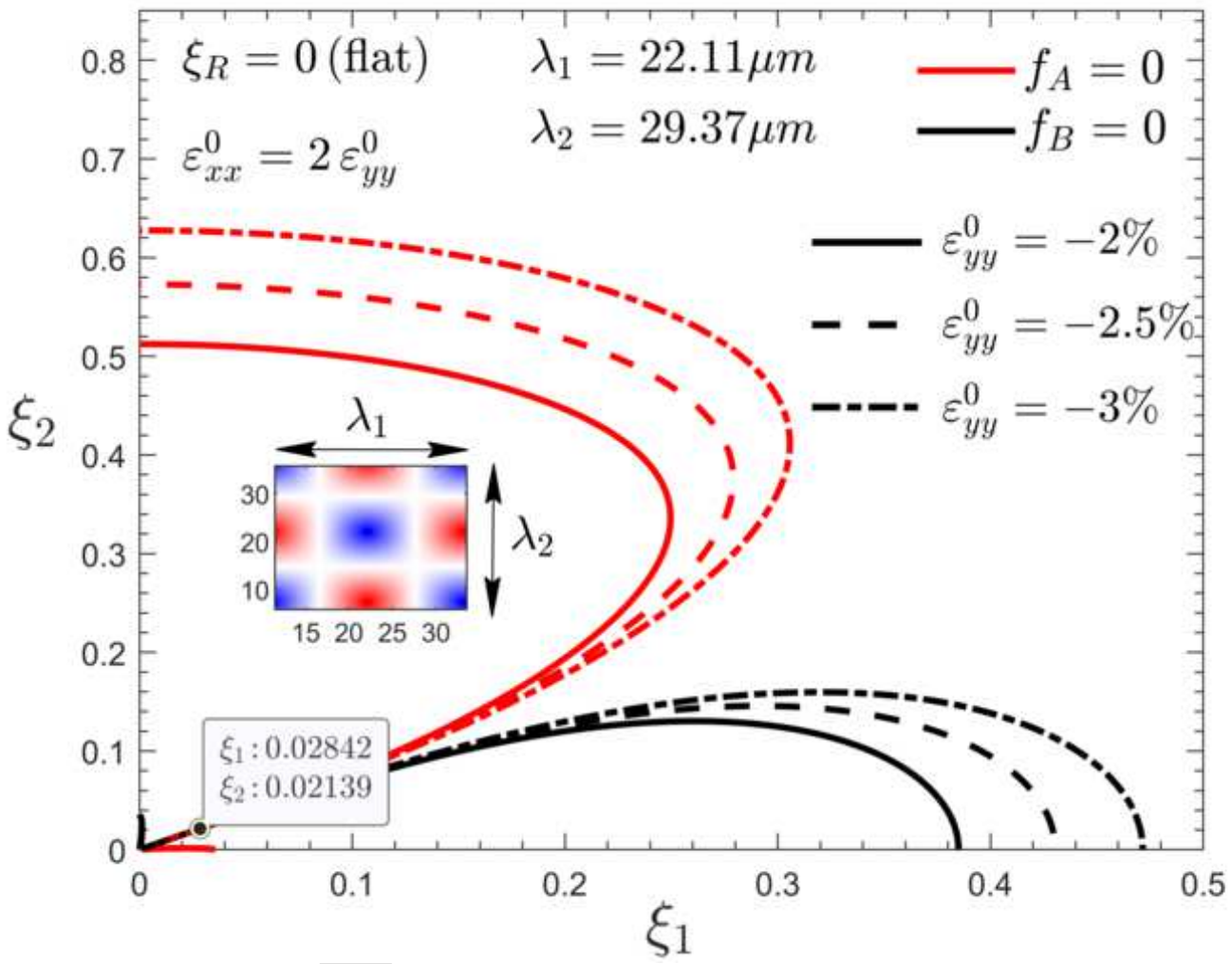
$\xi_R = 0$ (flat)
$\varepsilon^0_{xx} = 2\,\varepsilon^0_{yy}$
$\lambda_1 = 22.11\mu m$
$\lambda_2 = 29.37\mu m$
$f_A = 0$
$f_B = 0$
$\varepsilon^0_{yy} = -2\%$
$\varepsilon^0_{yy} = -2.5\%$
$\varepsilon^0_{yy} = -3\%$
λ_1
λ_2
30
20
10
15 20 25 30
$\xi_1 : 0.02842$
$\xi_2 : 0.02139$
0
0.1
0.2
0.3
0.4
0.5
0.6
0.7
0.8
ξ_1
ξ_2

Figure(s)

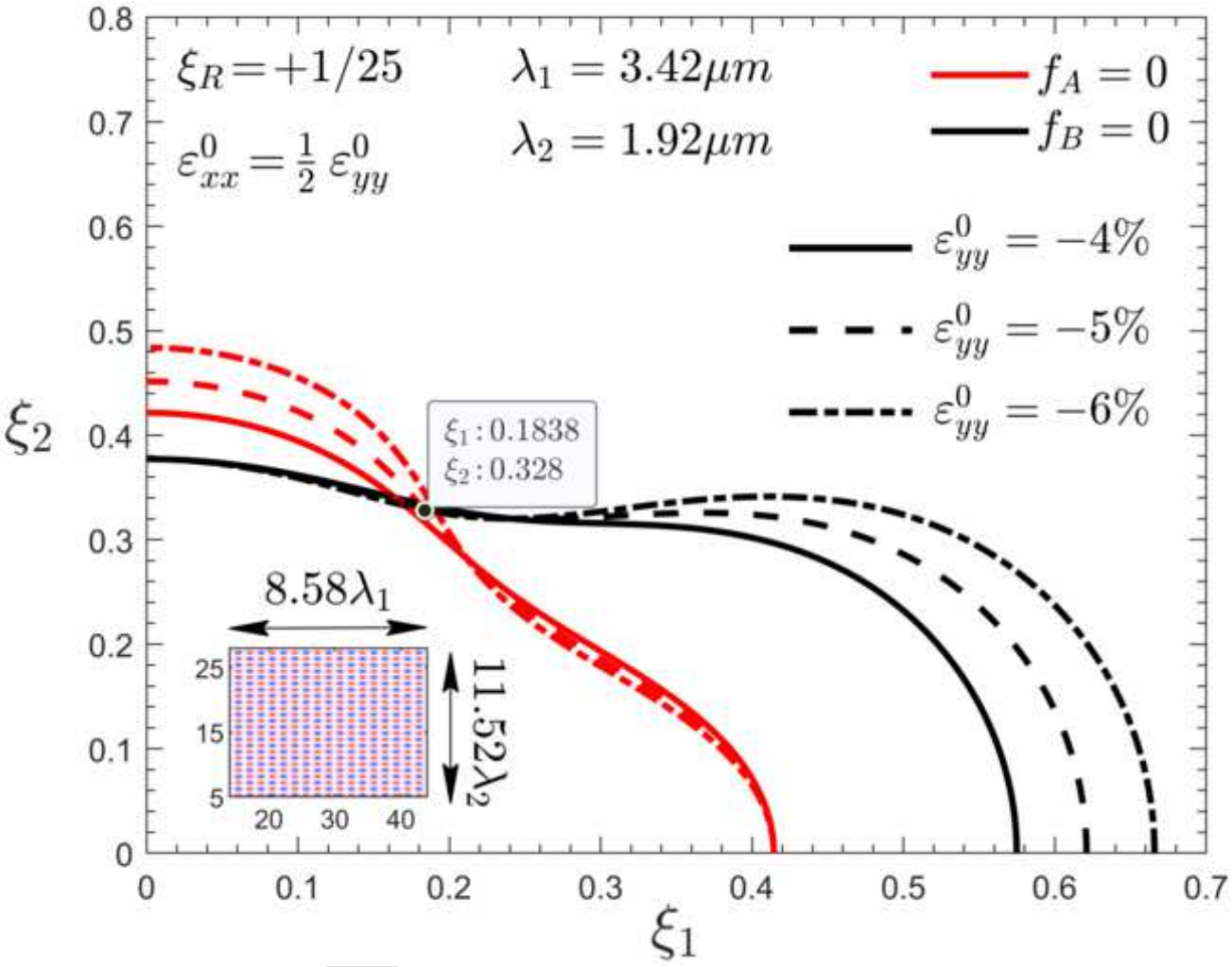
$\xi_R = +1/25$
$\varepsilon^0_{xx} = \frac{1}{2}\,\varepsilon^0_{yy}$
$\lambda_1 = 3.42\mu m$
$\lambda_2 = 1.92\mu m$
$f_A = 0$
$f_B = 0$
$\varepsilon^0_{yy} = -4\%$
$\varepsilon^0_{yy} = -5\%$
$\varepsilon^0_{yy} = -6\%$
$\xi_1 : 0.1838$
$\xi_2 : 0.328$
$8.58\lambda_1$
$11.52\lambda_2$
ξ_1
ξ_2

Figure(s)

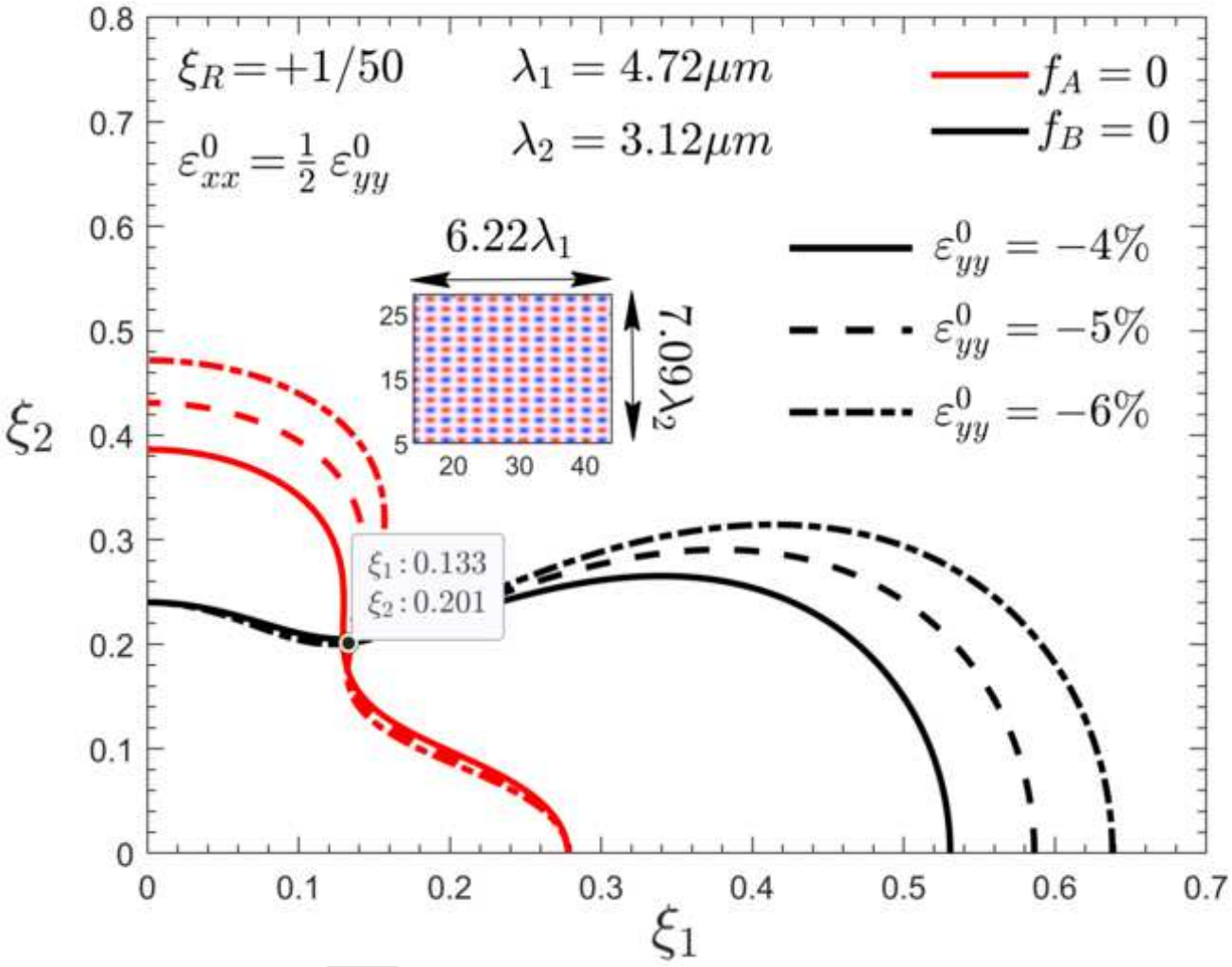
$\xi_R = +1/50$
$\varepsilon^0_{xx} = \frac{1}{2}\,\varepsilon^0_{yy}$
$\lambda_1 = 4.72\mu m$
$\lambda_2 = 3.12\mu m$
$f_A = 0$
$f_B = 0$
$6.22\lambda_1$
$7.09\lambda_2$
$\varepsilon^0_{yy} = -4\%$
$\varepsilon^0_{yy} = -5\%$
$\varepsilon^0_{yy} = -6\%$
$\xi_1 : 0.133$
$\xi_2 : 0.201$
ξ_1
ξ_2

Figure(s)

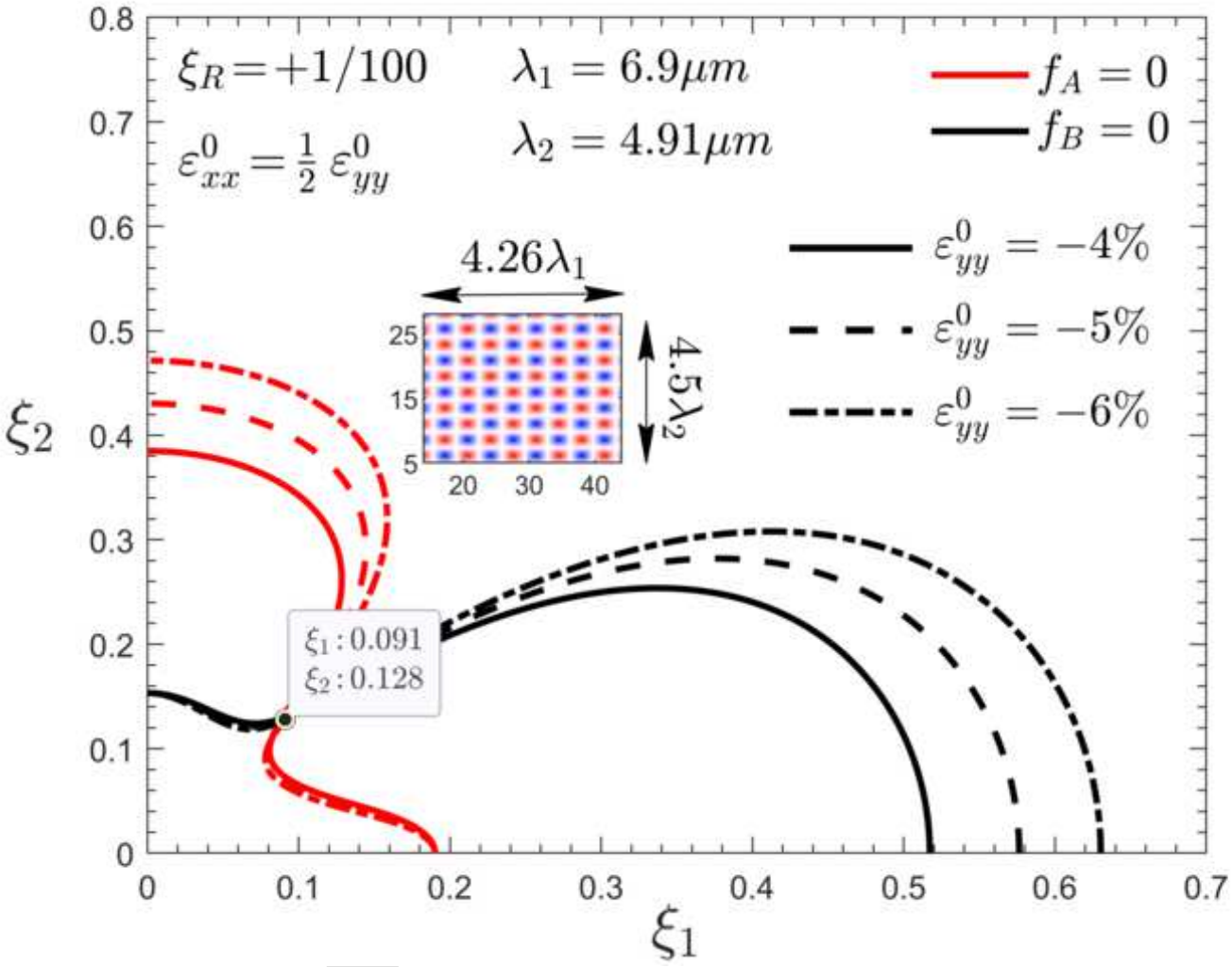
$\xi_R = +1/100$
$\lambda_1 = 6.9\mu m$
$\lambda_2 = 4.91\mu m$
$\varepsilon^0_{xx} = \frac{1}{2}\,\varepsilon^0_{yy}$
$f_A = 0$
$f_B = 0$
$\varepsilon^0_{yy} = -4\%$
$\varepsilon^0_{yy} = -5\%$
$\varepsilon^0_{yy} = -6\%$
$4.26\lambda_1$
$4.5\lambda_2$
$\xi_1 : 0.091$
$\xi_2 : 0.128$
ξ_1
ξ_2

Figure(s)

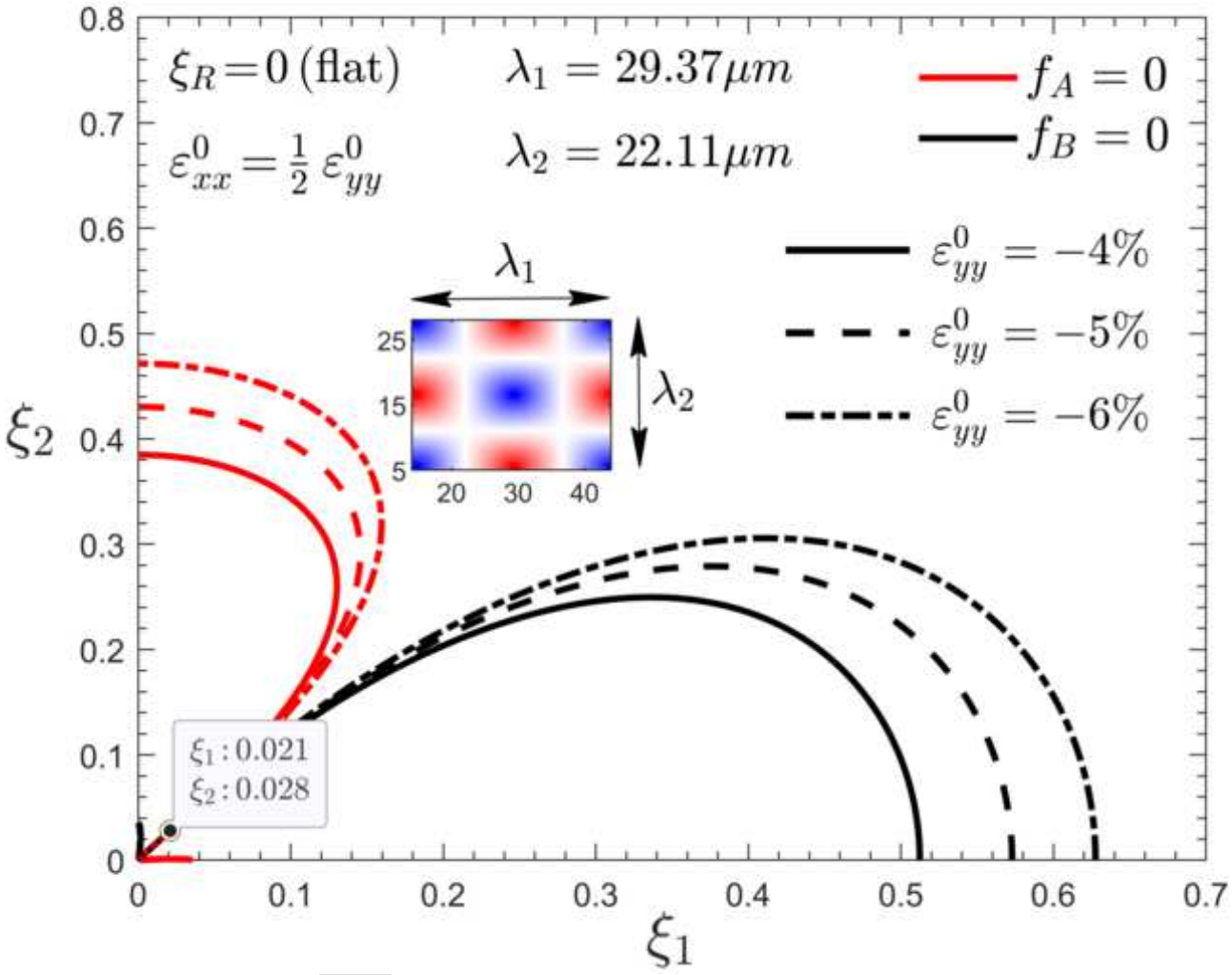
$\xi_R = 0$ (flat)
$\varepsilon^0_{xx} = \frac{1}{2}\,\varepsilon^0_{yy}$
$\lambda_1 = 29.37\mu m$
$\lambda_2 = 22.11\mu m$
$f_A = 0$
$f_B = 0$
$\varepsilon^0_{yy} = -4\%$
$\varepsilon^0_{yy} = -5\%$
$\varepsilon^0_{yy} = -6\%$
λ_1
λ_2
$\xi_1 : 0.021$
$\xi_2 : 0.028$
ξ_1
ξ_2

Figure(s)

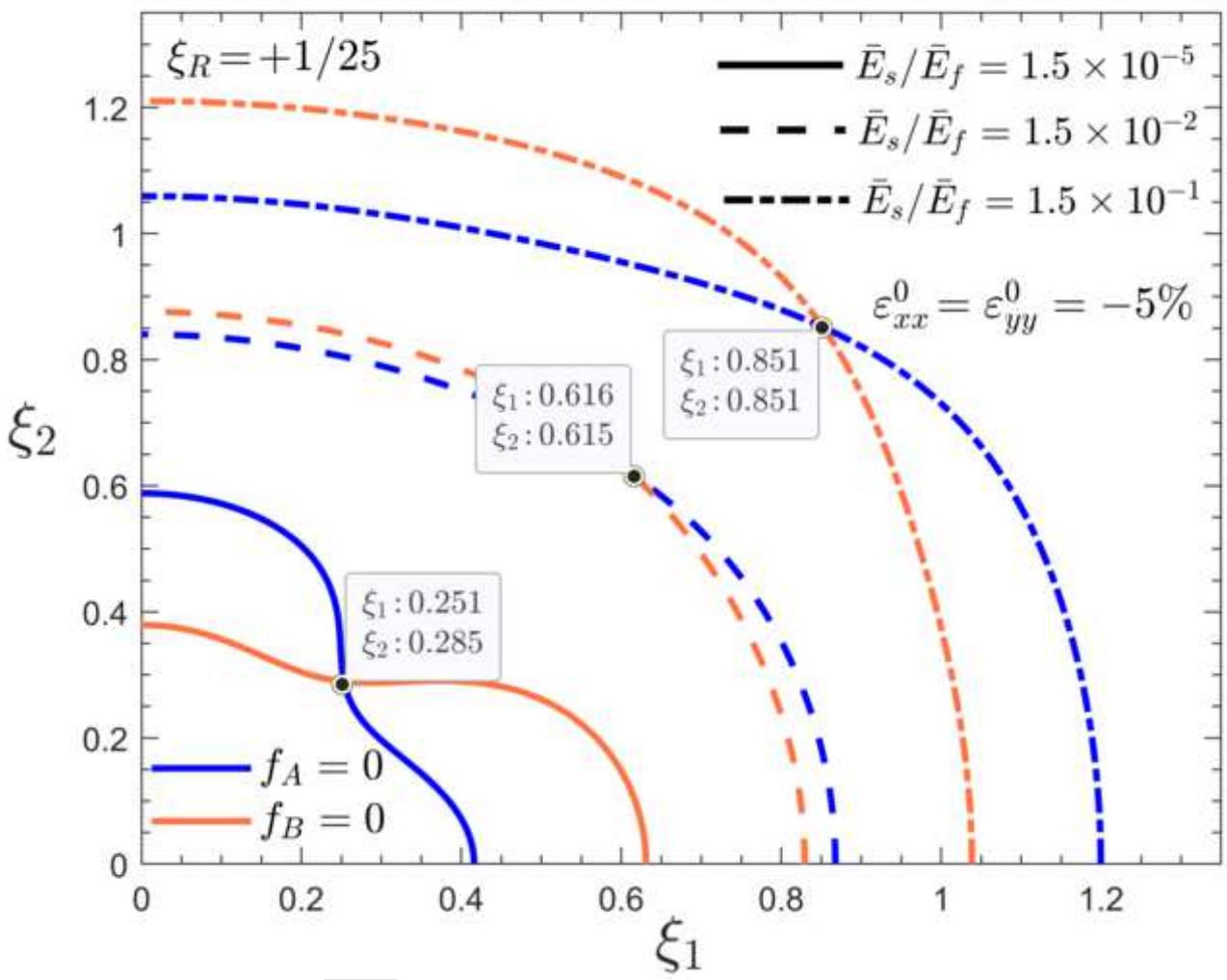
$\xi_R = +1/25$
$\bar{E}_s/\bar{E}_f = 1.5 \times 10^{-5}$
$\bar{E}_s/\bar{E}_f = 1.5 \times 10^{-2}$
$\bar{E}_s/\bar{E}_f = 1.5 \times 10^{-1}$
$\varepsilon^0_{xx} = \varepsilon^0_{yy} = -5\%$
$\xi_1 : 0.851$
$\xi_2 : 0.851$
$\xi_1 : 0.616$
$\xi_2 : 0.615$
$\xi_1 : 0.251$
$\xi_2 : 0.285$
$f_A = 0$
$f_B = 0$
ξ_2
ξ_1
0
0.2
0.4
0.6
0.8
1
1.2

Figure(s)

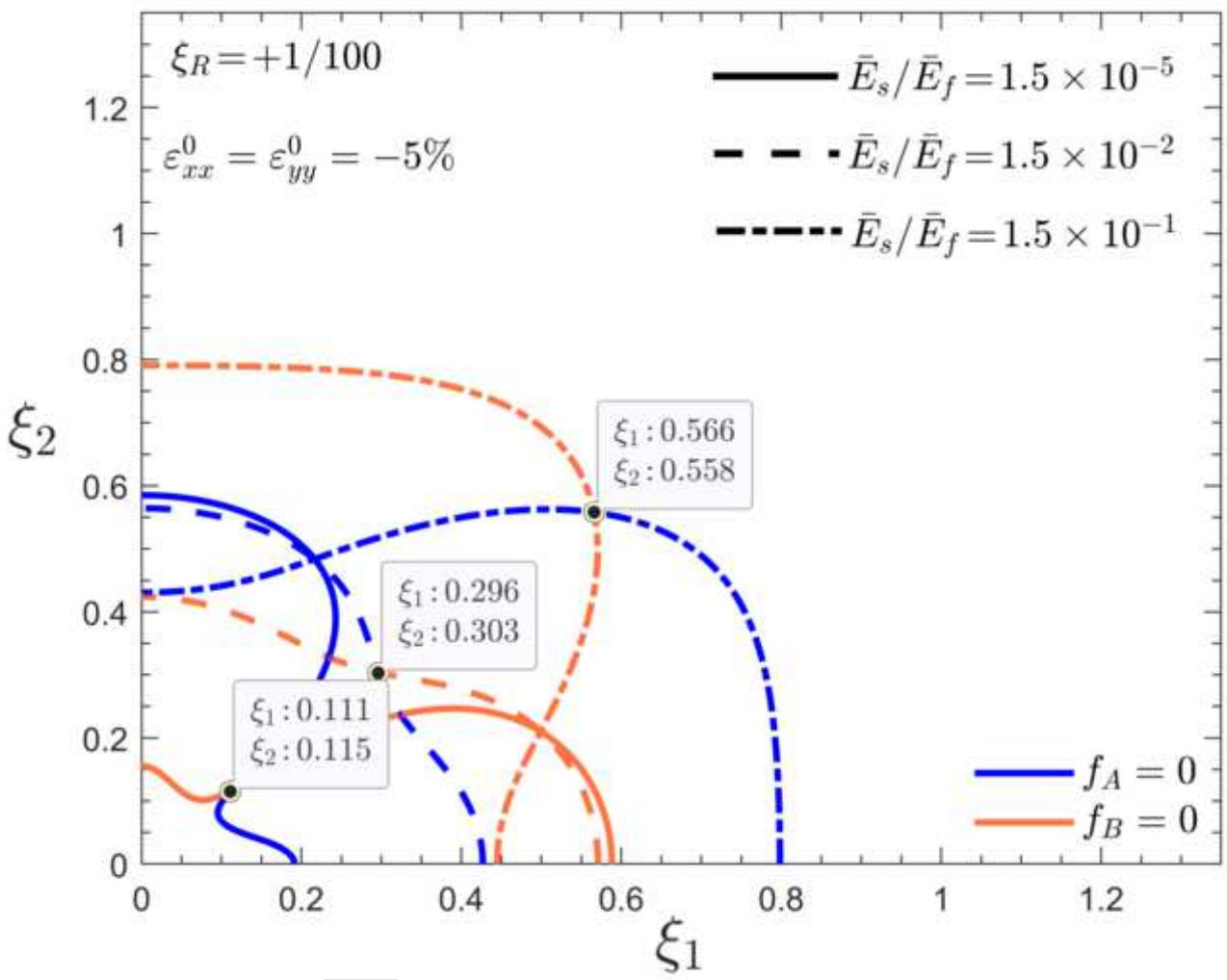
$\xi_R = +1/100$
$\varepsilon^0_{xx} = \varepsilon^0_{yy} = -5\%$
$\bar{E}_s/\bar{E}_f = 1.5 \times 10^{-5}$
$\bar{E}_s/\bar{E}_f = 1.5 \times 10^{-2}$
$\bar{E}_s/\bar{E}_f = 1.5 \times 10^{-1}$
$\xi_1 : 0.566$
$\xi_2 : 0.558$
$\xi_1 : 0.296$
$\xi_2 : 0.303$
$\xi_1 : 0.111$
$\xi_2 : 0.115$
$f_A = 0$
$f_B = 0$
ξ_2
ξ_1
0
0.2
0.4
0.6
0.8
1
1.2

Figure(s)

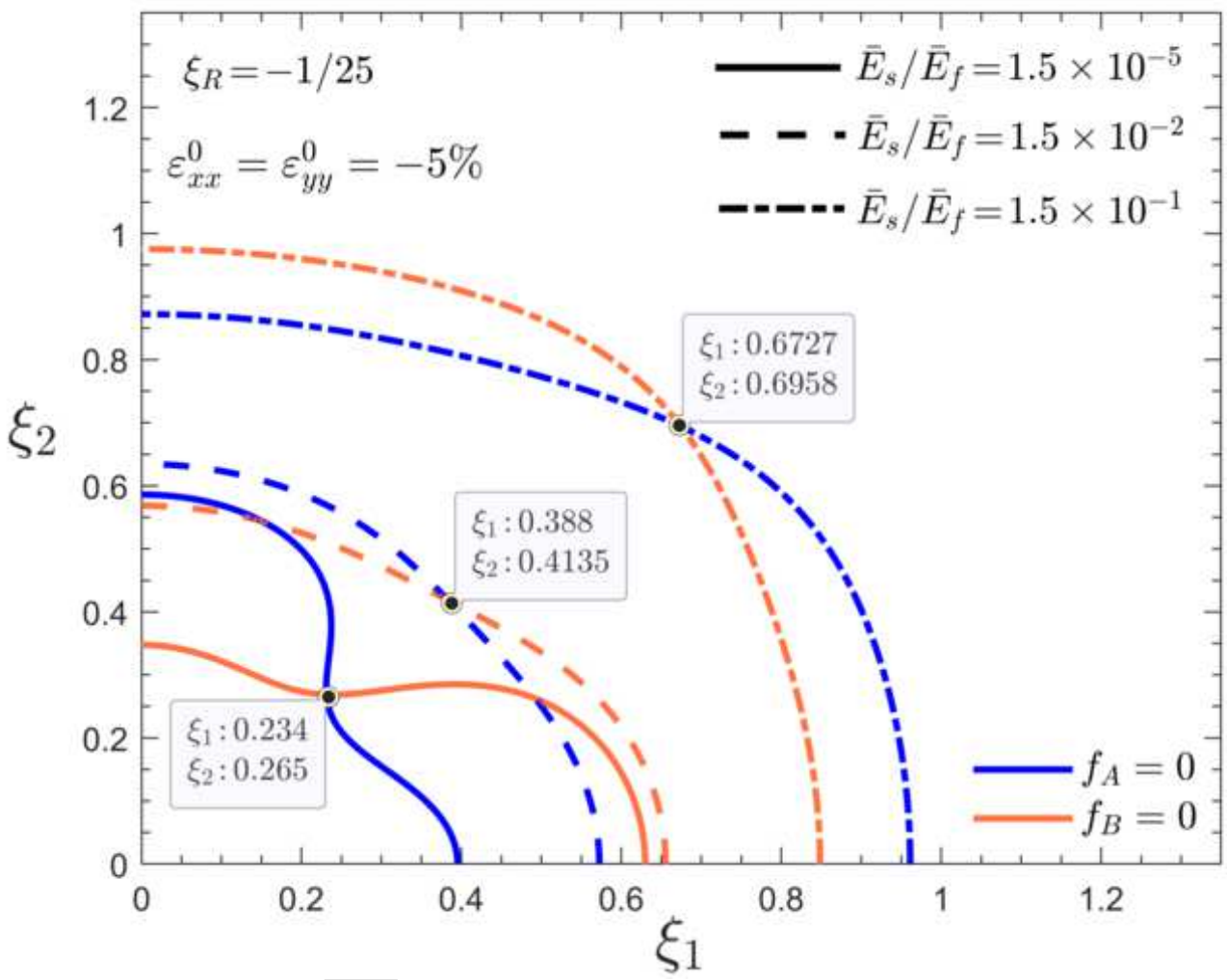
$\xi_R = -1/25$
$\varepsilon^0_{xx} = \varepsilon^0_{yy} = -5\%$
$\bar{E}_s/\bar{E}_f = 1.5 \times 10^{-5}$
$\bar{E}_s/\bar{E}_f = 1.5 \times 10^{-2}$
$\bar{E}_s/\bar{E}_f = 1.5 \times 10^{-1}$
$\xi_1 : 0.6727$
$\xi_2 : 0.6958$
$\xi_1 : 0.388$
$\xi_2 : 0.4135$
$\xi_1 : 0.234$
$\xi_2 : 0.265$
$f_A = 0$
$f_B = 0$
ξ_2
ξ_1
0
0.2
0.4
0.6
0.8
1
1.2

Figure(s)

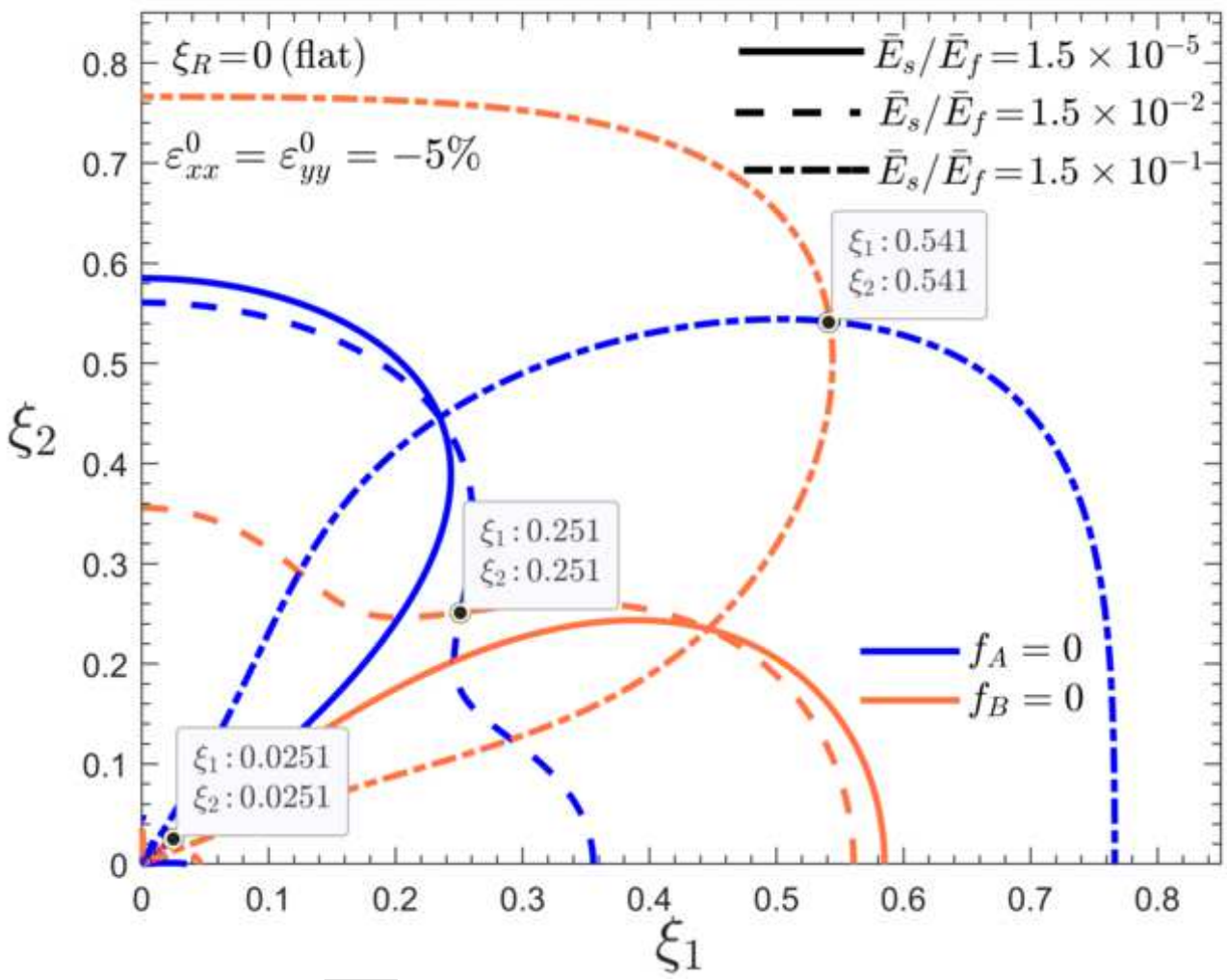
$\xi_R = 0$ (flat)
$\varepsilon^0_{xx} = \varepsilon^0_{yy} = -5\%$
$\bar{E}_s/\bar{E}_f = 1.5 \times 10^{-5}$
$\bar{E}_s/\bar{E}_f = 1.5 \times 10^{-2}$
$\bar{E}_s/\bar{E}_f = 1.5 \times 10^{-1}$
$\xi_1 : 0.541$
$\xi_2 : 0.541$
$\xi_1 : 0.251$
$\xi_2 : 0.251$
$\xi_1 : 0.0251$
$\xi_2 : 0.0251$
$f_A = 0$
$f_B = 0$
ξ_2
ξ_1
0
0.1
0.2
0.3
0.4
0.5
0.6
0.7
0.8

Figure(s)

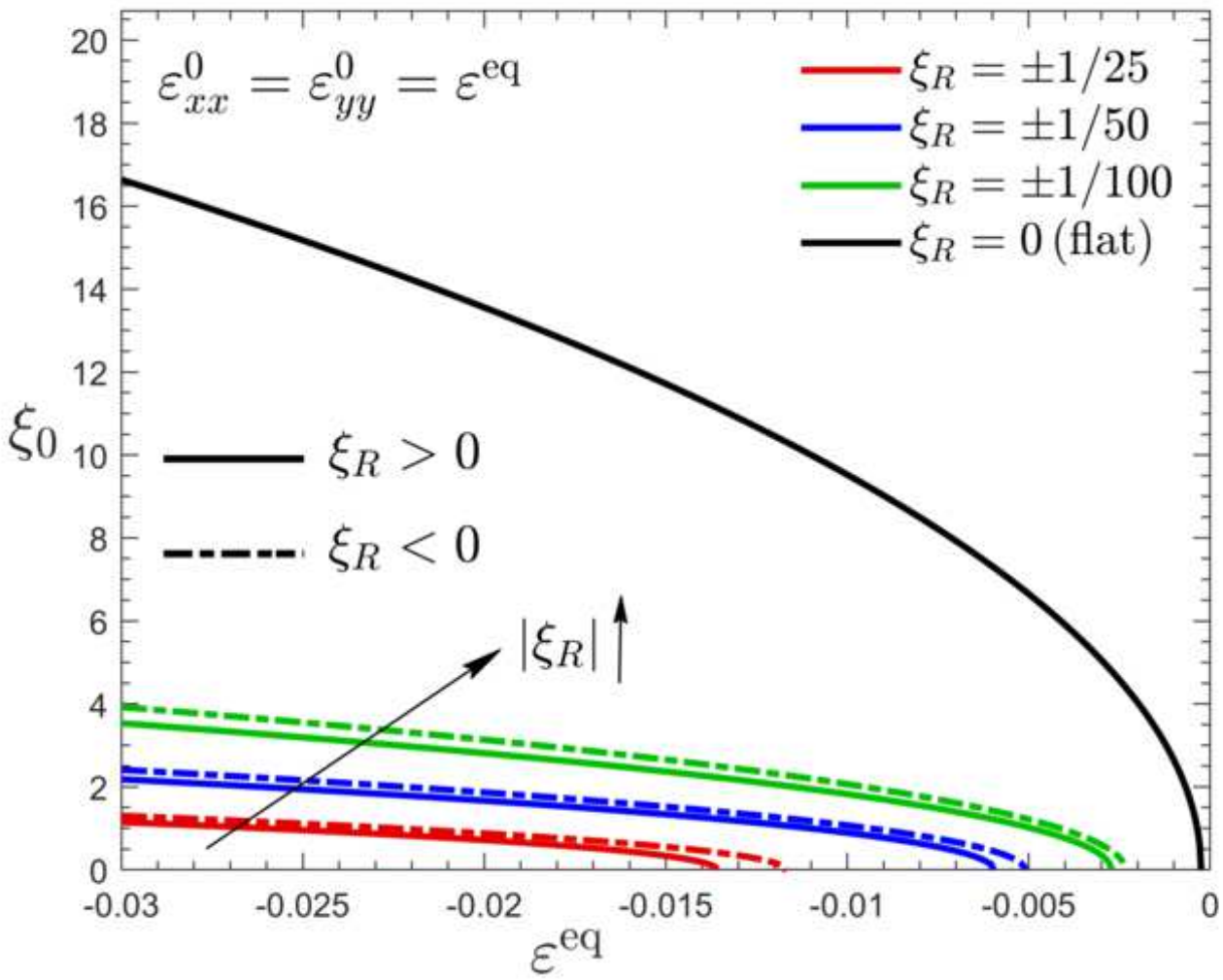
$\varepsilon^0_{xx} = \varepsilon^0_{yy} = \varepsilon^{\mathrm{eq}}$
$\xi_R = \pm 1/25$
$\xi_R = \pm 1/50$
$\xi_R = \pm 1/100$
$\xi_R = 0$ (flat)
$\xi_R > 0$
$\xi_R < 0$
$|\xi_R|$
ξ_0
$\varepsilon^{\mathrm{eq}}$
20
18
16
14
12
10
8
6
4
2
0
-0.03
-0.025
-0.02
-0.015
-0.01
-0.005
0

Figure(s)

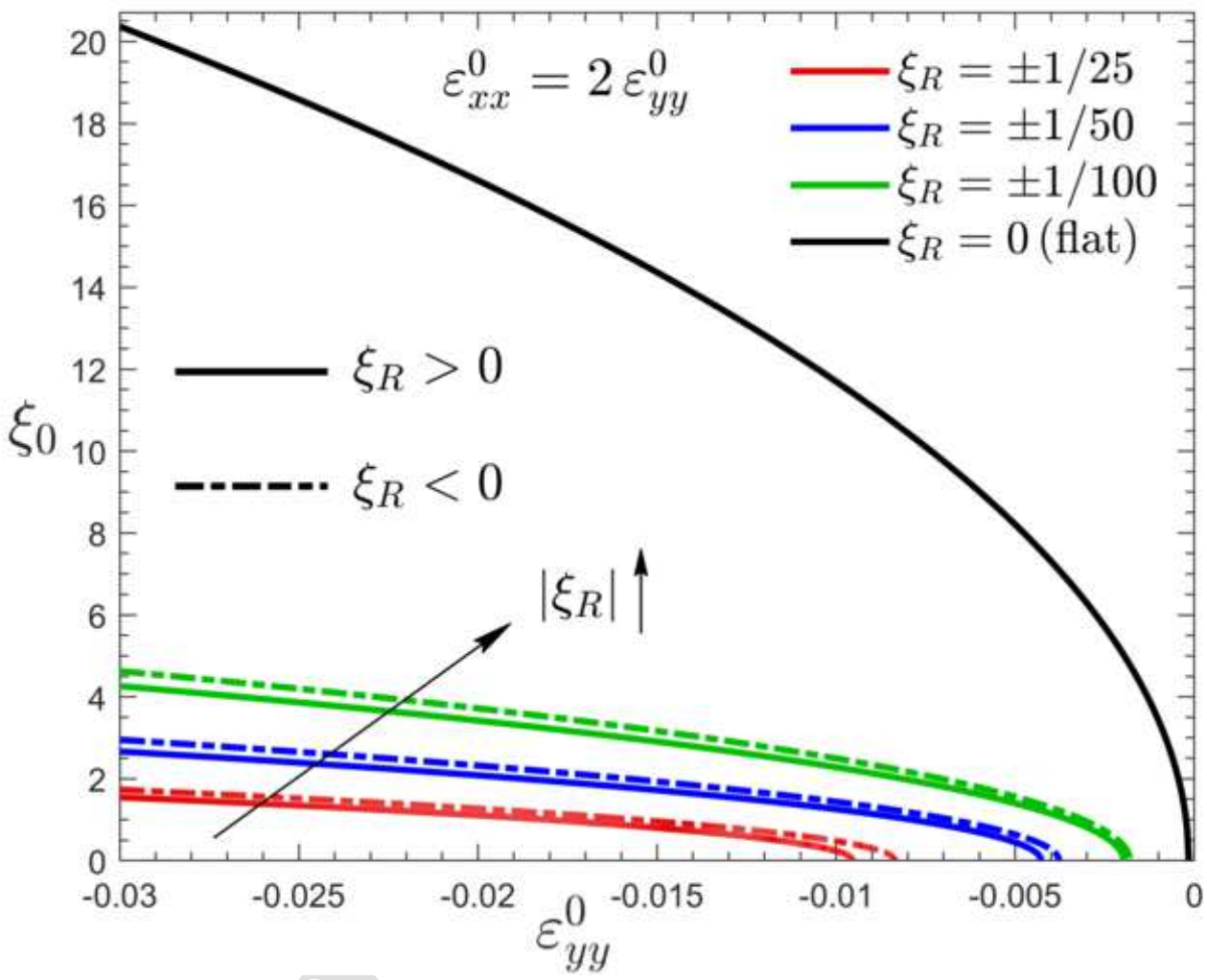
$\varepsilon^0_{xx} = 2\,\varepsilon^0_{yy}$
$\xi_R = \pm 1/25$
$\xi_R = \pm 1/50$
$\xi_R = \pm 1/100$
$\xi_R = 0$ (flat)
$\xi_R > 0$
$\xi_R < 0$
$|\xi_R|$
ξ_0
ε^0_{yy}
20
18
16
14
12
10
8
6
4
2
0
-0.03
-0.025
-0.02
-0.015
-0.01
-0.005
0

Figure(s)

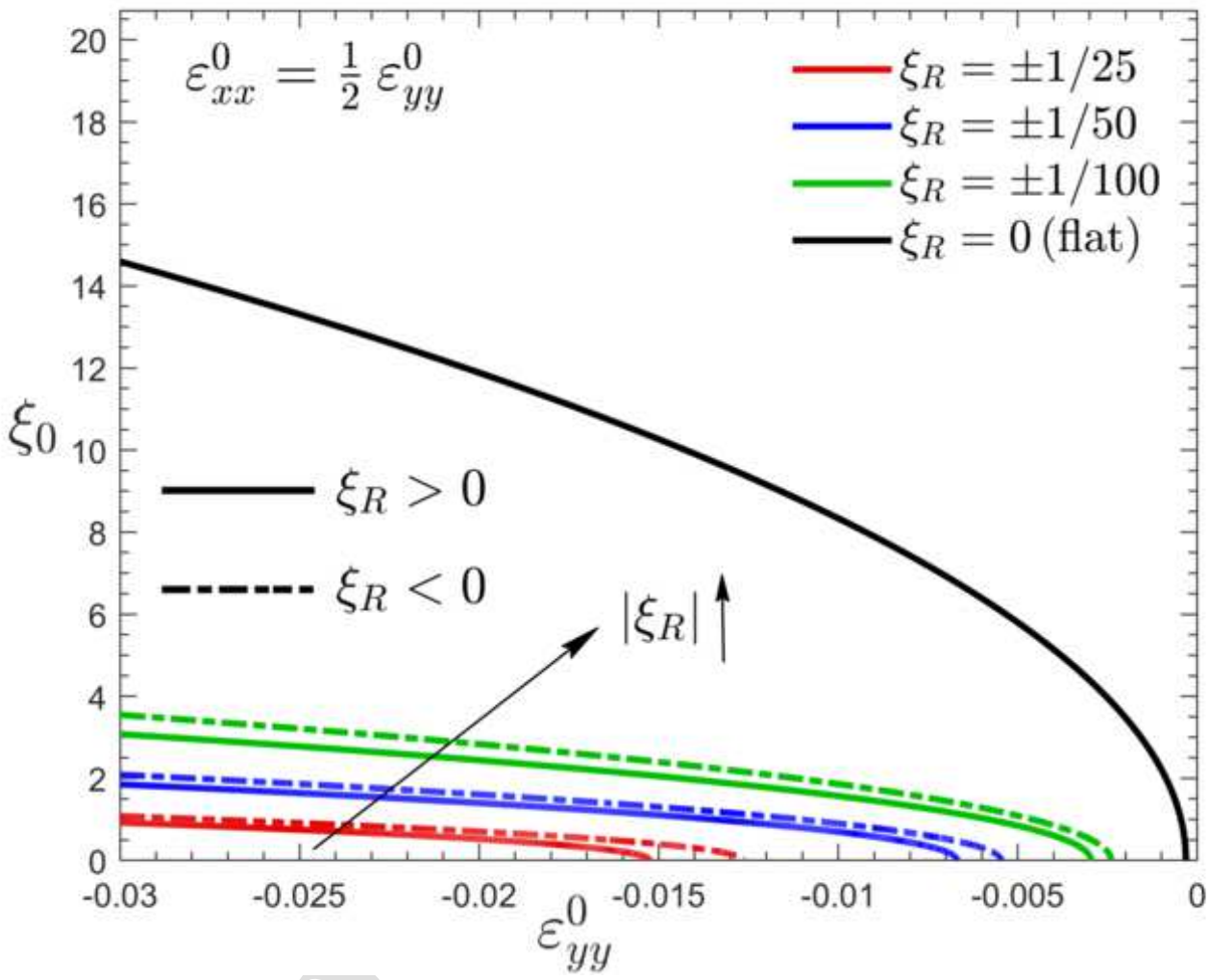
$\varepsilon^0_{xx} = \frac{1}{2}\,\varepsilon^0_{yy}$
$\xi_R = \pm 1/25$
$\xi_R = \pm 1/50$
$\xi_R = \pm 1/100$
$\xi_R = 0$ (flat)
$\xi_R > 0$
$\xi_R < 0$
$|\xi_R|$
ξ_0
ε^0_{yy}
20
18
16
14
12
10
8
6
4
2
0
-0.03
-0.025
-0.02
-0.015
-0.01
-0.005
0

Figure(s)

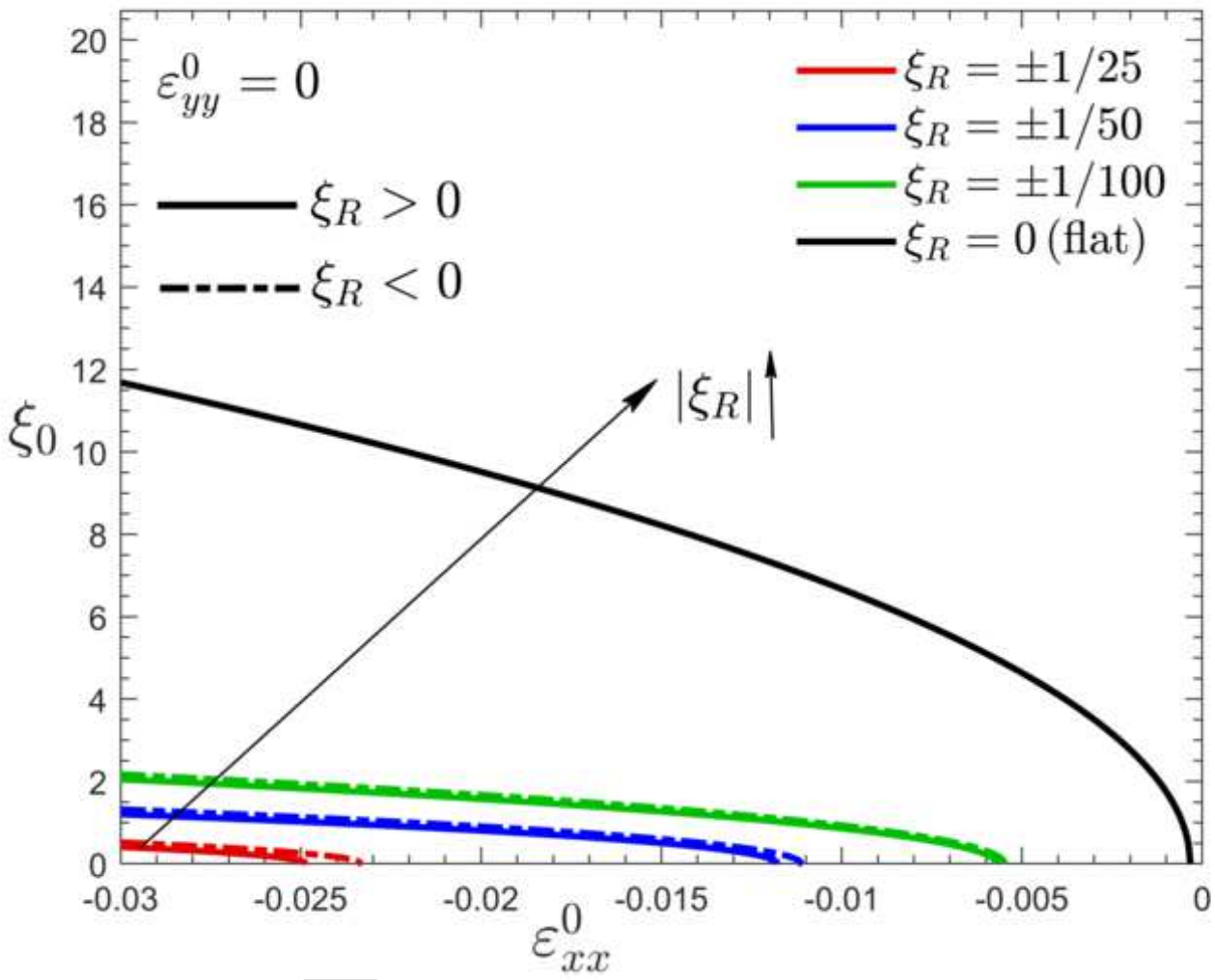
$\varepsilon^0_{yy} = 0$
$\xi_R > 0$
$\xi_R < 0$
$\xi_R = \pm 1/25$
$\xi_R = \pm 1/50$
$\xi_R = \pm 1/100$
$\xi_R = 0$ (flat)
$|\xi_R|$
ξ_0
ε^0_{xx}
20
18
16
14
12
10
8
6
4
2
0
-0.03
-0.025
-0.02
-0.015
-0.01
-0.005
0

Figure(s)

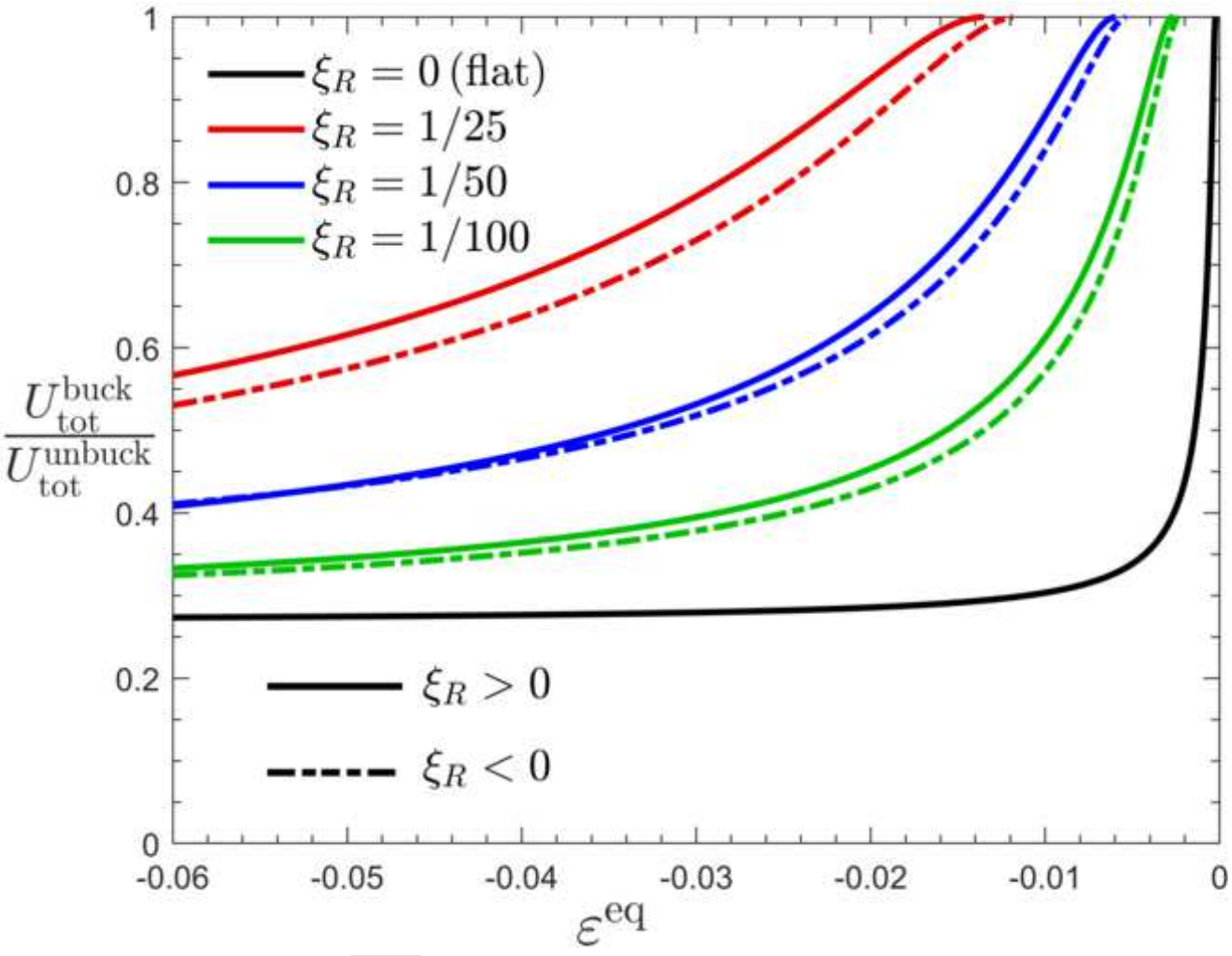
$\xi_R = 0$ (flat)
$\xi_R = 1/25$
$\xi_R = 1/50$
$\xi_R = 1/100$
$\xi_R > 0$
$\xi_R < 0$
$\frac{U_{\text{tot}}^{\text{buck}}}{U_{\text{tot}}^{\text{unbuck}}}$
ε^{eq}
1
0.8
0.6
0.4
0.2
0
-0.06
-0.05
-0.04
-0.03
-0.02
-0.01
0

Figure(s)

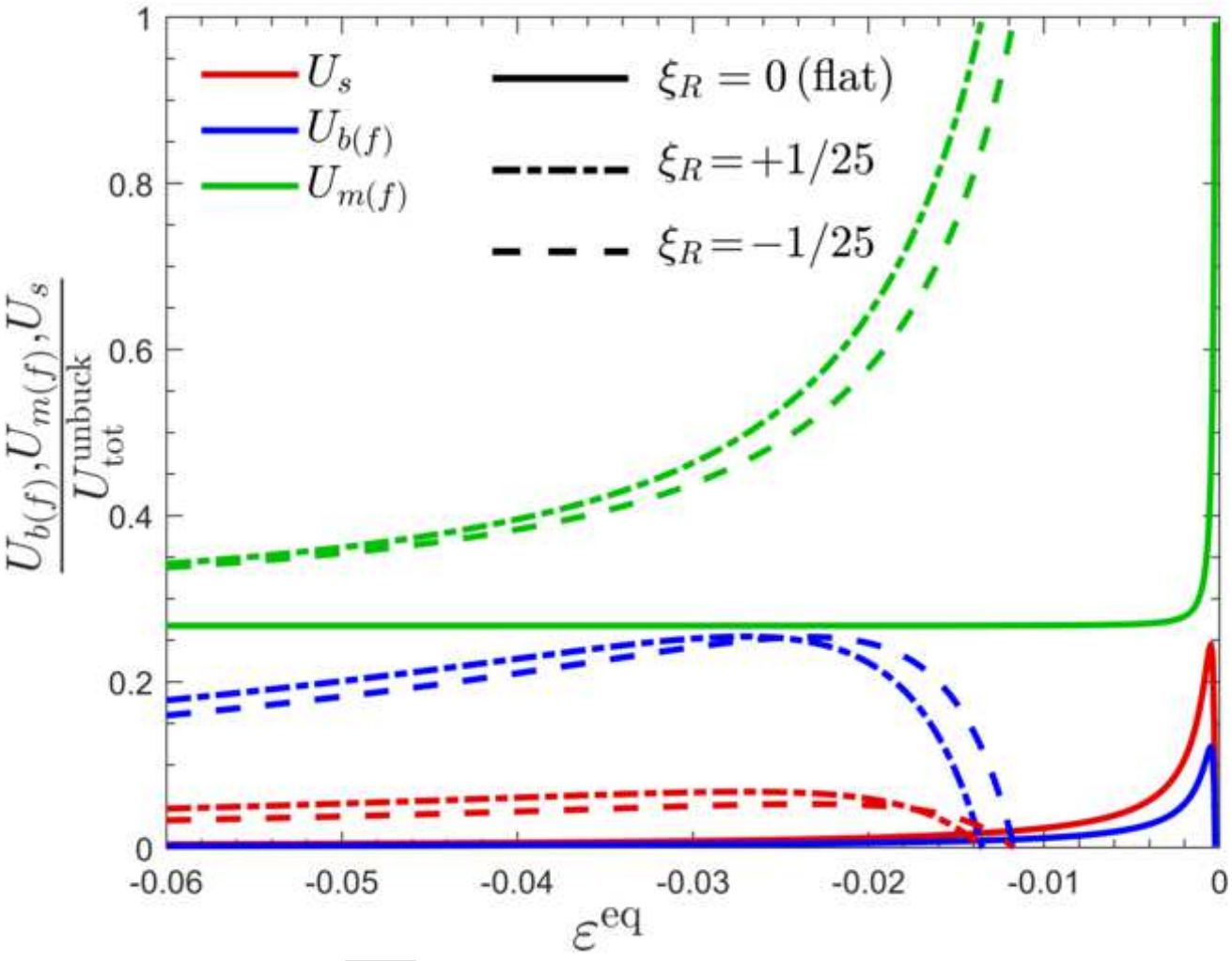

Figure(s)

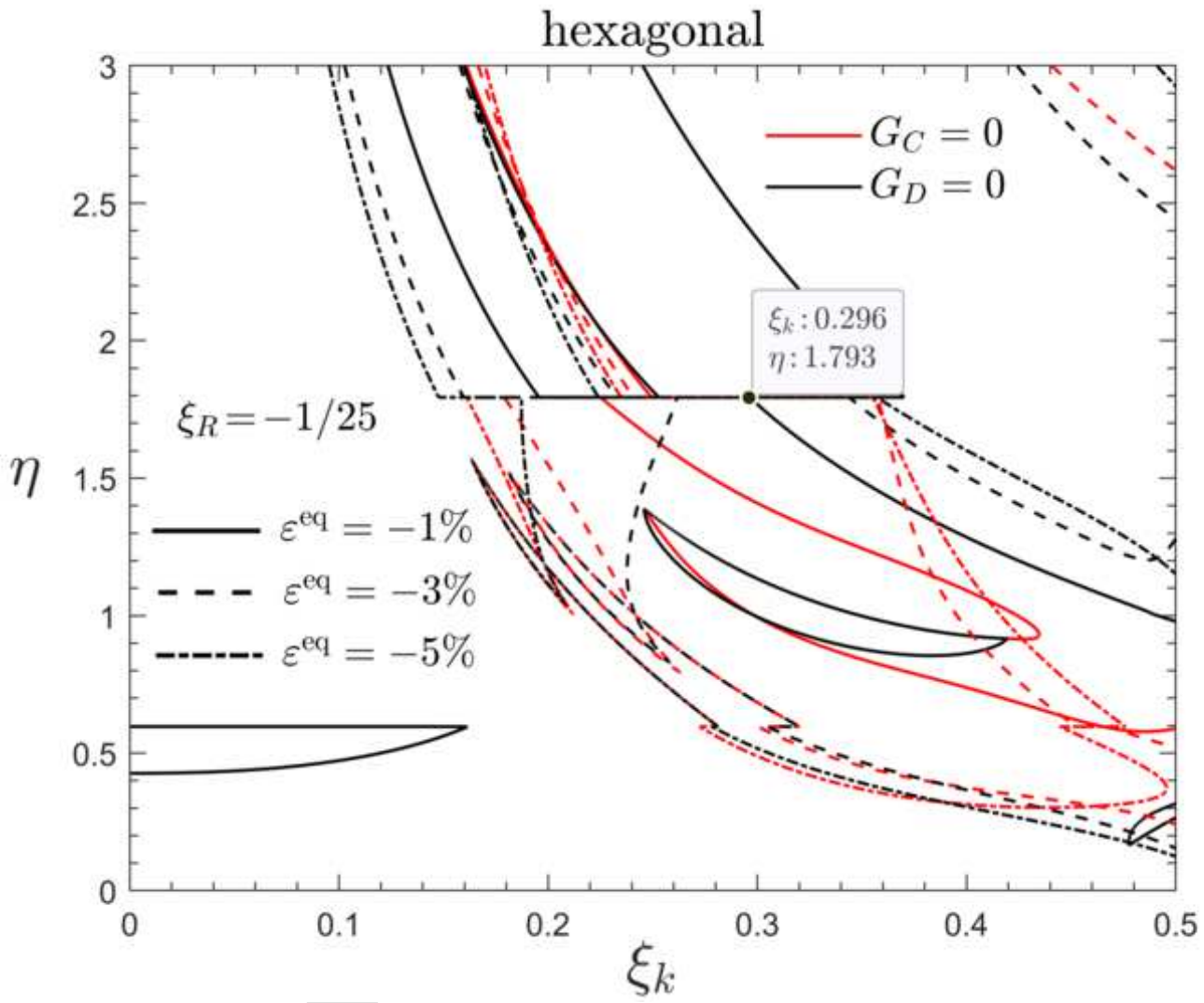
hexagonal
$G_C = 0$
$G_D = 0$
ξ_k : 0.296
η : 1.793
$\xi_R = -1/25$
$\varepsilon^{eq} = -1\%$
$\varepsilon^{eq} = -3\%$
$\varepsilon^{eq} = -5\%$
η
ξ_k
0
0.1
0.2
0.3
0.4
0.5
0.5
1
1.5
2
2.5
3

Figure(s)

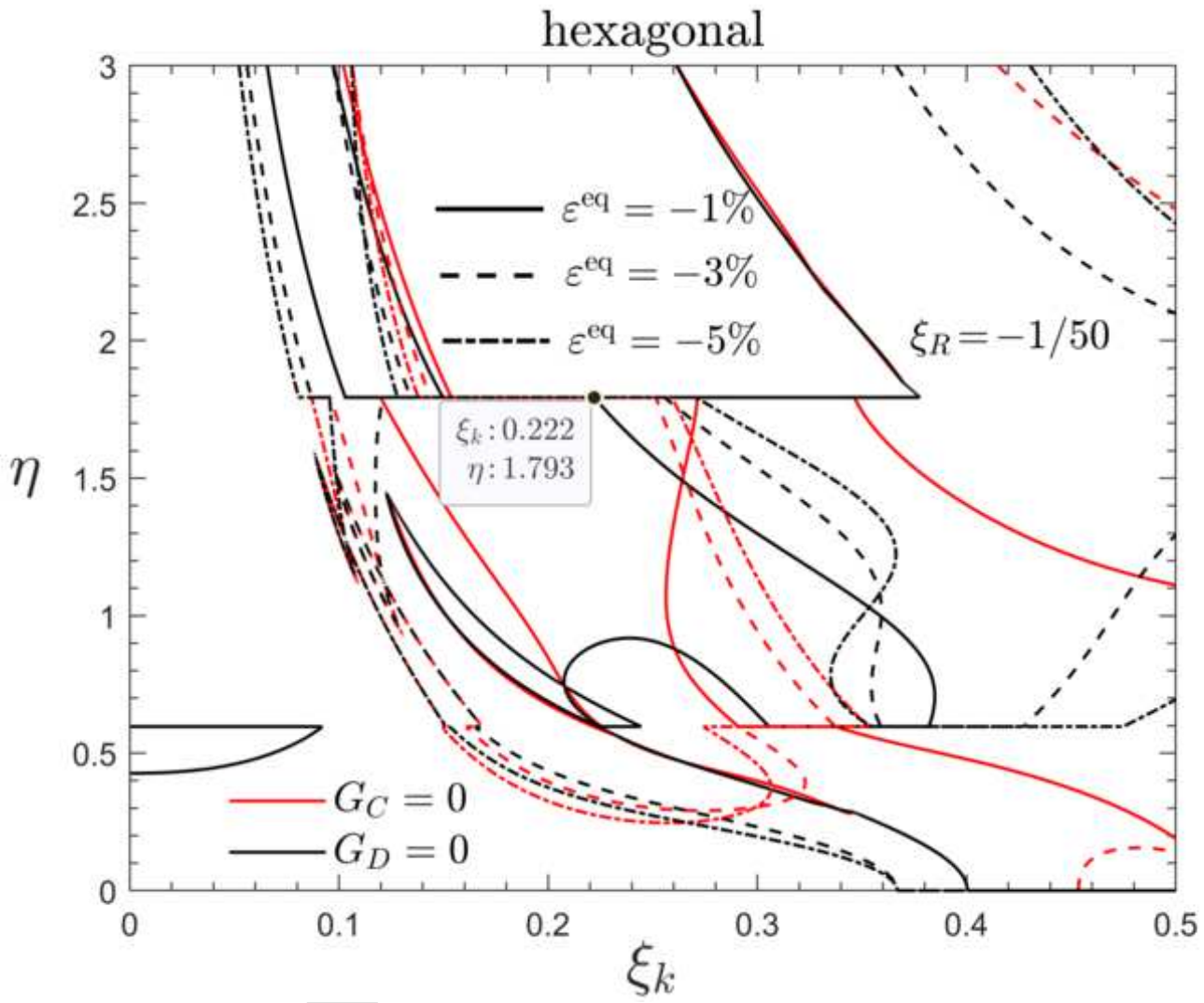

Figure(s)

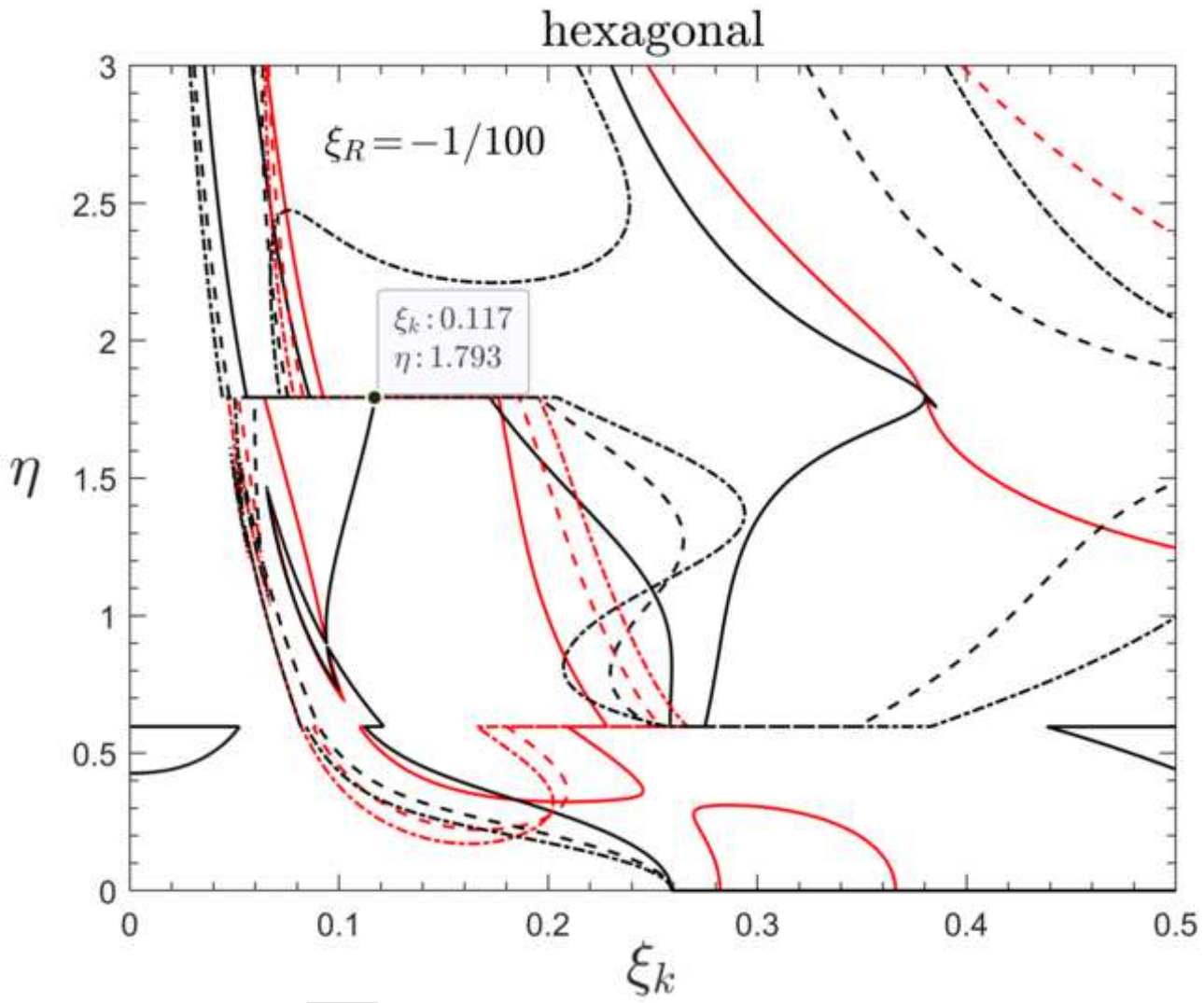

Figure(s)

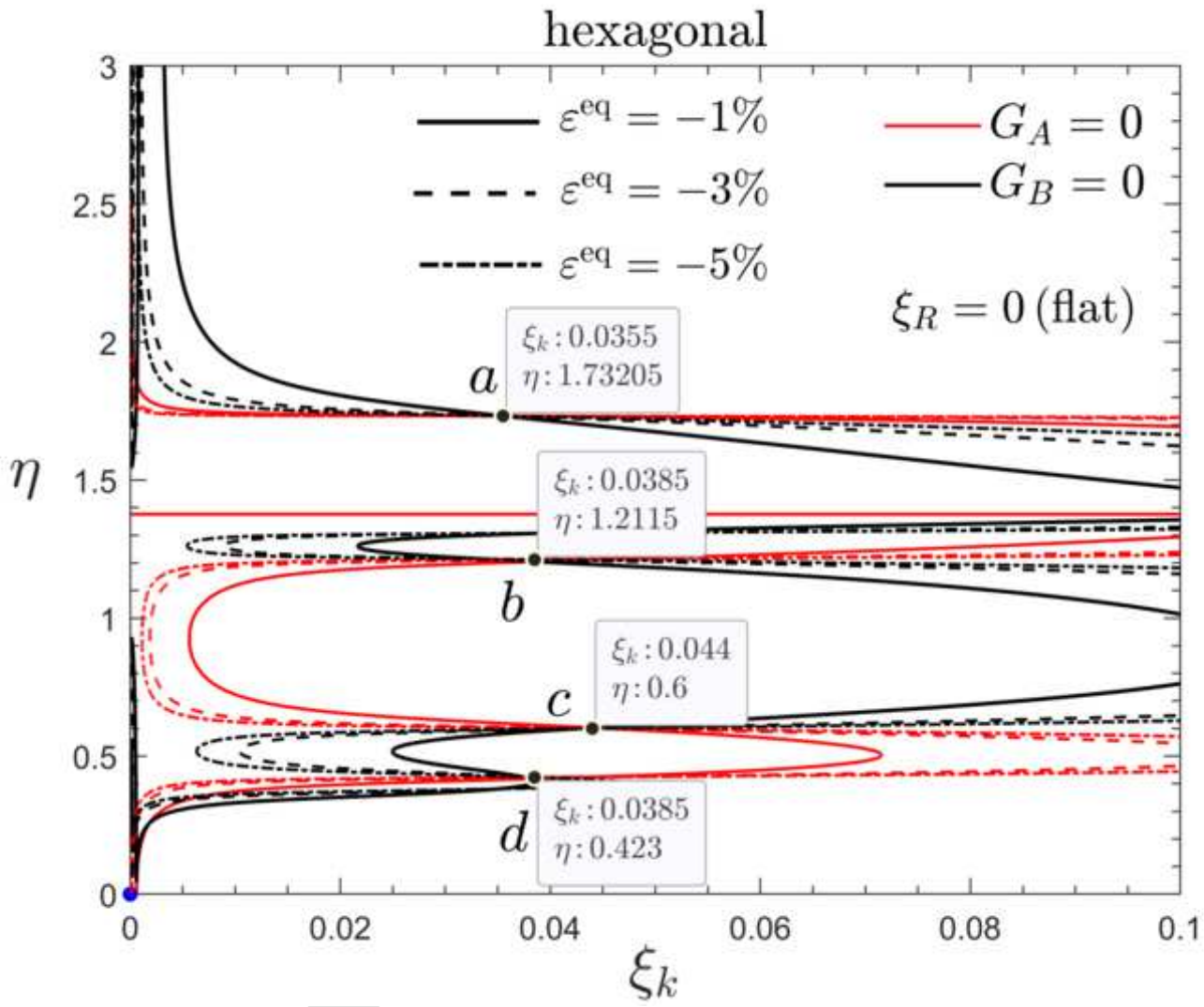
hexagonal
$\varepsilon^{\mathrm{eq}} = -1\%$
$\varepsilon^{\mathrm{eq}} = -3\%$
$\varepsilon^{\mathrm{eq}} = -5\%$
$G_A = 0$
$G_B = 0$
$\xi_R = 0$ (flat)
ξ_k : 0.0355
η : 1.73205
a
ξ_k : 0.0385
η : 1.2115
b
ξ_k : 0.044
η : 0.6
c
ξ_k : 0.0385
η : 0.423
d
η
ξ_k
0
0.5
1
1.5
2
2.5
3
0.02
0.04
0.06
0.08
0.1

Figure(s)

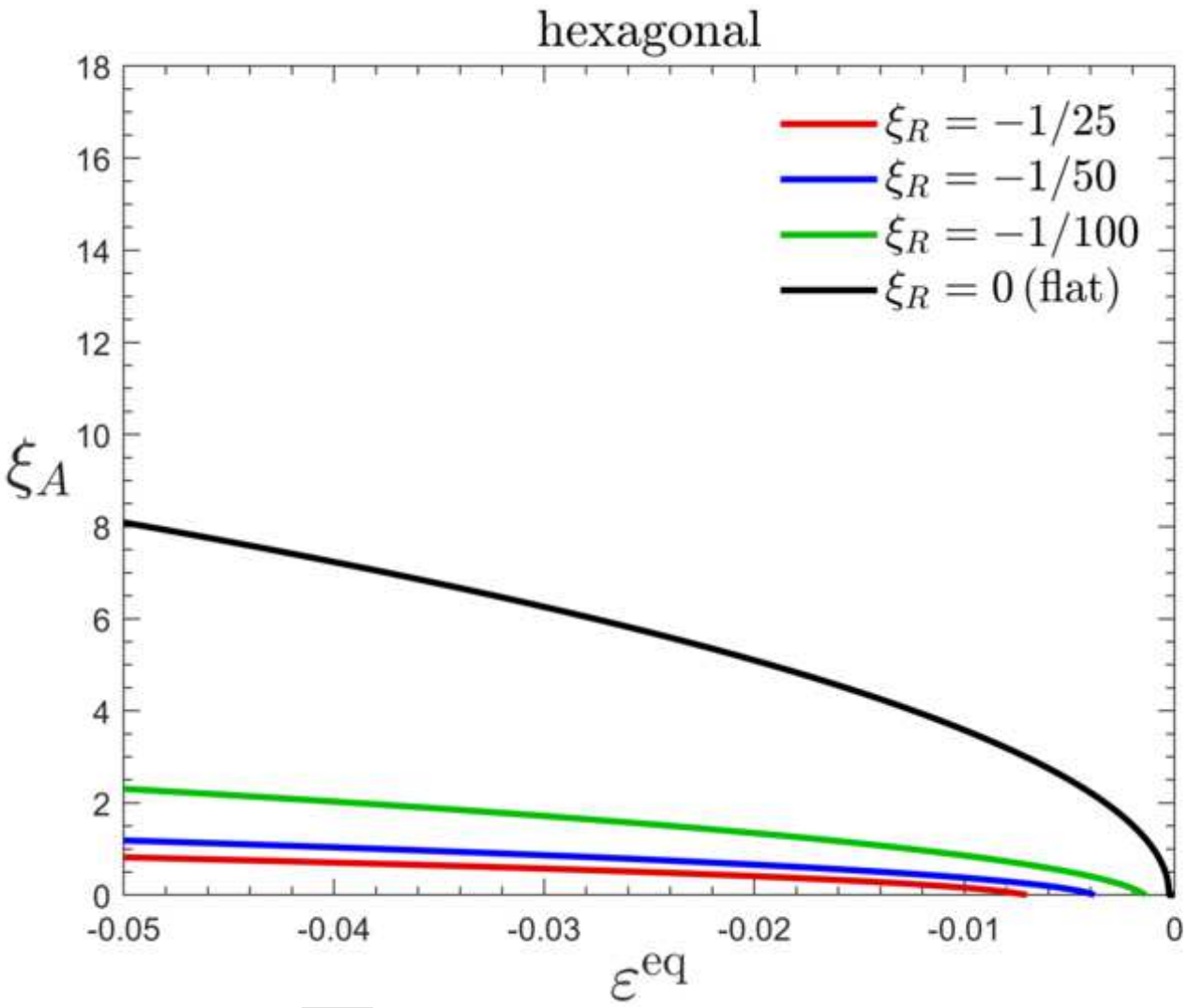

Figure(s)

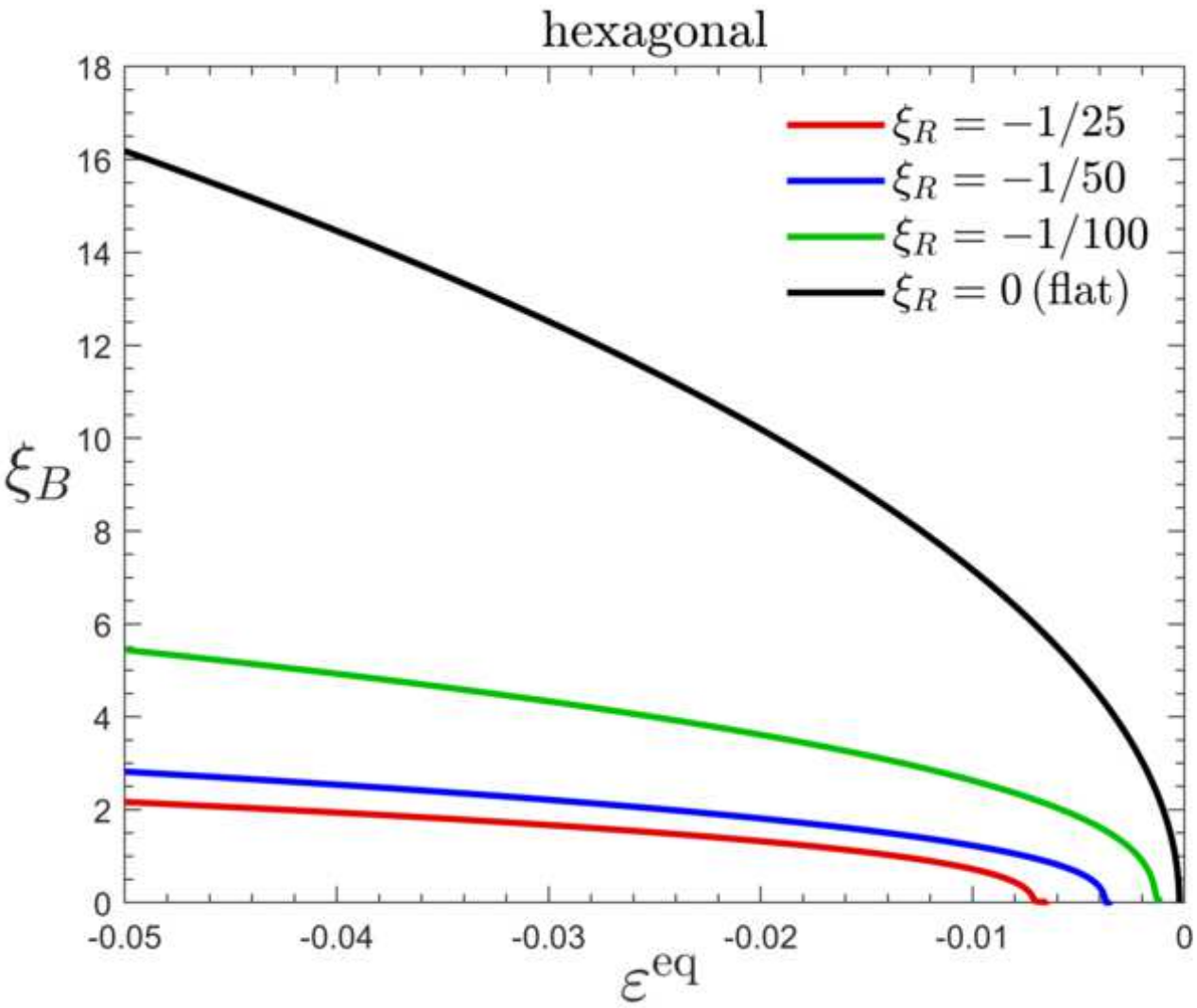

Figure(s)

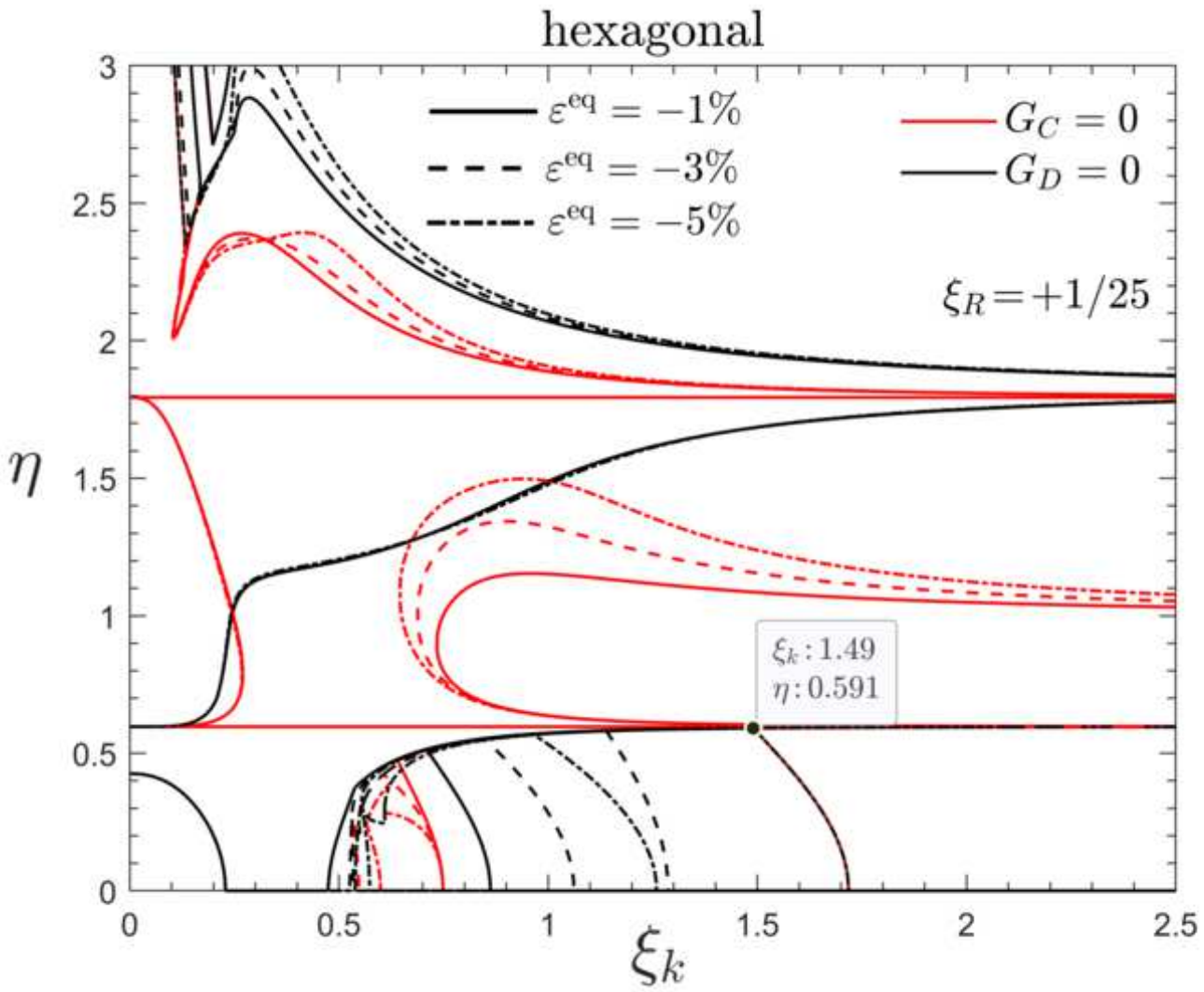

Figure(s)

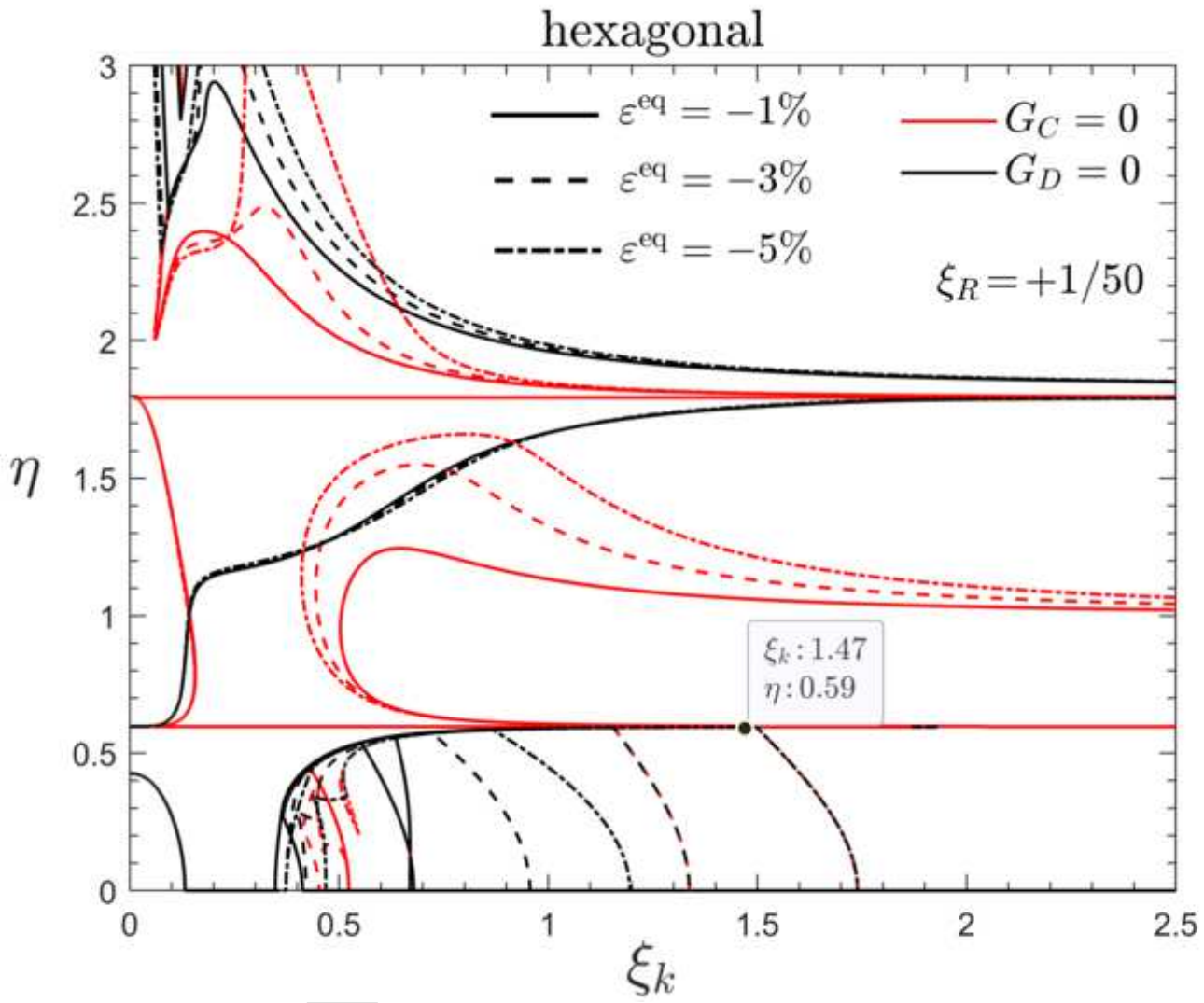

Figure(s)

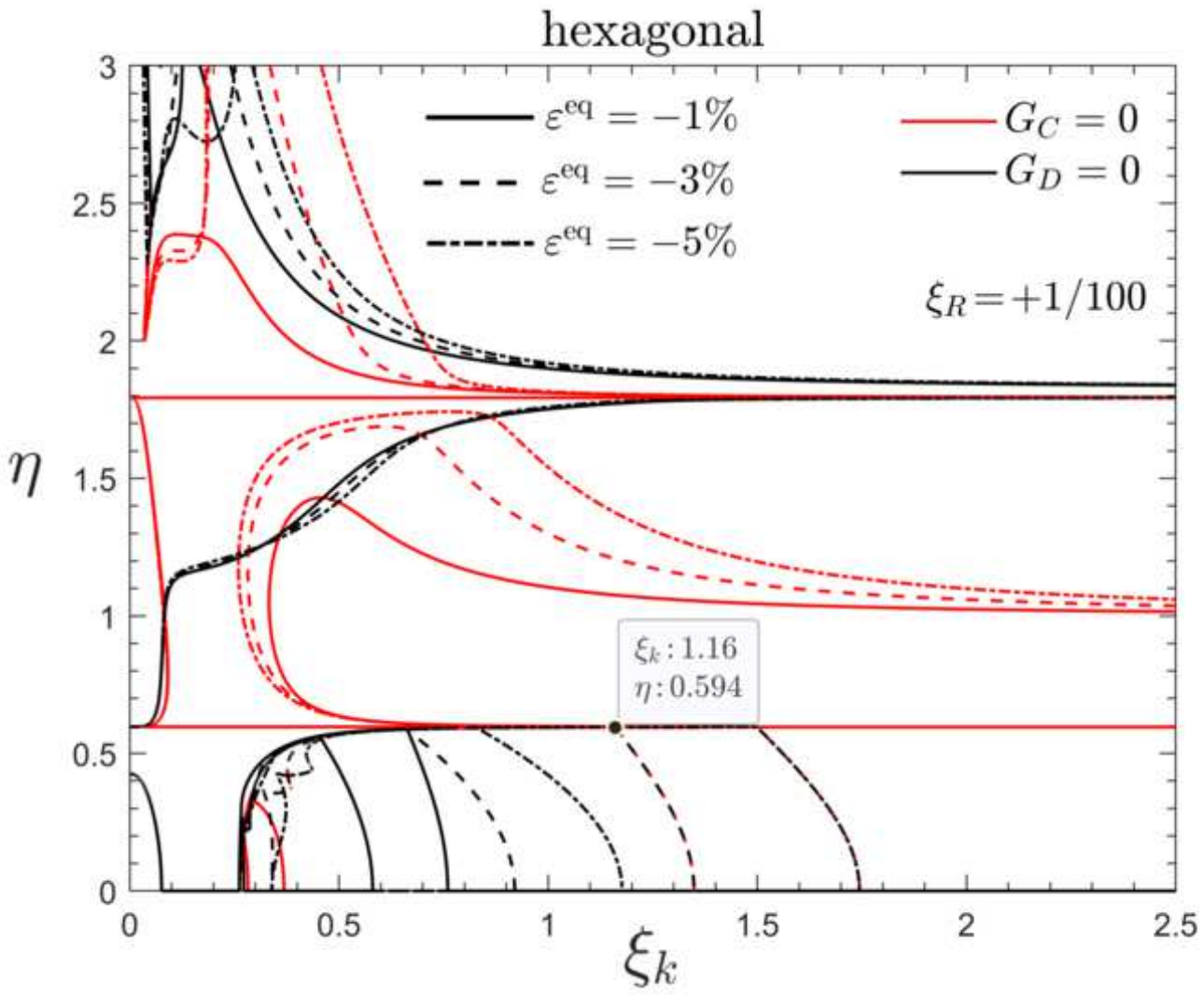

Figure(s)

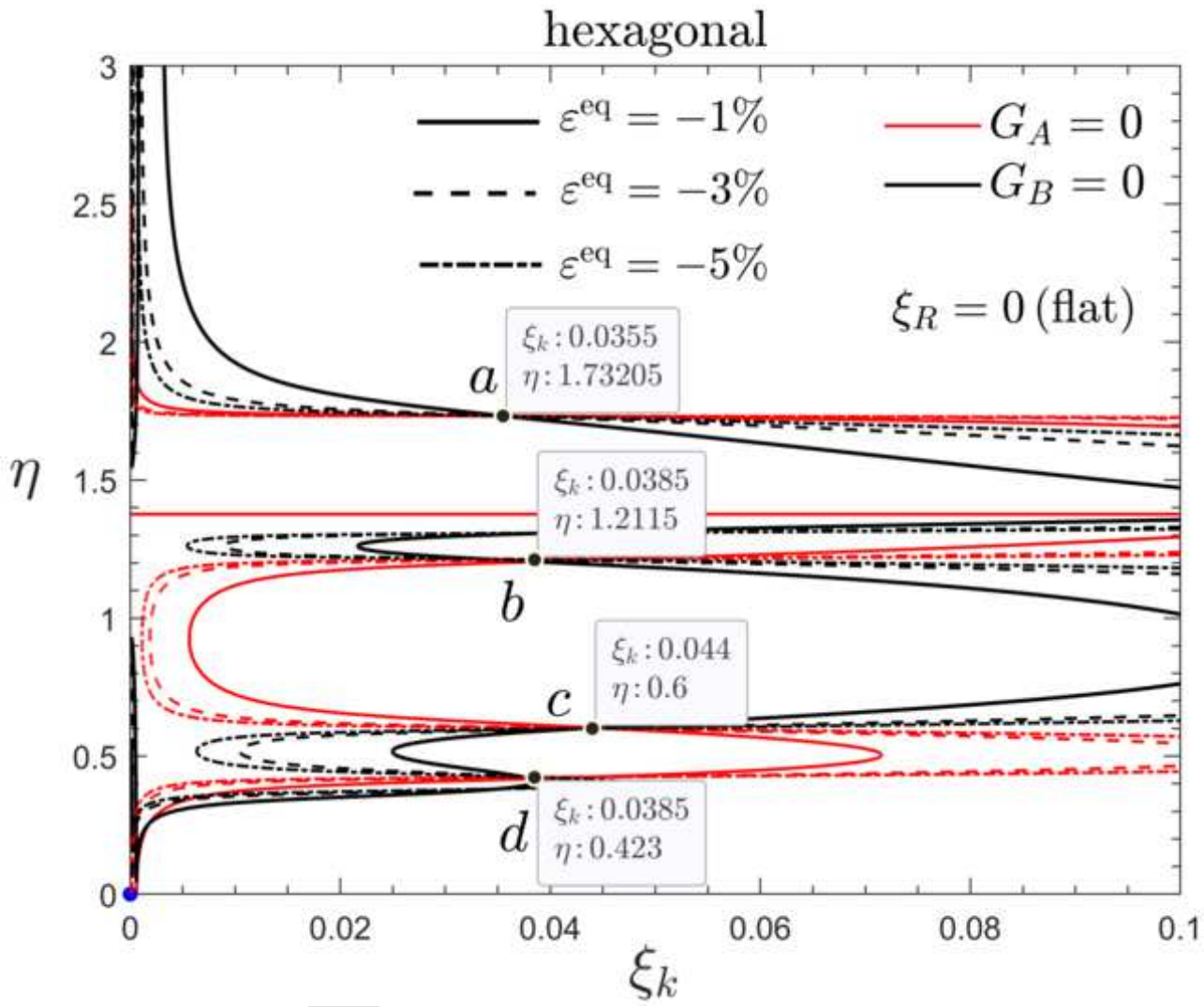
hexagonal
$\varepsilon^{\mathrm{eq}} = -1\%$
$\varepsilon^{\mathrm{eq}} = -3\%$
$\varepsilon^{\mathrm{eq}} = -5\%$
$G_A = 0$
$G_B = 0$
$\xi_R = 0$ (flat)
ξ_k : 0.0355
η : 1.73205
a
ξ_k : 0.0385
η : 1.2115
b
ξ_k : 0.044
η : 0.6
c
ξ_k : 0.0385
η : 0.423
d
η
ξ_k
0
0.5
1
1.5
2
2.5
3
0.02
0.04
0.06
0.08
0.1

Figure(s)

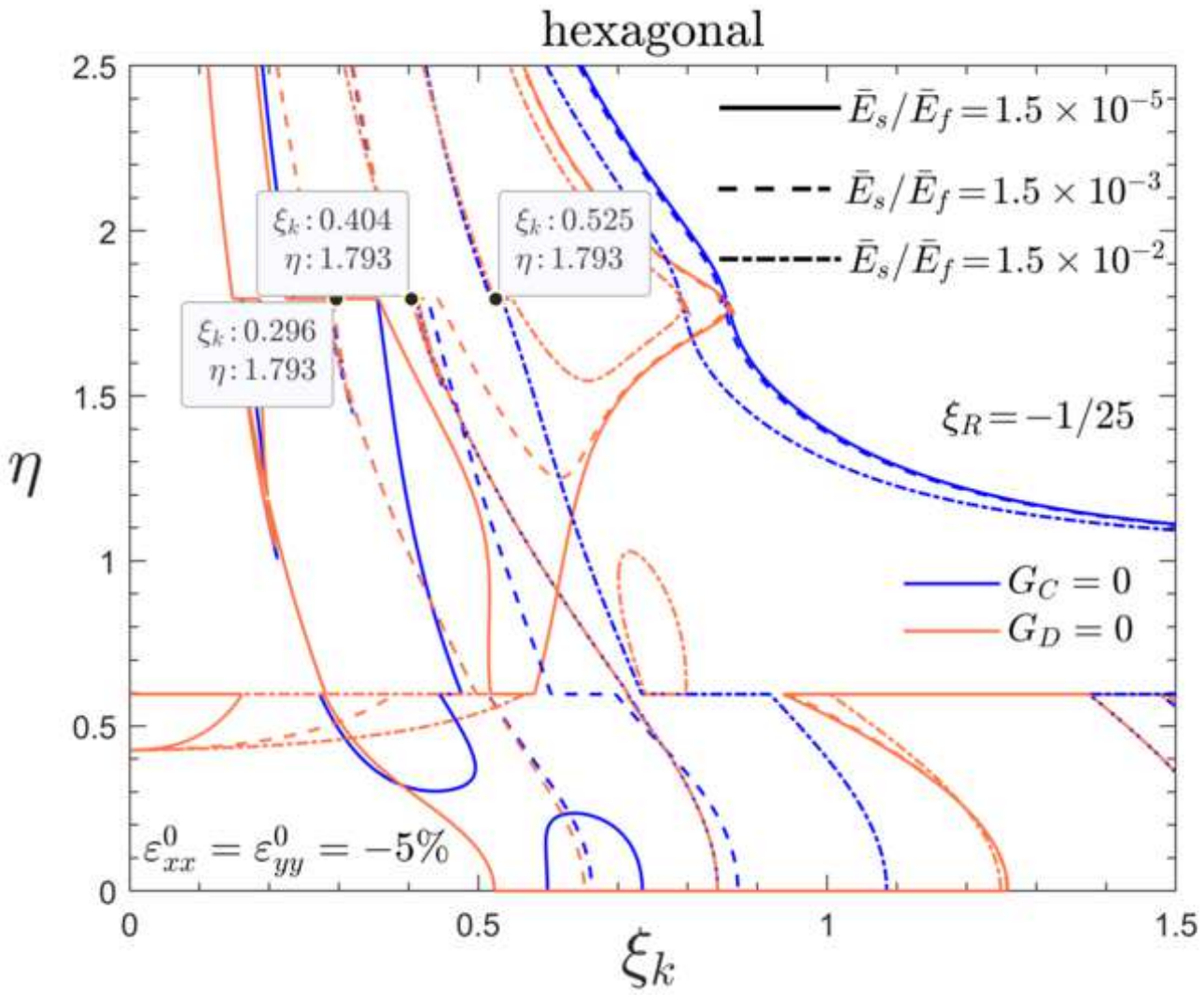
hexagonal
$\bar{E}_s/\bar{E}_f = 1.5 \times 10^{-5}$
$\bar{E}_s/\bar{E}_f = 1.5 \times 10^{-3}$
$\bar{E}_s/\bar{E}_f = 1.5 \times 10^{-2}$
$\xi_k: 0.404$
$\eta: 1.793$
$\xi_k: 0.525$
$\eta: 1.793$
$\xi_k: 0.296$
$\eta: 1.793$
$\xi_R = -1/25$
$G_C = 0$
$G_D = 0$
$\varepsilon^0_{xx} = \varepsilon^0_{yy} = -5\%$
η
ξ_k
0
0.5
1
1.5
2
2.5

Figure(s)

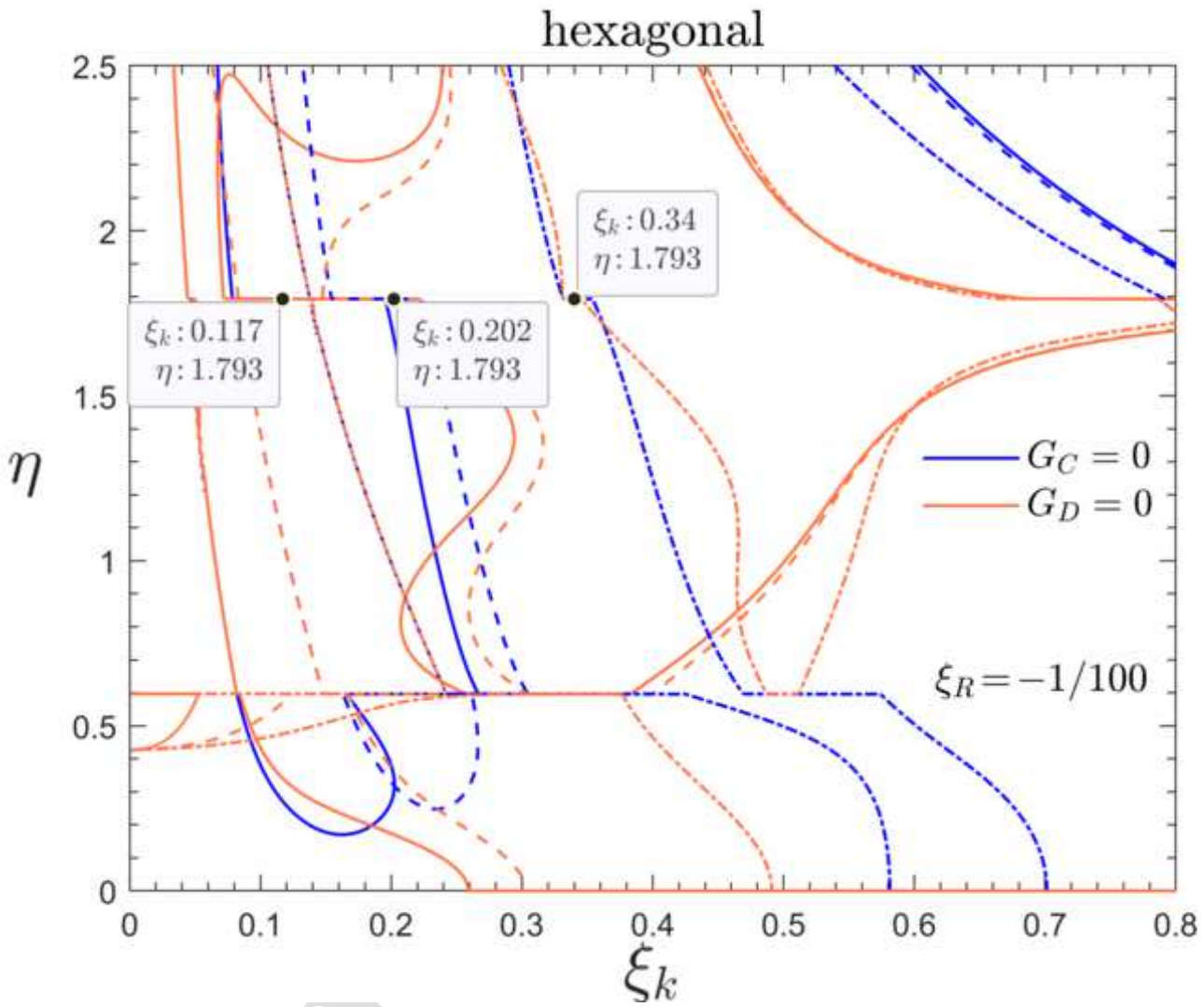

Figure(s)

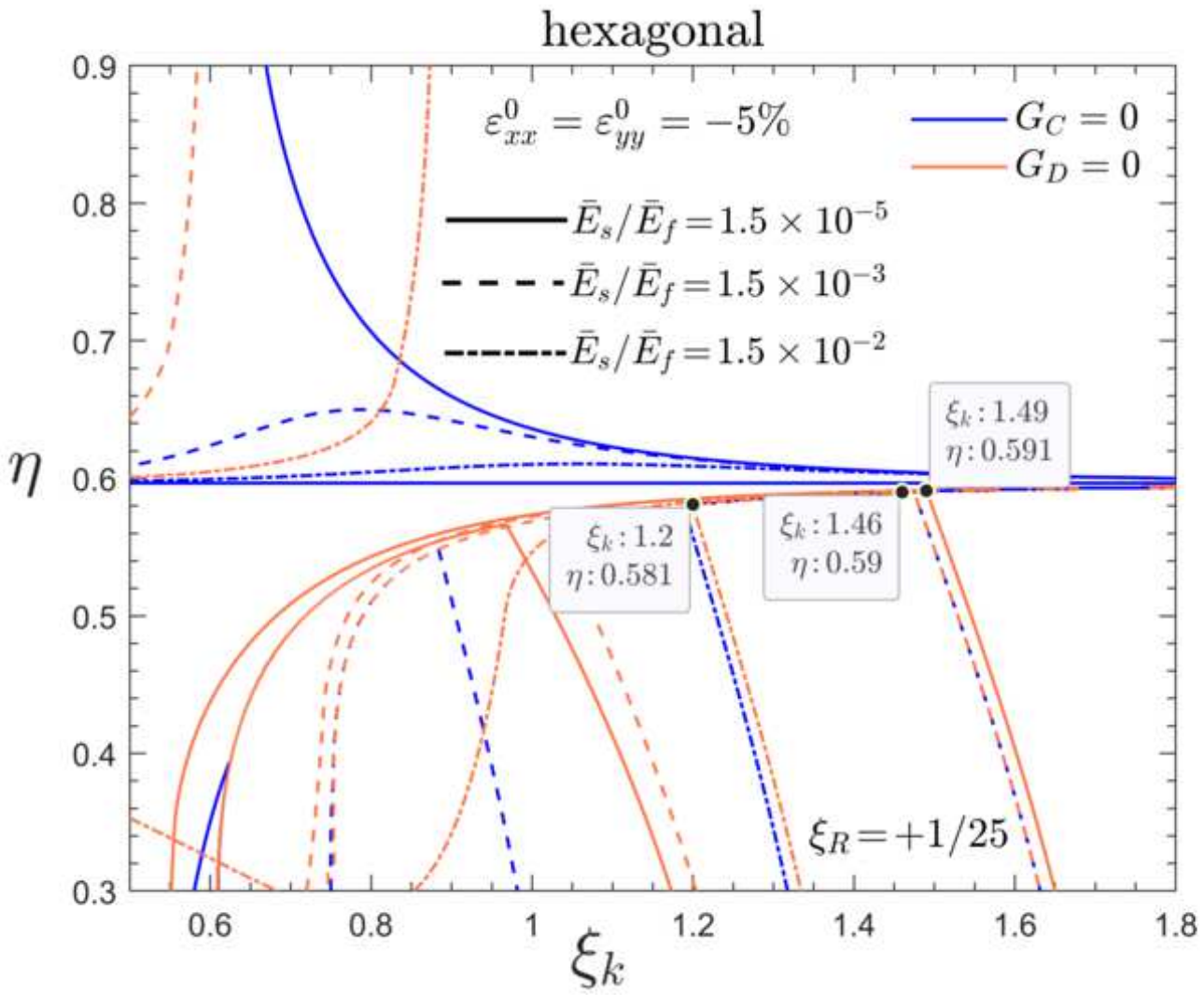
hexagonal
$\varepsilon^0_{xx} = \varepsilon^0_{yy} = -5\%$
$G_C = 0$
$G_D = 0$
$\bar{E}_s/\bar{E}_f = 1.5 \times 10^{-5}$
$\bar{E}_s/\bar{E}_f = 1.5 \times 10^{-3}$
$\bar{E}_s/\bar{E}_f = 1.5 \times 10^{-2}$
ξ_k: 1.49
η: 0.591
ξ_k: 1.2
η: 0.581
ξ_k: 1.46
η: 0.59
$\xi_R = +1/25$
η
ξ_k
0.9
0.8
0.7
0.6
0.5
0.4
0.3
0.6
0.8
1
1.2
1.4
1.6
1.8

Figure(s)

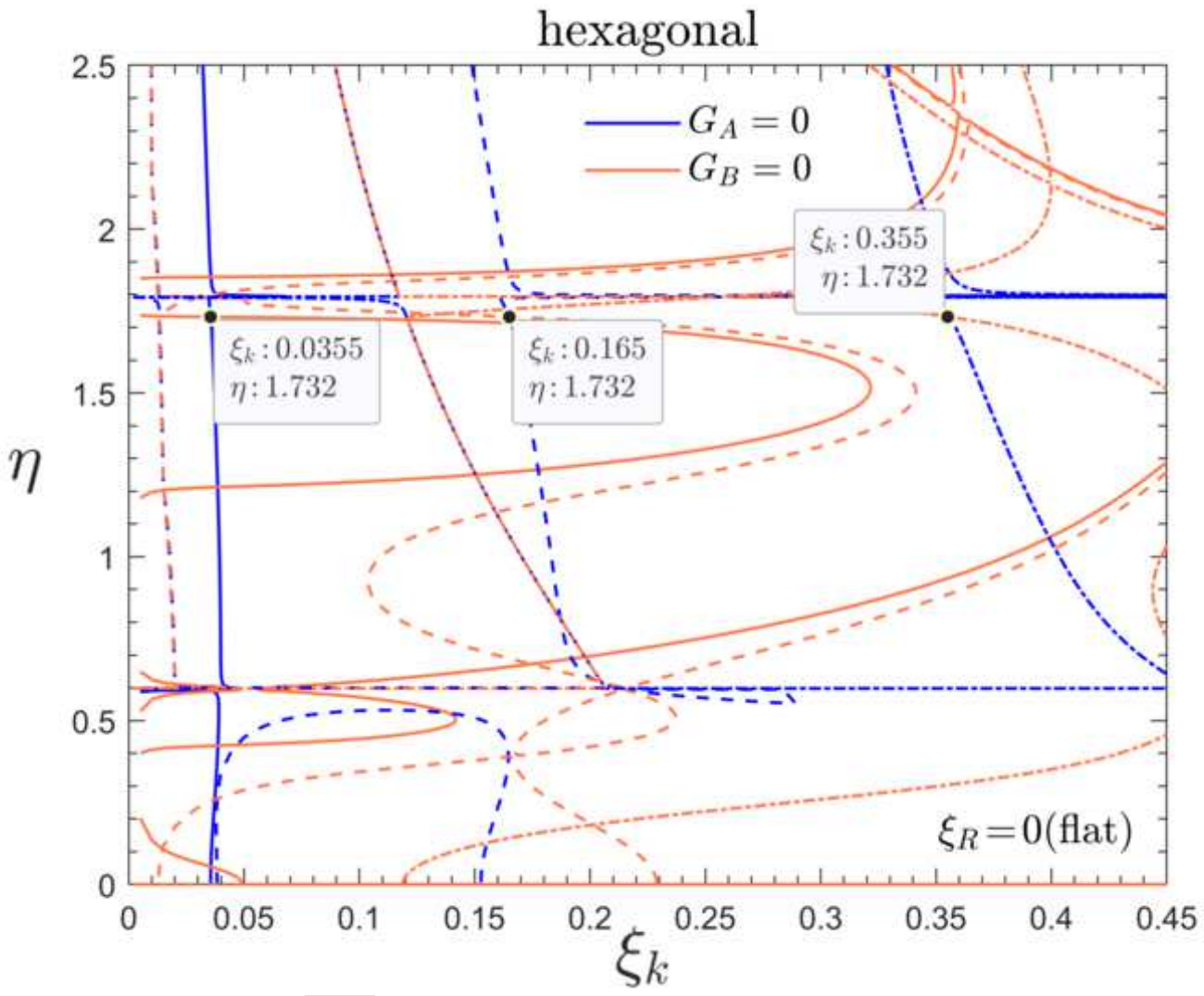

Figure(s)

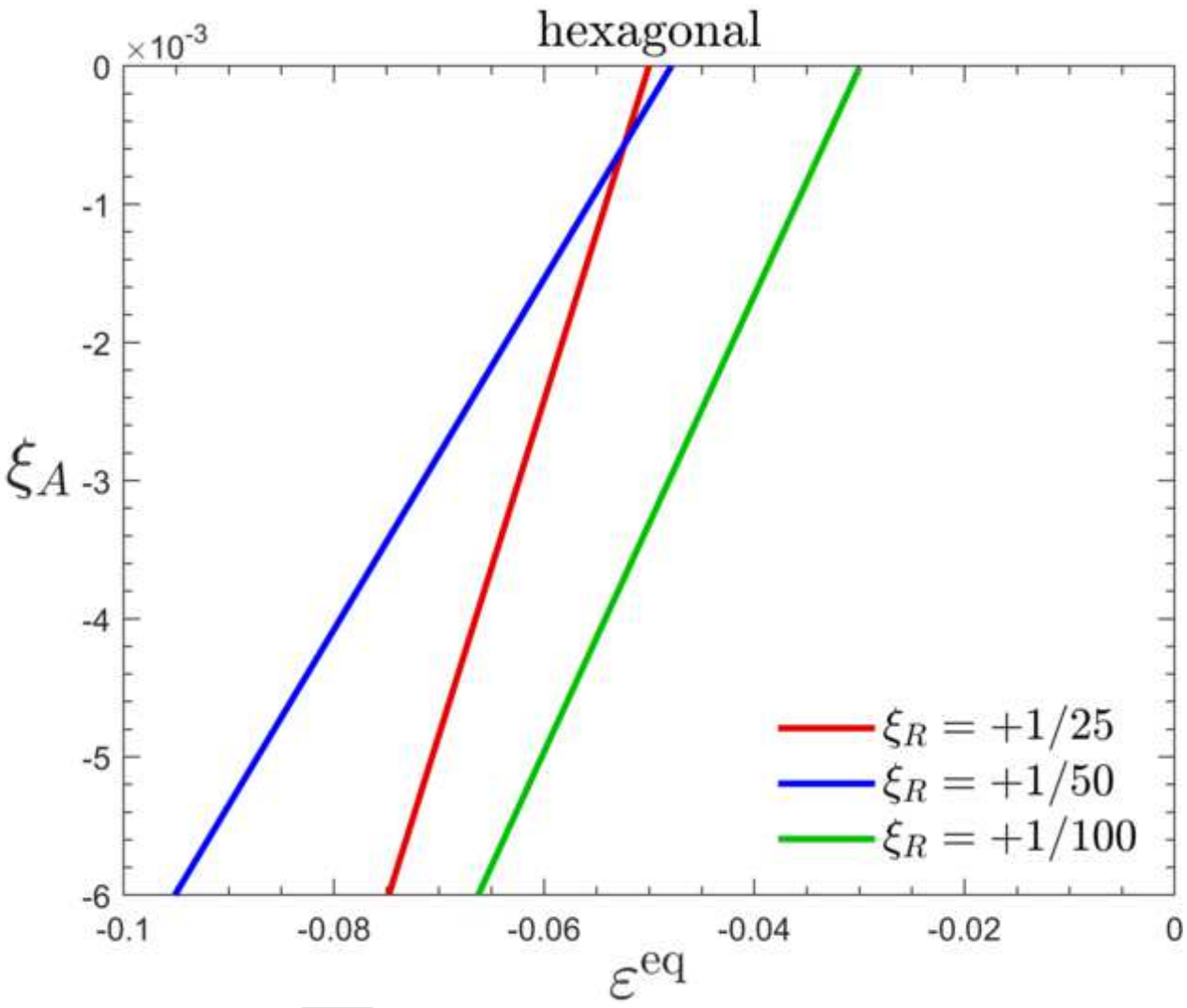

Figure(s)

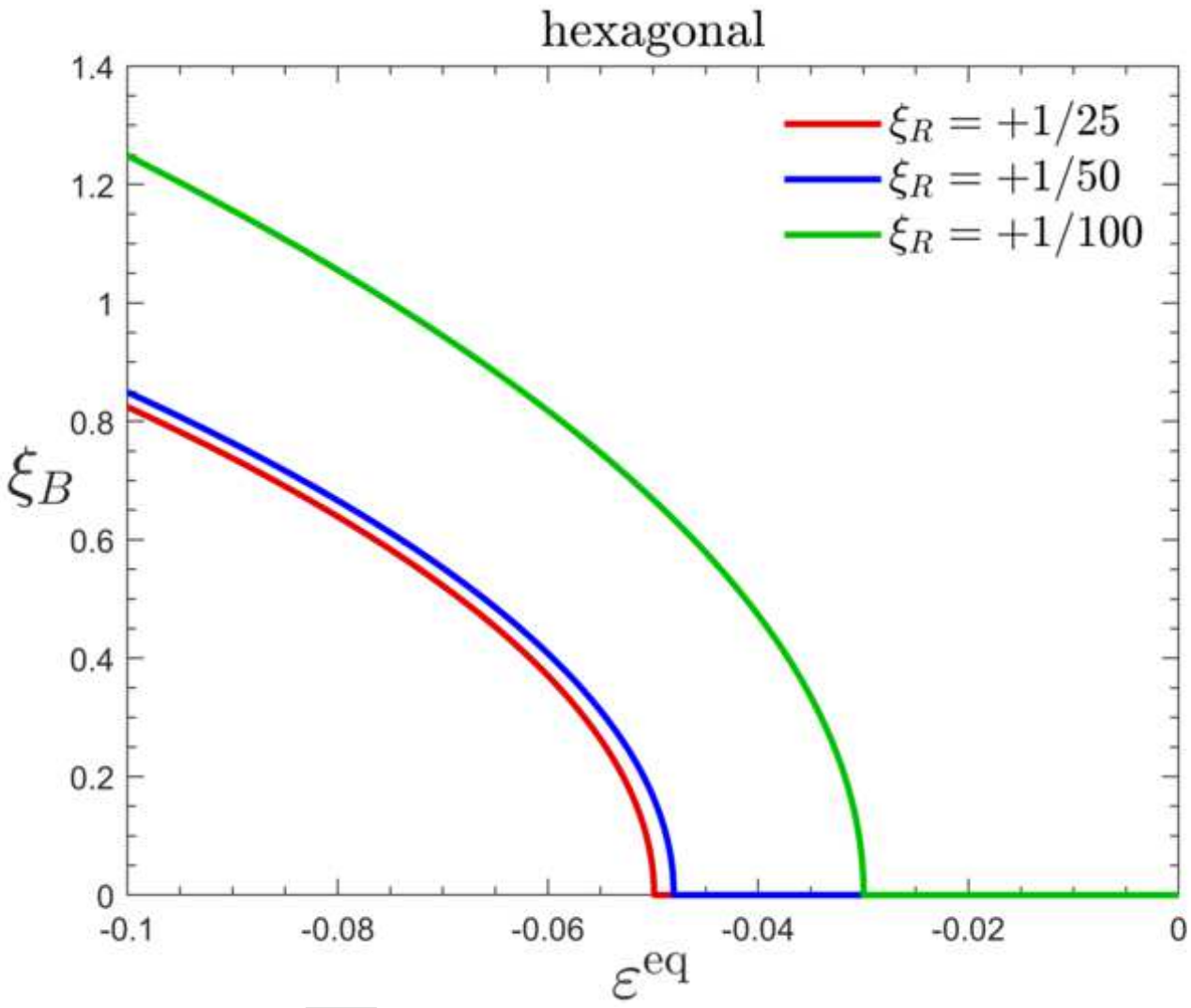

Figure(s)

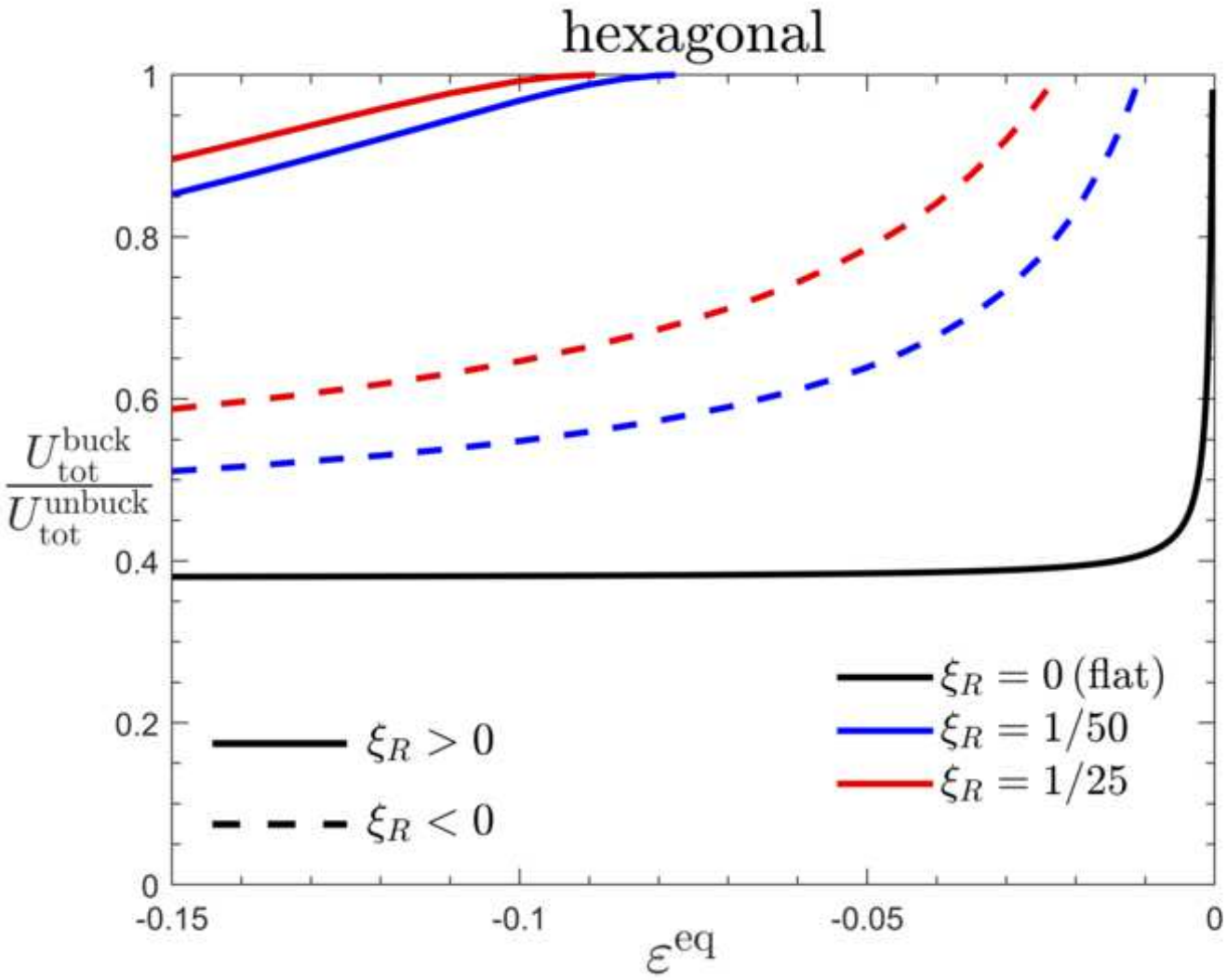
hexagonal
1
0.8
0.6
0.4
0.2
0
$\frac{U_{\text{tot}}^{\text{buck}}}{U_{\text{tot}}^{\text{unbuck}}}$
-0.15
-0.1
-0.05
0
ε^{eq}
$\xi_R > 0$
$\xi_R < 0$
$\xi_R = 0$ (flat)
$\xi_R = 1/50$
$\xi_R = 1/25$

Figure(s)

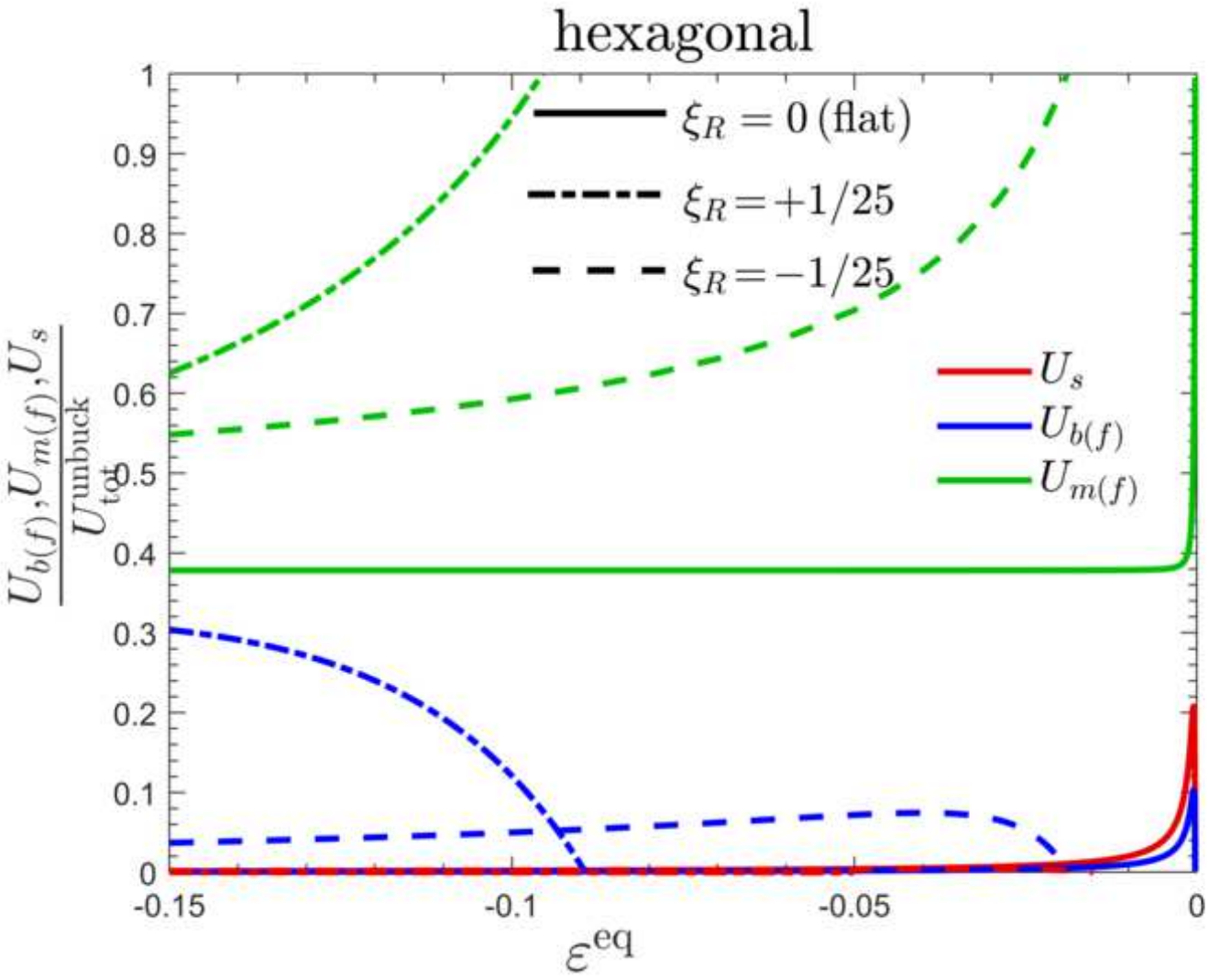
hexagonal
$\xi_R = 0$ (flat)
$\xi_R = +1/25$
$\xi_R = -1/25$
U_s
$U_{b(f)}$
$U_{m(f)}$
$\frac{U_{b(f)}, U_{m(f)}, U_s}{U_{\mathrm{tot}}^{\mathrm{unbuck}}}$
$\varepsilon^{\mathrm{eq}}$
1
0.9
0.8
0.7
0.6
0.5
0.4
0.3
0.2
0.1
0
-0.15
-0.1
-0.05
0

Figure(s)

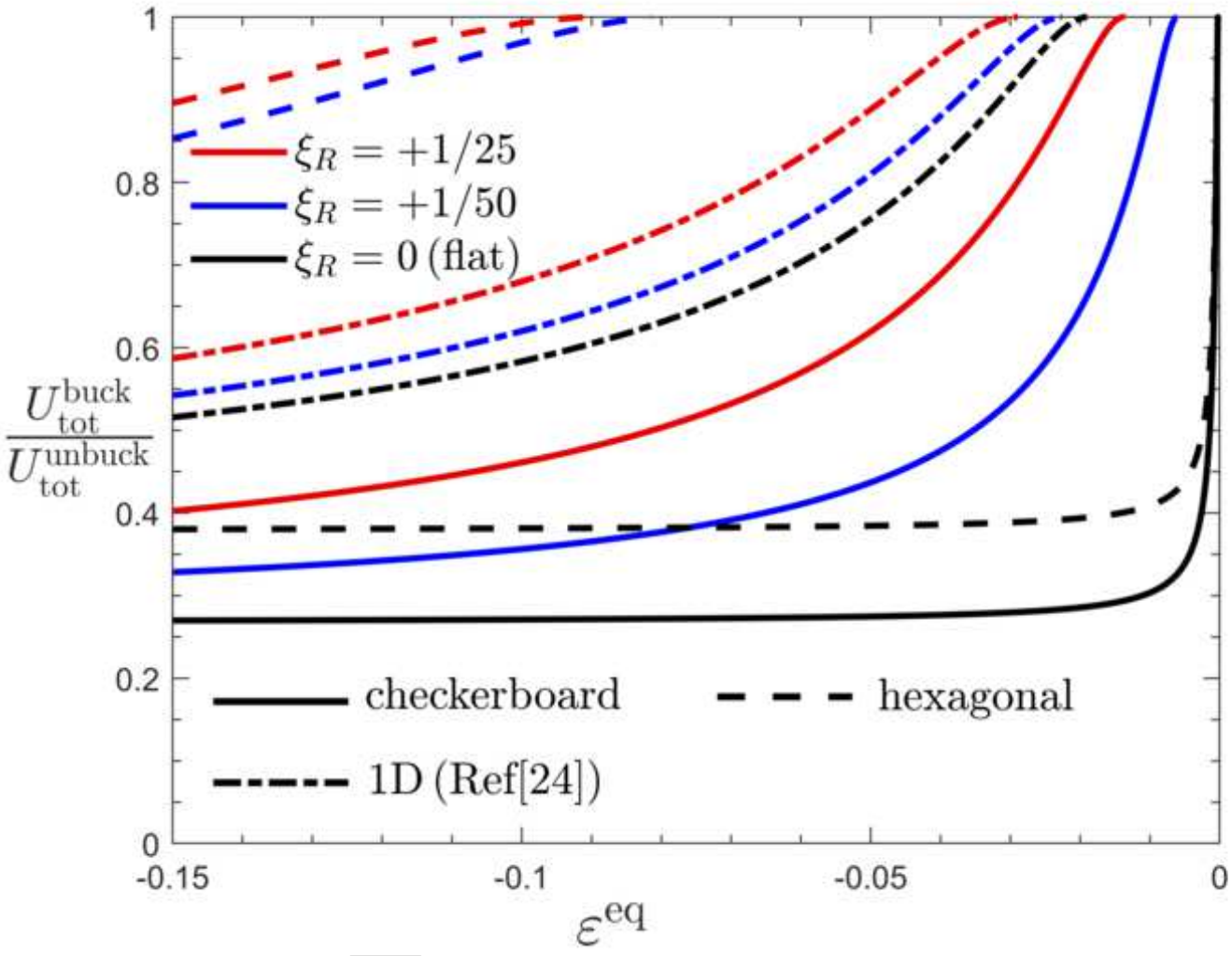
1
0.8
0.6
0.4
0.2
0
-0.15
-0.1
-0.05
0
$\frac{U_{\text{tot}}^{\text{buck}}}{U_{\text{tot}}^{\text{unbuck}}}$
ε^{eq}
$\xi_R = +1/25$
$\xi_R = +1/50$
$\xi_R = 0$ (flat)
checkerboard
hexagonal
1D (Ref[24])

Figure(s)

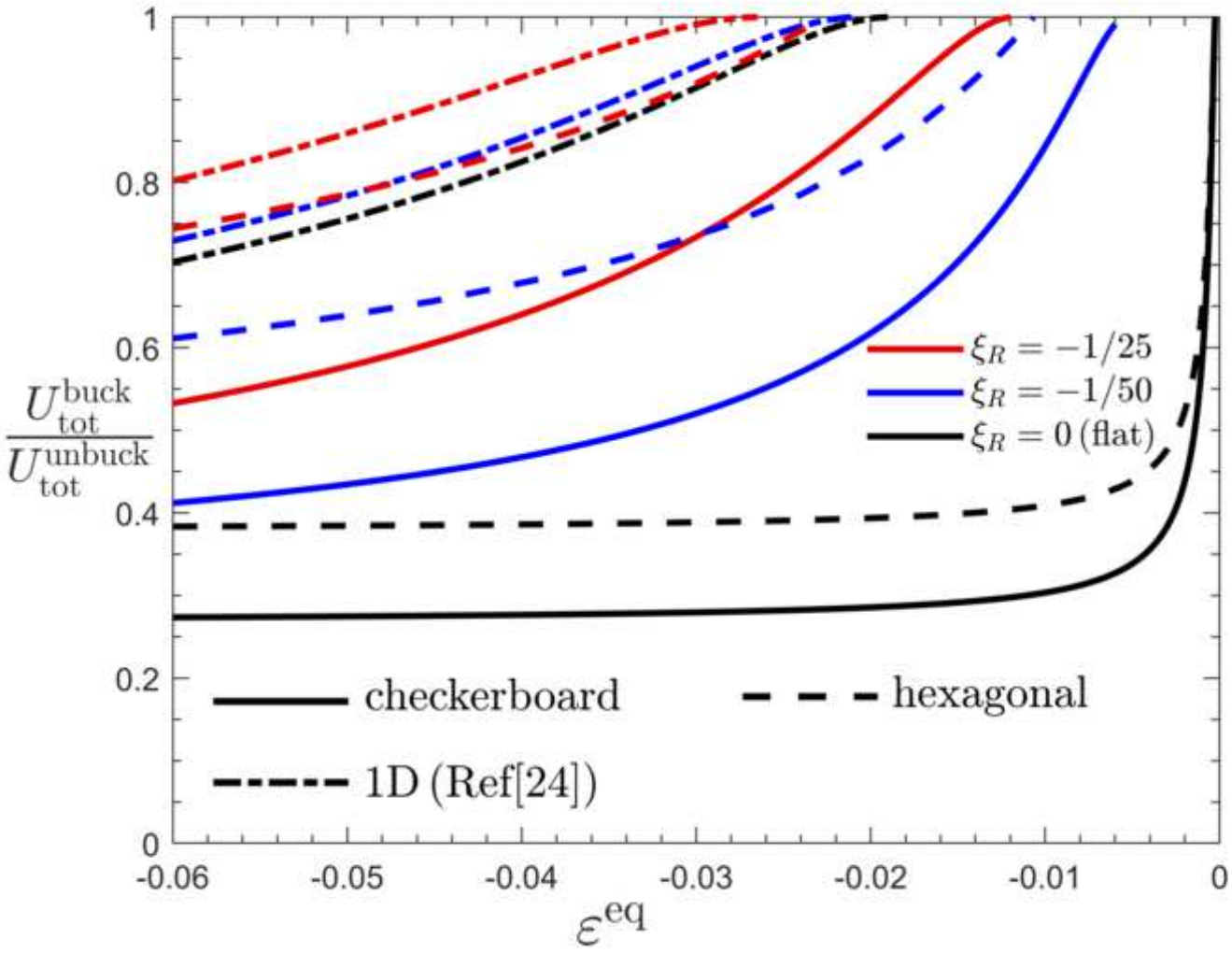

$\alpha_i\,(\nu_s)$	$\nu_s=-1/3$	$\nu_s=-1/4$	$\nu_s=0$	$\nu_s=1/4$	$\nu_s=1/3$	$\nu_s=0.48$
α_1	0.0755	0.0875	0.125	0.1666	0.1822	0.2138
α_2	0.1640	0.1625	0.1562	0.1458	0.1406	0.1274
α_3	0.2278	0.2438	0.2890	0.3342	0.3619	1.1629
α_4	0.4046	0.3866	0.3242	0.2534	0.2428	0.9879
α_5	0.3393	0.34834	0.3281	0.2065	0.3098	87.56
α_6	0.8696	0.8410	0.7851	1.0925	1.8421	106.01
α_7	1.2249	1.2062	1.125	1.2939	2.1412	193.57
α_8	618.3	568.3	376	1363.8	6797.1	6.9×10^{6}
α_9	3710.6	3898.9	5265	13595.3	29961.8	8.1×10^{6}
α_{10}	3613.8	3641.1	4284	12098.1	32393.2	1.5×10^{7}
α_{11}	1128	899.5	208	6150.7	41436.9	2.3×10^{8}
α_{12}	8629.2	9347.6	14403	50812	144838	2.6×10^{8}
α_{13}	4505.2	4611.3	7016	42068	161423	5×10^{8}
α_{14}	5311.8	3990.2	416	57665.1	484432	1.8×10^{10}
α_{15}	39424	42426.7	67539	341109	1.3×10^{6}	2.1×10^{10}
α_{16}	56894.4	60041	97939	651015	3×10^{6}	6.1×10^{10}
α_{17}	21122.8	19609.8	27424	361559	2.1×10^{6}	5.8×10^{10}

$\beta_i\,(\nu_s)$	$\nu_s = 1/3$	$\nu_s = 0.48$	$\beta_i\,(\nu_s)$	$\nu_s = 1/3$	$\nu_s = 0.48$
β_1	0.9166	1.4215	β_{18}	$1/3$	0.6915
β_2	0.0833	-0.7782	β_{19}	3.5	16.7459
β_3	2.7083	16.385	β_{20}	2.5729	15.4013
β_4	-11.3125	-182.544	β_{21}	9.1145	1490.82
β_5	14.2708	1581.59	β_{22}	48.3073	3284.61
β_6	16.2708	1583.59	β_{23}	39.3646	1793.87
β_7	122.518	108816	β_{24}	107.487	108627
β_8	121.518	108815	β_{25}	511.357	234999
β_9	-16.3125	-231.984	β_{26}	472.085	126982
β_{10}	-4.0833	-48.0185	β_{27}	610.129	3.72×10^6
β_{11}	-54.4167	-6498.78	β_{28}	2371.2	7.91×10^6
β_{12}	-43.0208	-6317.02	β_{29}	2124.14	4.2×10^6
β_{13}	701.868	3.73×10^6	β_{30}	1714.5	7.37×10^7
β_{14}	2082.97	7.42×10^7	β_{31}	7233.39	2.29×10^8
β_{15}	4.2812	96.4161	β_{32}	9747.39	2.37×10^8
β_{16}	-190.656	-309132	β_{33}	4169.55	8.21×10^7
β_{17}	0.625	0.5192			

t_f[nm]	$\nu_f[-]$	$\nu_s[-]$	E_f[MPa]	E_s[MPa]	$\bar{E}_s/\bar{E}_f[-]$
100	0.27	0.48	130000	1.65	1.53×10^{-5}

Critical compressive strain load (%)

ξ_R	$\varepsilon^0_{yy}\,(=\varepsilon^0_{xx})$	$\varepsilon^0_{yy}\,(=0.5\,\varepsilon^0_{xx})$	$\varepsilon^0_{yy}\,(=2\,\varepsilon^0_{xx})$
0 (flat)	-0.0249	-0.0157	-0.0315
$\pm 1/100$	$-0.273\,(-0.234)$	$-0.198\,(-0.180)$	$-0.296\,(-0.240)$
$\pm 1/50$	$-0.597\,(-0.511)$	$-0.428\,(-0.377)$	$-0.668\,(-0.546)$
$\pm 1/25$	$-1.359\,(-1.170)$	$-0.952\,(-0.835)$	$-1.523\,(-1.265)$

ξ_R	Present study	Ref.[35]
$1/25$	-2.48	-2.22
$1/50$	-1.18	-1.11
$1/100$	-0.571	-0.560
0 (flat)	-0.0335	-0.0316

Declaration of interests

☒ The authors declare that they have no known competing financial interests or personal relationships that could have appeared to influence the work reported in this paper.

☐ The authors declare the following financial interests/personal relationships which may be considered as potential competing interests: